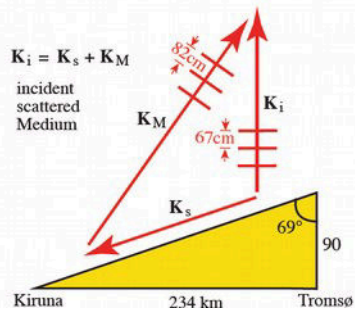
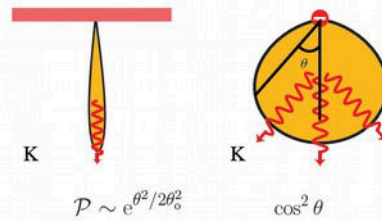


Tromsø–Kiruna Geometry



Aspect Sensitivity of PMSE
Anisotropic (specular) or Isotropic Scatterers ?



Ans: 11 July 2011, nearly isotropic, at least to $\theta = 69^\circ$

EISCAT

EUROPEAN INCOHERENT SCATTER
SCIENTIFIC ASSOCIATION

ANNUAL REPORT 2011



EISCAT Radar Systems

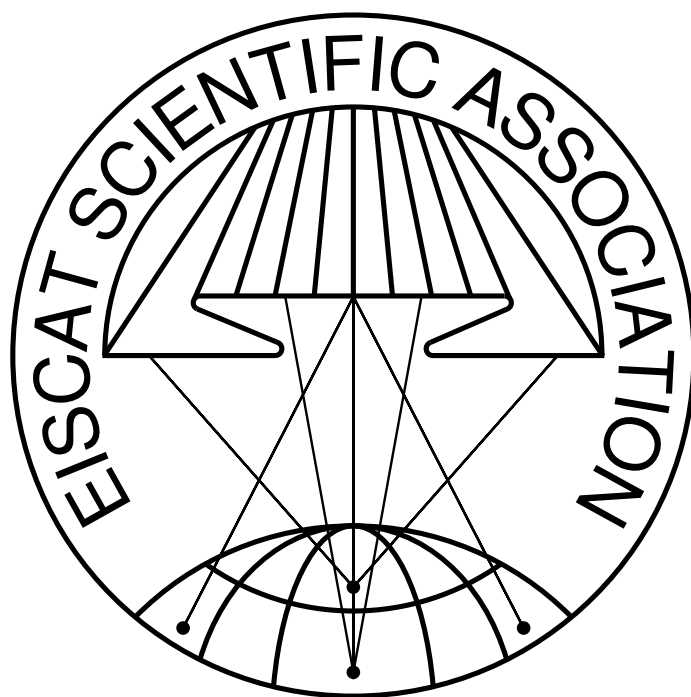
| Location | Tromsø | | Kiruna | Sodankylä | Longyearbyen | |
|-------------------------|---|----------------------------------|----------------------------------|----------------------------------|--|--|
| Geographic coordinates | 69°35'N 19°14'E | | 67°52'N 20°26'E | 67°22'N 26°38'E | 78°9'N 16°1'E | |
| Geomagnetic inclination | 77°30'N | | 76°48'N | 76°43'N | 82°6'N | |
| Invariant latitude | 66°12'N | | 64°27'N | 63°34'N | 75°18'N | |
| Band | VHF | UHF | UHF | UHF | UHF | |
| Frequency (MHz) | 224 | 929 | 929 | 929 | 500 | |
| Maximum bandwidth (MHz) | 3 | 8 | 8 | 8 | 10 | |
| Transmitter | 1 klystron | 2 klystrons | - | - | 16 klystrons | |
| Channels | 6 | 6 | 6 | 6 | 12 | |
| Peak Power (MW) | 1.6 | 2.0 | - | - | 1.0 | |
| Average power (MW) | 0.20 | 0.25 | - | - | 0.25 | |
| Pulse duration (ms) | 0.001–2.0 | 0.001–2.0 | - | - | 0.0005–2.0 | |
| Phase coding | binary | binary | binary | binary | binary | |
| Minimum interpulse (ms) | 1.0 | 1.0 | - | - | 0.1 | |
| Digital processing | 14 bit ADC on IF, 32 bit complex autocorrelation functions, parallel channels | | | | | |
| Antenna | parabolic cylinder 120 m × 40 m steerable | parabolic dish 32 m steerable | parabolic dish 32 m steerable | parabolic dish 32 m steerable | Antenna 1 parabolic dish 32 m steerable | Antenna 2 parabolic dish 42 m fixed |
| Feed system | line feed 128 crossed dipoles | Cassegrain | Cassegrain | Cassegrain | Cassegrain | Cassegrain |
| System temperature (K) | 250 | 90 | 50 | 50 | 80 | 65 |
| Gain (dBi) | 46 | 48.1 | 48.1 | 48.1 | 42.5 | 44.8 |
| Polarisation | circular | circular | any | any | circular | circular |

EISCAT Heating Facility in Tromsø

Frequency range: 4.0 MHz to 8.0 MHz, Maximum transmitter power: 12×0.1 MW, Antennas: Array 1 (5.5 MHz to 8.0 MHz) 30 dBi, Array 2 (4.0 MHz to 5.5 MHz) 24 dBi, Array 3 (5.5 MHz to 8.0 MHz) 24 dBi.

Additionally, a Dynasonde is operated at the heating facility.

Cover picture: Evidence of isotropic scattering from polar mesospheric summer echoes, from the work by C. La Hoz et al.



EISCAT Scientific Association
2011

EISCAT, the European Incoherent Scatter Scientific Association, is established to conduct research on the lower, middle and upper atmosphere and the ionosphere using the incoherent scatter radar technique. This technique is the most powerful ground-based tool for these research applications. EISCAT is also being used as a coherent scatter radar for studying instabilities in the ionosphere, investigating the structure and dynamics of the middle atmosphere, studying meteors and as a diagnostic instrument in ionospheric modification experiments with the heating facility.

There are fourteen incoherent scatter radars in the world, and EISCAT operates three of the highest-standard facilities. The EISCAT sites are located north of the Arctic Circle in Scandinavia. They consist of two independent radar systems on the mainland, together with a radar constructed on the island of Spitzbergen in the Svalbard archipelago — the EISCAT Svalbard Radar (see sketch and operating parameters on the inside of the front cover).

The EISCAT UHF radar operates in the 929 MHz band with a peak transmitter power of 2.0 MW, and employs fully steerable 32 m parabolic dish antennas. The transmitter for this system and one of the receivers are located in Tromsø (Norway). Receiving sites are also located in Kiruna (Sweden) and Sodankylä (Finland), allowing for tri-static radar measurements.

The monostatic VHF radar in Tromsø operates in the 224 MHz band with a peak transmitter power of 1.6 MW, using a 120 m × 40 m parabolic cylinder antenna which is subdivided into four sectors. This antenna can be steered mechanically in the meridional plane from vertical to 60° north of the zenith; limited east-west steering is also possible using alternative phasing cables.

The EISCAT Svalbard radar (ESR), located near Longyearbyen, operates in the 500 MHz band with a peak transmitter power of 1.0 MW, and employs a fully steerable parabolic dish antenna of 32 m diameter and a fixed antenna, aligned with the local magnetic field, with a 42 m diameter. The high latitude location of this facility is particularly aimed at studies of the cusp and the polar cap region.

The basic data measured with the incoherent scatter radar technique are profiles of electron density, electron and ion temperatures and bulk ion velocity. Subsequent processing allows derivation of a wealth of further parameters, describing the ionosphere and neutral atmosphere. A selection of well-designed radar pulse schemes are available to adapt the data-taking routines to many particular phenomena, occurring at altitudes from about 50 km to above 2000 km. Depending on geophysical conditions, a best time resolution of less than one second and an altitude resolution of a few hundred meters can be achieved.

Operations of 3000 h to 4000 h each year are distributed between Common Programmes (CP) and Special Programmes (SP). At present, six well-defined Common Programmes are run regularly, for between one and three days, typically about once per month, to provide a data base for long term synoptic studies. A large number of Special Programmes, defined individually by Associate scientists, are run to support national and international studies of both local and global geophysical phenomena.

Further details of the EISCAT system and its operation can be found in various EISCAT reports, including illustrated brochures, which can be obtained from EISCAT Headquarters in Kiruna, Sweden.

The investments and operational costs of EISCAT are shared between:

*China Research Institute of Radiowave Propagation, Peoples Republic of China
Deutsche Forschungsgemeinschaft, Germany
National Institute of Polar Research, Japan
Natural Environment Research Council, United Kingdom
Norges forskningsråd, Norway
Solar-Terrestrial Environment Laboratory, Nagoya University, Japan
Suomen Akatemia, Finland
Vetenskapsrådet, Sweden*

Contents

| | |
|--|-----------|
| EISCAT — from the Chairman’s perspective, fiscal year 2011 | 7 |
| EISCAT_3D | 8 |
| Scientific highlights 2011 | 12 |
| Ionospheric studies | 12 |
| First daytime thermospheric wind observation from a balloon-borne Fabry-Perot interferometer over Kiruna | 12 |
| Comparison of temporal fluctuations in the total electron content estimates from EISCAT and GPS along the same line of sight | 12 |
| Variance of the vertical ion speed in the polar lower ionosphere | 13 |
| A study of traveling ionospheric disturbances and atmospheric gravity waves using EISCAT Svalbard Radar IPY-data | 13 |
| Fine structure of a sporadic sodium layer | 14 |
| Sporadic E layer observation and analysis | 14 |
| EISCAT-Cluster observations of quiet-time near-Earth magnetotail fast flows and their signatures in the ionosphere | 14 |
| On the statistical relation between ion upflow and naturally enhanced ion-acoustic lines | 16 |
| Dependence of spectral width of ionospheric F region HF echoes on electric field | 17 |
| Solar zenith angle dependence of plasma density and temperature in the polar cap ionosphere and low-altitude magnetosphere | 17 |
| Auroral studies | 18 |
| Separating and quantifying ionospheric responses to proton and electron precipitation over Svalbard | 18 |
| Energy and flux variations across thin auroral arcs | 18 |
| A statistical investigation of the Cowling channel efficiency in the auroral zone | 19 |
| Dynamics and characteristics of black aurora as observed by high resolution ground-based imagers and radar | 19 |
| Polar mesospheric summer echoes | 21 |
| Evidence of isotropic scattering from PMSE | 21 |
| PMSE research highlights from German EISCAT users | 21 |
| EISCAT VHF measurements of aspect sensitivity in the vicinity of polar mesospheric summer echoes | 24 |
| Majority of PMSE spectral widths at UHF and VHF are compatible with a single scattering mechanism | 25 |
| Dusty space plasma diagnosis using temporal behavior of polar mesospheric summer echoes during active modification | 26 |
| Statistical survey of electron temperature enhancements in heater modulated polar mesospheric summer echoes | 26 |
| Active experiments | 26 |
| Temporal development of the magnetic zenith effect | 26 |
| EISCAT incoherent scatter radar measurements of artificial ionospheric modification at sub-ms time scales | 28 |

| | |
|---|-----------|
| Alternative estimation of the RF-enhanced plasma temperature during SPEAR experiments | 29 |
| Scientific highlights from Russian EISCAT users | 29 |
| Unusually broadened HF radar spectra from heater-induced artificial plasma irregularities | 32 |
| Investigation of the HF heater induced effects in the ionosphere | 32 |
| Angular dependence of pump-induced bottom- and top-side ionospheric plasma turbulence | 35 |
| Heating induced temperature enhancement in the polar summer ionosphere | 36 |
| Cosmic noise absorption changes due to radio heating of the D region ionosphere | 37 |
| New radar techniques | 38 |
| Fractional baud-length coding | 38 |
| Meteor head echo polarization at 930 MHz studied with the EISCAT UHF HPLA radar | 38 |
| Joule heating near an auroral arc and ion-neutral collision frequency in the polar cap E region | 39 |
| List of publications 2011 | 41 |
| EISCAT Operations 2011 | 44 |
| EISCAT organisational diagram 2011 | 48 |
| Committee Membership and Senior Staff | 49 |
| Appendix: EISCAT Scientific Association Annual Report, 2011 | 51 |
| The EISCAT Associates, December 2011 | 65 |
| Contact Information | 66 |

EISCAT — from the Chairman's perspective, fiscal year 2011

Slowly gliding closer to the possible realisation of EISCAT_3D and a third antenna on Svalbard while still considering the needs of the current EISCAT system, the fiscal year 2011 contained many important issues to deal with.

The information gathered in the EU funded projects EISCAT_3D Design Study (finished) and the currently ongoing EISCAT_3D Preparatory Phase pictures a modular system where the total cost for construction and operation is dependent of the size of the system to be designed. During the year EISCAT decided that an appropriate aim for the cost would be approximately 1 000 000 000 SEK for construction with a yearly operational and administrative budget of approximately 70 000 000 SEK. This decision made detailed strategy decisions easier about what should be expected with regard to associate funding, and the picture of the possible future system became easier to see. It was also agreed to have a look at the current agreement and statues, with the aim to make it easier for the current associates and possible new candidate associates to fund the system, creating a stable, but also more dynamic, funding model for EISCAT. This EISCAT agreement group started their work in 2011.

Concerning the intentions of the Chinese associates to contribute to EISCAT a third antenna for the Svalbard site, the early stages of a feasibility study continued. These activities were driven by the consultant Arvid Øvergård, with the expenses kindly covered by the Chinese associates. During

the year, the Svalbard community was informed and asked for opinions about the plans and the Norwegian frequency authority was approached for frequency allowances.

The current EISCAT mainland systems are operated with two different frequency ranges. The VHF system (222.8 MHz to 225.4 MHz) is monostatic, while the UHF system (926.6 MHz to 930.5 MHz) has tristatic capabilities. However, the UHF frequencies will soon be lost to mobile operators. In order to secure the tristatic mode of operation, a reliable and not too costly method to convert the UHF receivers at Kiruna and Sodankylä has been developed by EISCAT personnel. At the autumn meeting in Bonn, EISCAT Council decided that EISCAT should convert the present UHF receivers to VHF receivers.

The year 2011 was also the last year DFG (Germany) acted as an EISCAT associate. In their instruction, DFG can only finance research through projects and programmes, in contrast to infrastructure. During the years, DFG has sponsored a programme with the German researchers. This programme has now ended meaning that DFG sadly has to withdraw from EISCAT. Efforts will be made by EISCAT to be able to welcome the German research community again in the future.

In summary, 2011 was a year where many important decisions were made for a bright future, though under heavy economical constraints.

*Dr. Tomas Andersson
Chairperson, EISCAT Council*

EISCAT_3D

This is a short report of the progress of the work in the EISCAT_3D Preparatory Phase project during 2011.

Background of the Preparatory Phase

The high-latitude atmosphere and ionosphere are critically important for the study of Solar-Terrestrial relationships as well as the physical processes and the coupling of the different altitude regions in the Earth's atmosphere. The Arctic areas of Northern Europe provide a unique opportunity to observe this region from the ground with instruments placed within a well-developed infrastructure of observational facilities and research institutions. EISCAT_3D will be a world-leading international Research Infrastructure, using the incoherent scatter technique to study the atmosphere in the Scandinavian Arctic and to investigate how the Earth's atmosphere is coupled to space. EISCAT_3D will provide an advanced tool for studying plasma physics phenomena in the atmosphere, a key atmospheric monitoring instrument for climate and space weather studies and an essential element in international global multi-instrument campaigns for studying the environment.

EISCAT_3D will consist of several phased-array antenna sites for transmission of high-power radio waves and reception of faint signals back-scattered by charged particles in the atmosphere. Measuring and analysing the radio signal accurately probes the composition and physical parameters of the upper atmosphere. Each antenna array will consist of a large number of single antennas whose individual signals are digitally manipulated and combined to provide a cutting-edge atmospheric radar system. This will enable new types of volumetric imaging observations, multi-static observations, detailed studies on small scales, and quasi-continuous observations of the upper atmosphere. In order to reach the measurement objectives the radar will be distributed over several

sites in Northern Scandinavia. The flexibility of the new instrument requires new measurement strategies and opens the radar observations to an expanding user community.

EISCAT_3D will contribute to the growing field of research based on accumulating, handling and analysing large data volumes for Earth system studies. The fully working array will produce a data rate of several TB/s and the expected stored data volume in the initial phase of operation will be of the order of 1000 TB per year. Exploitation of its full potential requires collaboration with regional e-infrastructures and close connection to global e-infrastructures for the environment.

EISCAT Scientific Association is the Coordinator of the EISCAT_3D Preparatory Phase project. EISCAT is currently funded and operated by research councils of Norway, Sweden, Finland, Japan, China and the United Kingdom and has its headquarters in Kiruna, Sweden. It runs a radar system on Svalbard and a system on the Northern Scandinavian mainland consisting of a main transmitting and receiving radar site in Tromsø, Norway, and receiving sites in Sodankylä, Finland, and Kiruna, Sweden. The latter mainland system, that has successfully been producing incoherent scatter data for more than 30 years, will be replaced by the new EISCAT_3D system. The EISCAT host institutions actively participate in the project.

The current Preparatory Phase, that started in October 2010, aims to ensure that the project will reach a sufficient level of maturity so that the implementation of EISCAT_3D can begin immediately after its conclusion in September 2014.

Progress during the year

The Preparatory Phase is concerned with forming a consortium, procuring the financing, selecting the sites, preparing for the data handling, considering the scientific requirements and planning construction and operation. For all these tasks researchers and other stakeholders are involved.



The team responsible for the site surveys during 2011. From the left: “the ALIS bus”, Peter Bergqvist, Tarmo Laakso and Lars-Göran Vanhainen.

The project actively involves the scientific user community and all relevant documents can be found on the project website¹, the major fraction being open to the public.

EISCAT Scientific Association will provide the basis for the future EISCAT_3D consortium. The current EISCAT Associates have stated their support for the new EISCAT_3D. A letter of intent in order to support the EISCAT_3D project was fixed by the Council in October, to be signed by the current EISCAT Associates and possibly also by potential new members of the association. EISCAT Council has formed a working group together with the project to negotiate a new consortium agreement for the EISCAT Association that should be more suitable for constructing and operating EISCAT_3D and for attracting new members. Procedures will also be implemented within the research infrastructure to safeguard good scientific practice and to ensure the commitment to excellent research.

To procure the finances, major investments will be needed from several countries. The current estimate of costs for EISCAT_3D that assumes a total budget of 120 M€ to be invested over five to eight years, needs to be confirmed based on de-

tailed planning and site selection. Funding opportunities for research infrastructures for possible investment into EISCAT_3D in the coming years are identified in Norway, Sweden and Japan. The Finnish user community plans submitting a proposal next autumn to include EISCAT_3D in the national roadmap for research infrastructures. Funding situations in China and the United Kingdom are currently explored. Several other countries are either actively pursuing research based on EISCAT measurements or planning to do so in the near future. These are Belgium, Germany, Ireland, Italy, Poland, Russia and Ukraine. Some of these countries currently consider possible future participation in the EISCAT_3D consortium. The outreach activities of the project, conference presentations by the project participants and the EISCAT_3D project meetings are particularly important in this context.

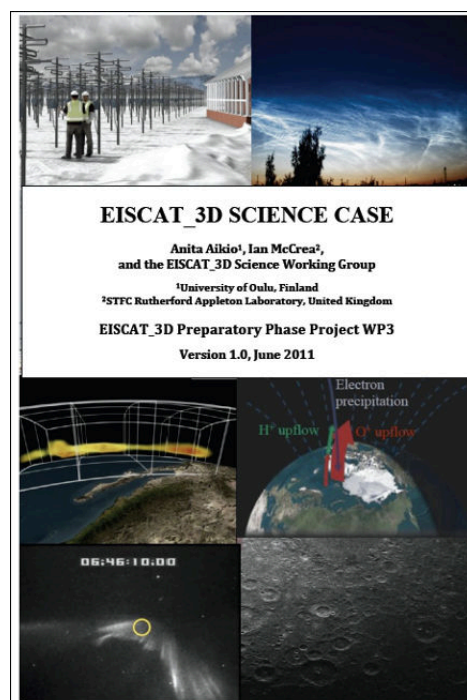
The site selection makes progress, though the requirements for site location vary for the different measurement objectives and need to be balanced. The project has also realised that site selection would not only be based on scientific considerations. The site surveys, that are carried out by the project, investigate the radio environment as well as the local infrastructure conditions. These

¹www.eiscat3d.se

can not be made during the Arctic winter which constrains the schedule to the summer. Allocations for the frequency range of the EISCAT_3D system were obtained in Norway, but not in Finland and Sweden. Progress in frequency allocation can be made as soon as the sites are selected and the first construction funding for the project is granted.

Planning for the data handling covers issues ranging from the direct connection of radar sites to the internet to the maintenance of the data and its placement within the framework of international geospace observatories and environmental research infrastructures. Some of the Work Packages related to data handling and data management have not formally started yet, since they for instance require knowledge of the detailed instrument performance and the radar sites. Nonetheless, some more general issues of data handling can be addressed by using the current EISCAT data and this approach is currently pursued. Preparatory work is also carried out in the frame of other projects. EISCAT, as Coordinator of the EISCAT_3D Preparatory Phase, participates in consortia funded by the European Union through Framework Programme 7: ENVRI is related to the common needs of ESFRI projects in terms of data handling, storage and management. ESPAS will facilitate user access to space weather data from ground-based and satellite experiments. COOPEUS that is currently under negotiation will facilitate collaboration with US environmental research institutions for common data policies and standards relevant to global research infrastructures in the environment field.

The scientific requirements have a major influence on the system design and for this a Science Case is continuously revised in collaboration with the present EISCAT user community and with prospective future users. Communication with the scientific user community is facilitated through outreach activities, conference presentations and a series of dedicated meetings organized by the project. The website for EISCAT_3D has been online since March 2009 and is regularly maintained and updated. A user account system on the website was introduced at the beginning of the project and facilitates the close connection of the project to the community. The project sets a high priority on expanding the user base into the space weather and middle atmosphere communities, which have not been major users of EISCAT in the past. Nonetheless, discussions also showed that in order to prepare competitive proposals to the national



Cover of the first version of the EISCAT_3D Science Case.

funding bodies it is important to clearly state the primary objectives of the project and to emphasise the key scientific issues that focus on those measurement capabilities of EISCAT_3D that are unique: the capability of continuous observations, of both small and large scale observations and the flexibility of changing the modes in order to directly respond to observed phenomena.

Planning the construction and operation of the new system requires a detailed instrument design. The design planning is based on a previous Design Study (funded within FP6) and on the long experience with the existing EISCAT radars. The project also aims to make use of innovative theoretical studies in signal processing, radar coding, data handling and data analysis. This recent progress is summarised in a handbook of measurement principles, whose initial version was prepared during the first months of the Preparatory Phase for consideration during the planning. The new instrument will carry out signal processing using Software-Defined Radio (SDR) receiver systems. In order to use the aperture synthesis imaging radar technique with the new instrument, simulations for optimal receiving outlier configuration were carried out and completed. A simple double triangular configuration was suggested as a result of this work. While work on specific tech-

nical tasks makes good progress, the results still need to be combined within an instrument design.

The project faces a wide range of expectations from researchers and other stakeholders. User expectations are in some cases contradictory, ranging from the desire to have a new system workable as quickly as possible to the desire to design the system in a sophisticated way based on the results of mathematically rigorous considerations. Combined with some gaps in the technical work that was proposed in the original project plan and with a deficiency in available engineering workforce at the project Coordinator, this has delayed the preparation of the instrument performance specification. This delay of a Deliverable in the project has an impact on some of the technical Work Packages and imposes uncertainties on budget and experiment description needed for the consortium negotiations. The project Coordinator approaches this problem with an additional recruitment planned for next year and continued efforts to communicate with the user community. Further recruitments are also envisioned later next year. Other delays of Milestones and Deliverables have less impact on the work plan. Delayed starts of some of the Work Packages have also required minor changes in the project planning that will be compensated by an intensified activity later in the project. The project benefits from its location within a network of well-developed observational facilities and research institutions that are very supportive of the project. At the same time they have different expectations that have to be met in a way so that all stakeholders are satisfied. To meet this challenge the project Coordinator benefits from exchange of experience, networking and training on managing international research infrastructures that is offered by projects within the Framework Programme 7. Swedish Research Council will support the development of the project with a 7 MSEK planning grant for 2012 and 2013 from its funding programme for research infrastructures. A major fraction of this funding is planned for negotiations and organisational preparation of the project.

Expectations

The goal of the Preparatory Phase is to bring the EISCAT Scientific Association in the position to be-

gin implementing the new infrastructure in 2014. While not all of the Deliverables of the project have yet been delivered on time, the reasons for delays have been identified and measures have been taken to compensate for these delays so that there is confidence within the project that the EISCAT_3D Preparatory Phase will end successfully. Regional and national enterprises from a wide range of industrial sectors are expected to participate in building the new system. The project expects that the EISCAT_3D data will be managed in collaboration with the local e-infrastructure in the Nordic countries. The Research Infrastructure will be connected to universities and research institutions locally in Northern Scandinavia close to the sites, and globally through the members of the association and the international research community. EISCAT_3D will also provide young researchers and engineers the opportunity to gain experience in the maintenance and handling of huge data volumes and will introduce young scientists to environmental research on internationally competitive level.

Project partners

There are eight partners in the EISCAT_3D Preparatory Phase:

- EISCAT Scientific Association (EISCAT)
- University of Oulu (UOULU)
- Luleå University of Technology (LTU)
- Swedish Institute of Space Physics (IRF)
- University of Tromsø (UiT)
- Science & Technology Facilities Council (STFC)
- Swedish Research Council (VR)
- National Instruments Belgium NV (NI)

The host institutions for the present EISCAT systems are Sodankylä Geophysical Institute (independent department of University of Oulu), University of Tromsø and Swedish Institute of Space Physics.

Scientific highlights 2011

Ionospheric studies

First daytime thermospheric wind observation from a balloon-borne Fabry-Perot interferometer over Kiruna

HIWIND (High altitude Interferometer WIND Observation) is the first balloon Fabry-Perot interferometer (FPI) to achieve successful thermospheric wind measurement for both day and night. By flying at ~ 40 km altitude, HIWIND avoids the high solar scattering background and enables daytime remote sensing of Doppler shift in airglow for thermospheric wind observation. During its first flight in June 2011 from Kiruna, (68°N , 65 MLAT), HIWIND observed persistent equatorward winds (Figure 1), while the NCAR TIEGCM model predicted poleward winds on the dayside. Combined with simultaneous EISCAT incoherent scatter radar observation, HIWIND yielded a daytime Burnside factor value of 0.85 (Figure 1). HIWIND data appear to suggest that upward vertical winds near the auroral oval may be the cause for large differences between the FPI measured and radar derived winds near midnight.

Q. Wu, et al., "First Daytime Thermospheric Wind Observation from a balloon-borne Fabry-Perot interferometer over Kiruna (68°N)", *Geophys. Res. Lett.* 39, L14104, doi:10.1029/2012GL052533, 2012.

Comparison of temporal fluctuations in the total electron content estimates from EISCAT and GPS along the same line of sight

The impact of space weather events onto satellite based technologies (e.g. satellite navigation and precise positioning) is typically quantified on the basis of the total electron content (TEC) and temporal fluctuations associated with it. GNSS (Global Navigation Satellite Systems) TEC measurements are integrated over a long distance and thus may include contributions from different regions of the ionised atmosphere which may pre-

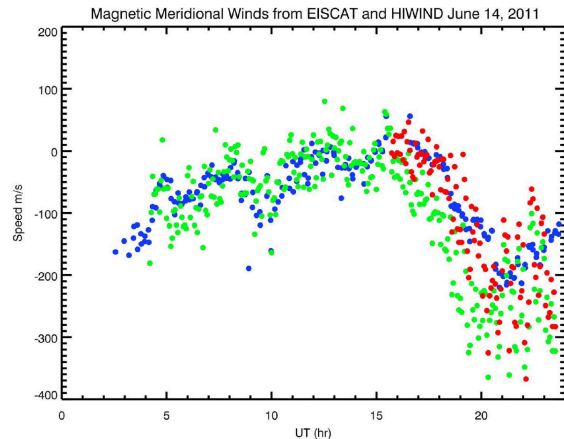


Figure 1: Winds in the magnetic meridian from HIWIND and EISCAT. The green dots are EISCAT derived winds with a Burnside factor of 0.85. The blue dots are HIWIND observed winds. The red dots are EISCAT winds after estimating the upward vertical wind effects.

vent the resolution of the mechanisms ultimately responsible for given observations. The purpose of the experiment presented here was to compare TEC estimates from EISCAT and GPS measurements. The EISCAT measurements were obtained along the same line of sight of a given GPS satellite observed from Tromsø. The present analyses focused on the comparison of temporal fluctuations in the TEC between aligned GPS and EISCAT measurements. A reasonably good agreement was found between temporal fluctuations in TEC observed by EISCAT and those observed by a co-located GPS ionospheric monitor along the same line of sight (Figure 2), indicating a contribution from structures at E and F altitudes mainly onto the total TEC in the presence of ionisation enhancements possibly caused by particle precipitation in the nighttime sector. The experiment suggests the great potential in the measurements to be performed by the future EISCAT_3D system, limited only in the localised geographic region to be covered.

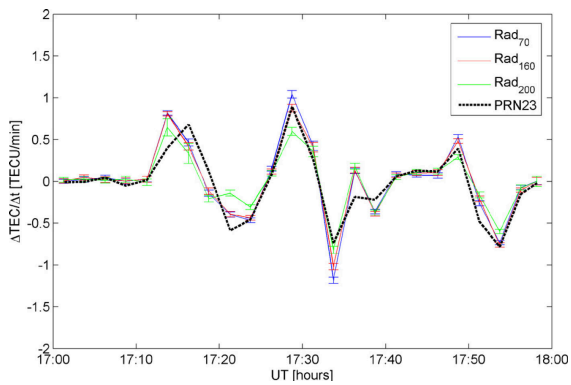


Figure 2: Temporal fluctuations in slant TEC along the EISCAT (Tromsø, 12 December 2011) line of sight as integrated from altitudes 70 km (blue), 150 km (red), 200 km (green) upwards until range 500 km. Temporal fluctuations in slant TEC from PRN23 (dashed black) along the same direction are shown as well. The temporal fluctuations are calculated over an interval of approximately 150 s.

B. Forte, et al., "Comparison of temporal fluctuations in the total electron content estimates from EISCAT and GPS along the same line of sight", *Ann. Geophys.*, IN PRESS.

Variance of the vertical ion speed in the polar lower ionosphere

The vertical component of the ion velocity measured with the European Incoherent Scatter (EISCAT) Tromsø UHF radar (69.6°N, 19.2°E) in the lower ionosphere (from 95 km to 130 km) was found to be characterised by notably large variances at oscillation periods of 2 min to 8 min. Of particular interest was the geomagnetic activity dependence above ~106 km, which showed larger variances ($100 \text{ m}^2 \text{ s}^{-2}$ to $500 \text{ m}^2 \text{ s}^{-2}$) during periods of geomagnetic disturbance than during quiet periods. Below 106 km, the variance was less sensitive to the geomagnetic activity. Height profiles of the variance during the disturbed period showed steep increases with heights above 106 km, then reaching a peak at 120 km, where the ion gyrofrequency is equal to the modelled ion-neutral collision frequency. A theoretical prediction well reproduced the height profile for the geomagnetically disturbed period by assuming oscillations in the meridional component of the electric field (Figure 3). The theoretical study suggested that the electric field oscillation is a possible cause of large variances of the vertical ion speed in the polar lower ionosphere. However, below 106 km, other mechanisms were necessary.

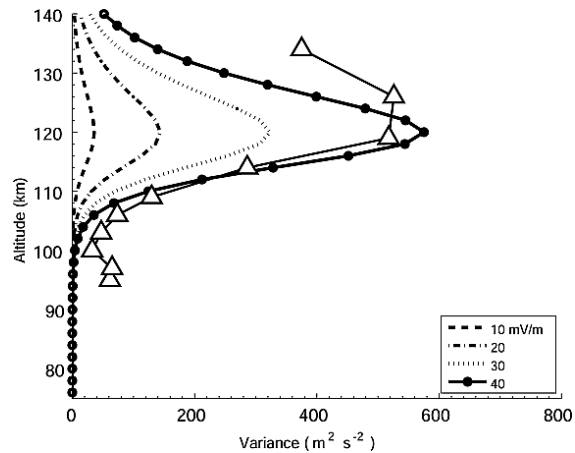


Figure 3: Comparison of the vertical ion speed variance between the theoretical predictions and the observed result (open triangles).

S. Oyama, et al., "Variance of the vertical ion speed measured with the EISCAT UHF radar in the polar lower ionosphere at Tromsø, Norway", *J. Geophys. Res.* 116, A00K06, doi:10.1029/2010JA016129, 2011.

A study of traveling ionospheric disturbances and atmospheric gravity waves using EISCAT Svalbard Radar IPY-data

Vlasov et al. (2011) presented a statistical study of Traveling Ionospheric Disturbances (TIDs) as observed by the EISCAT Svalbard Radar (ESR) during the continuous IPY-run (March 2007 – February 2008) with field-aligned measurements. A semi-automatic routine was developed for searching and extracting Atmospheric Gravity Wave (AGW) activity. The collected data shows that AGW-TID signatures (Figure 4) are common in the high-latitude ionosphere especially in the field-aligned ion velocity data (244 cases of AGW-TID signatures in daily records), but they can be observed also in electron density (26 cases), electron temperature (12 cases) and ion temperature (26 cases). During the IPY campaign (in solar minimum conditions) AGW-TID events appear more frequently during summer months than during the winter months. It remains a topic for future studies whether the observed seasonal variation in the performance of the observational method that was used (AGW-TID signature may be more pronounced in a dense ionosphere). In the AGW-TID dataset the distribution of the oscillation periods has two peaks, one around 0.5 h to 0.7 h and the other around 1.1 h to 1.3 h. The diurnal oc-

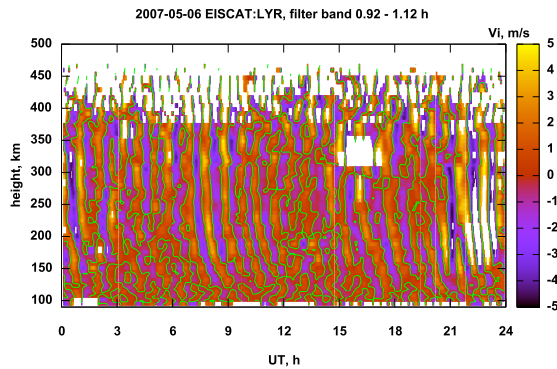


Figure 4: Filtered field-aligned ion velocity data on 6 May 2007, which clearly shows the quasi-periodic disturbances with “downward” phase progression in time as typical AGW-TID signatures.

currence rate has a deep minimum in the region of magnetic midnight, which might be partly explained by irregular auroral activity obscuring the TID signatures from our detection routines. As both the period and horizontal phase speed estimates (as derived from the classical AGW dispersion relation) show values typical both for large scale TIDs and mesoscale TIDs it is difficult to distinguish whether the generator for high-latitude AGW-TIDs resides typically in the troposphere or in the near-Earth space. The results of the statistical analysis give anyway some valuable reference information for the future efforts to learn more about the dominating TID source mechanisms in polar cap conditions, and to improve AGW simulations.

A. Vlasov, et al., “A study of Traveling Ionospheric Disturbances and Atmospheric Gravity Waves using EISCAT Svalbard Radar IPY-data”, *Ann. Geophys.* 29, 2101–2116, 2011.

Fine structure of a sporadic sodium layer

A sporadic sodium layer (SSL) was studied, in particular its fine structure, that was observed at 92 km to 98 km between 20:00 and 23:30 UT (21:00–24:30 LT) on 11 January 2011 using a sodium lidar, which was installed in the European incoherent scatter (EISCAT) radar site at Tromsø, Norway (69.6°N, 19.2°E) in early 2010 (Figure 5). The sodium lidar measurement with 5-seconds time-resolution reveals the details of dramatic sodium-density increase as well as short-period wavelike structure in the SSL. The rate of increase of height-integrated sodium density at the begin-

ning of the SSL event was $6.4 \times 10^{10} \text{ m}^{-2} \text{ s}^{-1}$ to $9.6 \times 10^{10} \text{ m}^{-2} \text{ s}^{-1}$. Dominant oscillation periods in the wavelike structures were 7 min to 11 min at 95 km to 98 km and 3 min at 92 km to 95 km. The calculated power spectral densities are well represented by power laws, implying the presence of the short-period waves and turbulence in the frequency range of 10^{-4} Hz to 10^{-1} Hz .

T. T. Tsuda, et al., “Fine structure of sporadic sodium layer observed with a sodium lidar at Tromsø, Norway”, *Geophys. Res. Lett.* 38, L18102, doi:10.1029/2011GL048685, 2011.

Sporadic E layer observation and analysis

Based on the theory of wave propagation in the layered media, a sporadic E layer observed by the UHF radar in Tromsø (Figure 6) on 3 July 2008 was analysed. The electron density profile was obtained by inverting the UHF observation, thus a simulated ionogram (Figure 7) was calculated and compared with the measurements by the dynasonde in Tromsø, as shown in Figure 8. The result shows that the sporadic E layer ionogram traces by the theory of partial reflection agrees well with the observation.

EISCAT-Cluster observations of quiet-time near-Earth magnetotail fast flows and their signatures in the ionosphere

Pitkänen et al. (2011) report observations of a sequence of quiet-time Earthward bursty bulk flows (BBFs) measured by the Cluster spacecraft in the near-tail plasma sheet in the evening sector, and by simultaneous high-resolution measurements in the northern conjugate ionosphere by the EISCAT radars, a MIRACLE all-sky camera, magnetometers, and a meridian-scanning photometer (MSP) on 17 October 2005.

The BBFs at Cluster show signatures that are consistent with the plasma “bubble” model, eg. deflection and compression of the ambient plasma in front of the Earthward moving bubble, magnetic signatures of a flow shear region, and the proper flows inside the bubble. In addition, clear signatures of tailward return flows around the edges of the bubble can be identified. The duskside return flows are associated with significant decrease in plasma density, giving support to the recent suggestion of formation of a depleted wake. However, the same feature is not seen for

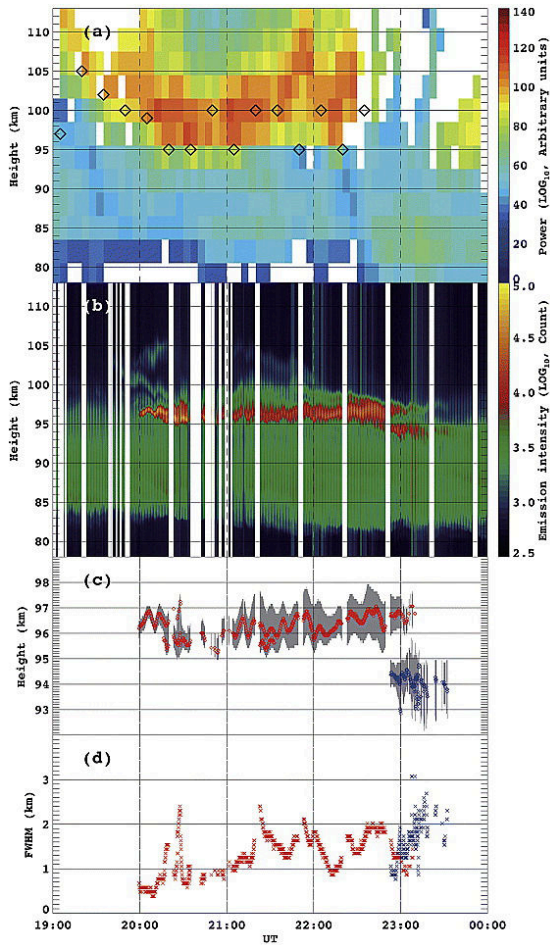


Figure 5: (a) The MF-radar (2.8 MHz) received power data with a resolution of 5 min and 3 km, at 74 km to 109 km for 19:00–24:00 UT on 11 January 2011. Diamond symbols indicate $h'E_s$ determined with the ionosonde at Tromsø. It should be noted that the height information of the strong echoes and the $h'E_s$ could be affected by a time delay, i.e. group retardation, in the radio propagation. (b) The sodium lidar received emission intensity data with a resolution of 5 s and 96 m. It should be noted that the emission intensity includes an artificial variation due to changing of the laser frequency at every 1 min. (c) The peak height and (d) the FWHM in the emission intensity of the sporadic sodium layer. Red symbols indicate those at 95 km to 98 km, and blue symbols indicate those at 92 km to 95 km. The FWHM is also described by vertical grey bar in Figure panel c.

the dawnside return flows, but rather an increase in density.

In the ionosphere, EISCAT and optical measurements show that each of the studied BBFs is associated with an auroral streamer (Figure 9) that starts from the vicinity of the polar cap bound-

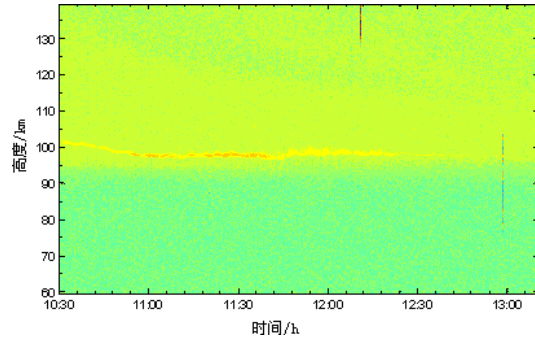


Figure 6: Sporadic E layer observation by the EISCAT UHF radar on 3 July 2008.

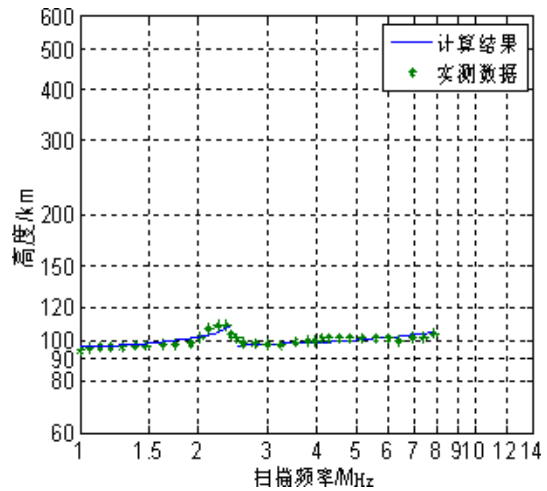


Figure 7: Simulated ionogram obtained through inversion of the EISCAT UHF data. Blue line: calculated profile, green stars: EISCAT measurements.

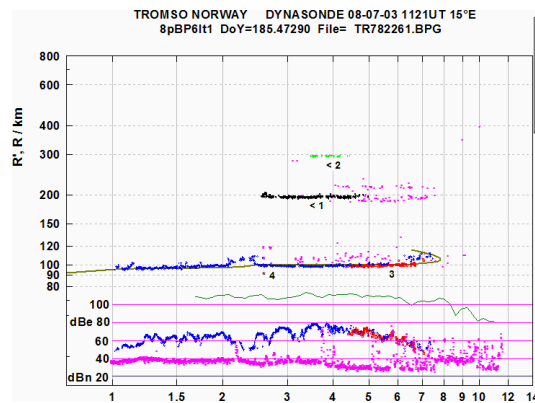


Figure 8: The sporadic E layer as observed by the dynasonde in Tromsø.

ary, intrudes equatorward, brakes at 68° MLAT to 70° MLAT and drifts westward along the proton oval. Within the streamer itself and poleward of it, the ionospheric plasma flow has an equator-

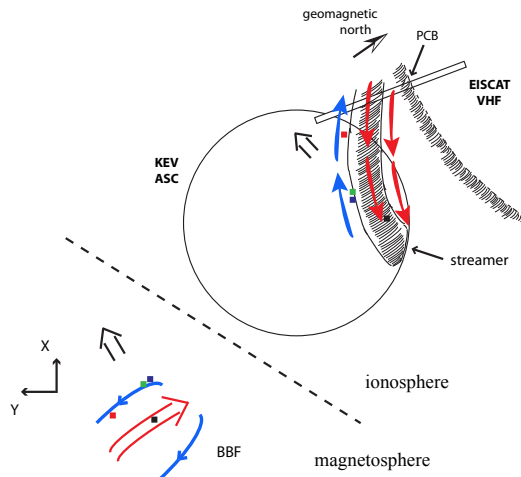


Figure 9: Schematic illustration of the situation in the ionosphere and possible configuration of the BBF in the tail close to the XY(GSM) plane at around 18:31 UT to 18:34 UT when C1 sees the BBF proper flow. Red arrows indicate the BBF proper flow and blue arrows the return flows. Wide black open arrows indicate the drift direction of the flow pattern.

ward component, which is the ionospheric manifestation of the Earthward BBF channel. A sharp velocity shear appears at the equatorward edge of a streamer. It is suggested that each BBF creates a local velocity shear in the ionosphere, in which the plasma flow poleward of and inside the streamer is in the direction of the streamer and southeastward. A northwestward return flow is located on the equatorward side. The return flow is associated with decreased plasma densities both in the ionosphere and in the magnetosphere as measured by EISCAT and Cluster, respectively. In summary, the first simultaneous high-resolution observations are presented of BBF return flows both in the plasma sheet and in the ionosphere, and those are in accordance with the bubble model. The results apply for the duskside return flows, but the manifestation of dawnside return flows in the ionosphere requires further studies.

Finally, EISCAT measurements indicate increased night-side reconnection rate during the ≈ 35 min period of BBFs. It is suggested that the observed temporal event of IMF rotation to a more southward direction produces enhanced open flux transport to the nightside magnetotail, and consequently, the nightside reconnection rate is increased.

T. Pitkänen et al., "EISCAT-Cluster observations of quiet-time near-Earth magnetotail fast flows and their

signatures in the ionosphere", *Ann. Geophys.* 29, 299, 2011.

On the statistical relation between ion upflow and naturally enhanced ion-acoustic lines

Characteristics have been investigated of ion upflow and naturally enhanced ion-acoustic lines (NEIALs) based on the European Incoherent Scatter (EISCAT) Svalbard radar (ESR) data continuously obtained between March 2007 and February 2008. For the ion upflow study approximately 78,000 field-aligned profiles obtained with the ESR were used. For the NEIAL study approximately 1500 NEIALs were identified in the ESR data at altitudes from 100 km to 500 km. The occurrence frequency of ion upflow shows two peaks (Figure 10), at about 08:00 and 13:00 magnetic local time (MLT), while only one strong peak is seen around 09:00 MLT for NEIALs. The upward ion flux also has only one peak around 11:00–1300 MLT. The occurrence frequency of ion upflow varies strongly over season. It is higher in winter than in summer, whereas NEIALs are more frequent in summer than in winter. NEIALs frequently occur under high geomagnetic activity and also high solar activity conditions. Approximately 10% of NEIALs in the F region ionosphere were accompanied by NEIALs in the E region (occurred at altitudes below 200 km). About half of the E region enhanced echoes did not have an F region counterpart. Upshifted NEIALs dominate in the E region whereas downshifted NEIALs are usually stronger above an altitude of 300 km. The high occurrence frequency of NEIALs in the pre-noon region (08:00–10:00 MLT) might be associated with acceleration of thermal ions to suprathermal ones. At the same MLT and geomagnetic latitude suprathermal ions and broadband extremely low frequency (BBELF) wave activity have been observed, according to previous studies.

Y. Ogawa, et al., "On the statistical relation between ion upflow and naturally enhanced ion-acoustic lines observed with the EISCAT Svalbard radar", *J. Geophys. Res.* 116, A03313, doi:10.1029/2010JA015827, 2011.

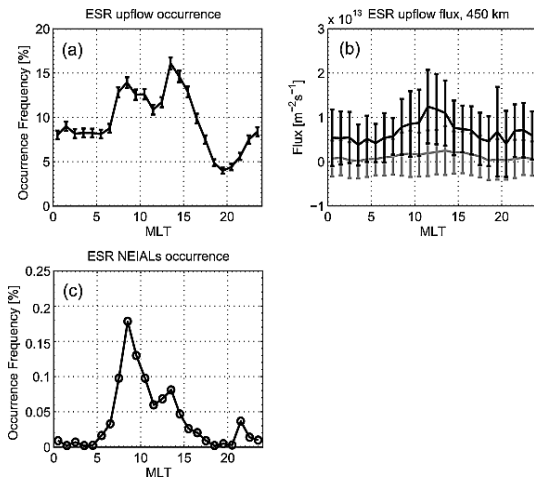


Figure 10: MLT distribution of (a) the occurrence frequency of ion upflow, (b) the upward ion flux at 450 km altitude, (c) the occurrence frequency of NEIALs in the F region ionosphere. The black line in Figure panel b indicates the average flux in upflow events, while the gray line indicates the average flux of all data (upflow, downflow, and no flow events).

Dependence of spectral width of ionospheric F region HF echoes on electric field

The EISCAT Svalbard radar monitors plasma parameters in the ionospheric region that is frequently located near the polar cap boundary. The SuperDARN radar at Hankasalmi, Finland, detects coherent echoes from this region, and these echoes typically show increased spectral width. By combining SuperDARN spectral width with ESR measurements of the ambient electric field, it was found that the spectral width of echoes tends to increase with the electric field (Figure 11). To explain these observations, it was assumed that the irregularities observed were excited through the $\vec{E} \times \vec{B}$ gradient drift plasma instability with energy cascading to shorter wavelengths. It was assumed that once the waves in the decametre range (detectable by the HAN radar) reach large amplitudes, their evolution is fully controlled by the non-linear three-wave interaction with waves of a smaller size. It was found that the decay time of these irregularities depends on the intensity of smaller-scale irregularities but not the ones seen by the radar. The quantitative estimates performed show that the inverse decay time of decametre irregularities increases with the electric field magnitude and the trend was found to be similar to the reported experimental data.

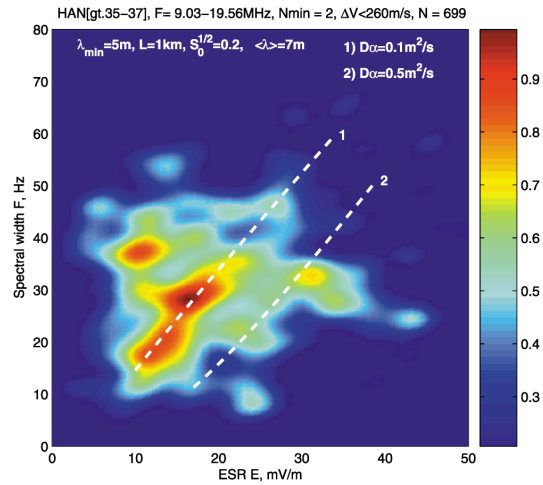


Figure 11: The occurrence distribution of the spectral width as a function of the electric field magnitude. Dashed lines show theoretical dependencies for two values of the diffusion coefficient. The model curves were obtained by using parameters indicated on the plot.

A. Kozlovsky, et al., "Dependence of spectral width of ionospheric F region HF echoes on electric field", *J. Geophys. Res.* 116 (A07302), 1–6, 2011.

Solar zenith angle dependence of plasma density and temperature in the polar cap ionosphere and low-altitude magnetosphere

The solar zenith angle (SZA) dependence of the ion and electron temperatures is investigated statistically on the basis of data obtained by the Akebono and Intercosmos satellites, and European Incoherent Scatter (EISCAT) Svalbard radar (ESR) (Figure 12). A drastic change in the electron temperature occurs near the terminator, similarly to that in the electron density profile obtained by the Akebono satellite. The sum of the ion and electron temperatures obtained by the ESR (~ 6500 K at ~ 1050 km altitude under sunlit conditions and ~ 3000 K at ~ 750 km altitude under dark conditions) agrees well with the scale height at low altitudes obtained from the Akebono observations, assuming that the temperature is constant and that O^+ ions are dominant. Comparisons between the present statistical results (SZA dependence of the electron density and ion and electron temperatures) and modeling studies of the polar wind indicate that the plasma density profile (especially of the O^+ ion density) in the polar cap is strongly controlled by solar radiation onto the ionosphere

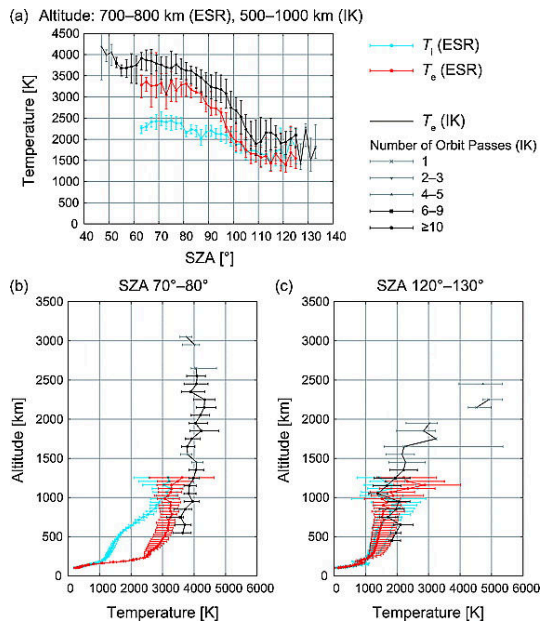


Figure 12: (a) SZA dependence of the ion (T_i) and electron (T_e) temperatures obtained by the Intercomcos (IK) satellites (500 km to 1000 km altitude) and ESR (700 km to 800 km altitude). Altitude profiles of the ion and electron temperatures in the SZA ranges of (b) 70° to 80° and (c) 90° to 120°. Blue and red points and lines show T_i and T_e obtained by ESR, respectively. Black (number of orbit passes ≥ 6) and grey (number of orbit passes ≤ 5) points and lines show T_e observed by the IK satellites. Points denote median temperatures. Error bars indicate quartiles.

by changing ion and electron temperatures in the ionosphere during geomagnetically quiet periods.

N. Kitamura, et al., “Solar zenith angle dependence of plasma density and temperature in the polar cap ionosphere and low-altitude magnetosphere during geomagnetically quiet periods at solar maximum”, *J. Geophys. Res.* 115, A07310, doi:10.1029/2009JA014766, 2011.

Auroral studies

Separating and quantifying ionospheric responses to proton and electron precipitation over Svalbard

Lanchester et al. (2011) used the EISCAT Svalbard Radar, together with data from the ASK optical imager, to study an auroral event observed during a period of high solar wind velocity, but low solar wind density (Figure 13). The radar

data were used in conjunction with satellite observations from IMAGE, NOAA-16 and DMSP-F14. The ground-based and space-based data provided inputs to a coupled electron deposition and ion chemistry model which predicted the overall emission rate. The predicted rates were compared to multi-wavelength optical data ($H\beta$, N_2^+ 1N(0,2) and O^+ 4P-4D emissions) measured from the ground, showing that, at the time of the closest approach of NOAA-16, the model predictions were in good agreement with the ground-based optical data, based on precipitating protons and electrons with total fluxes of 0.23 mW m^{-2} and 3.0 mW m^{-2} , respectively (Figure 14). It was deduced that the variations in F region electron density, and in the emissions from transitions of O^+ and N_2^+ , could largely be explained by electron precipitation, whereas the E region density changes and emissions could largely be accounted for by proton precipitation.

B. Lanchester, et al., “Separating and quantifying ionospheric responses to proton and electron precipitation over Svalbard”, *J. Geophys. Res.* 116, A09322, doi:10.1029/2011JA016474, 2011.

Energy and flux variations across thin auroral arcs

Two discrete auroral arc filaments, with widths of less than 1 km, have been analysed using multi-station, multi-monochromatic optical observations from small and medium field-of-view imagers and the EISCAT radar. The energy and flux of the precipitating electrons, volume emission rates and local electric fields in the ionosphere have been determined at high temporal (up to 30 Hz) and spatial (down to tens of metres) resolution. A new time-dependent inversion model is used to derive energy spectra from EISCAT electron density profiles. The energy and flux are also derived independently from optical emissions combined with ion-chemistry modelling, and a good agreement is found. A robust method to obtain detailed 2-D maps of the average energy and number flux of small scale aurora is presented. The arcs are stretched in the north-south direction, and the lowest energies are found on the western, leading edges of the arcs. The large ionospheric electric fields (250 mV m^{-1}) found from tri-static radar measurements (Figure 15) are evidence of strong currents associated with the region close to the optical arcs. The different data sets indicate that the arcs appear on the boundaries between regions with different average energy of

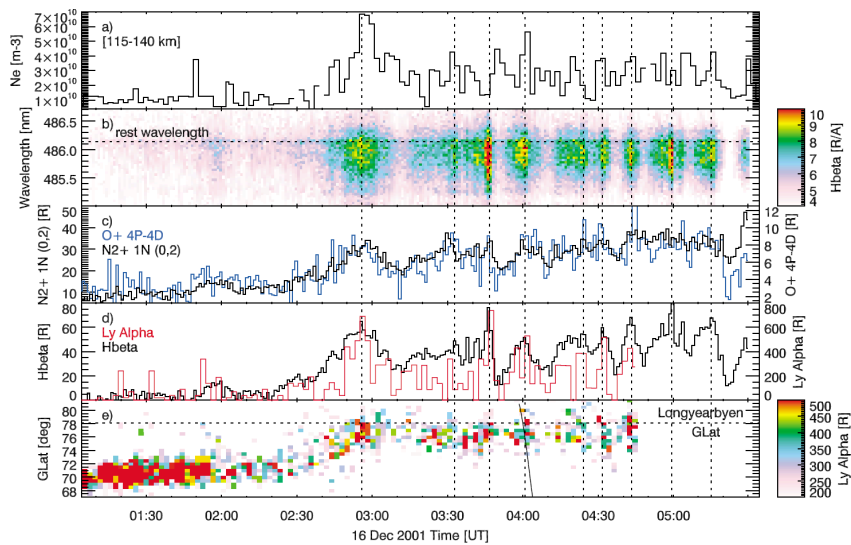


Figure 13: Overview of ground-based measurements for 01:00–05:30 UT on 16 December 2001: (a) ESR averaged electron density between 115 km and 140 km, (b) HiTIES H β brightness as a function of wavelength, (c) HiTIES N $_2^+$ and O $^+$ integrated brightness, (d) IMAGE Ly α brightness over Svalbard and integrated HiTIES H β , and (e) IMAGE Ly α brightness as a function of geographic latitude. The NOAA-16 track is seen at 04:00 UT. The vertical lines correspond to peaks in the HiTIES integrated H β brightness. The SI12 data do not extend to the end of the interval.

diffuse precipitation, caused by pitch-angle scattering. The two thin arcs on these boundaries are found to be related to an increase in number flux (and thus increased energy flux) without an increase in energy. Figure 16 compares height profiles of the EISCAT electron density for the time interval around one arc, with the corresponding modelled electron density.

H. Dahlgren et al., “Energy and flux variations across thin auroral arcs”, *Ann. Geophys.* 29, 1699–1712, doi:10.5194/angeo-29-1699-2011, 2011.

A statistical investigation of the Cowling channel efficiency in the auroral zone

During the late evening and night of 14 September 2004, the nightside auroral oval shows a distinct double-oval configuration for several hours after substorm onset, observed by the IMAGE satellite as well as the MIRACLE network. During the recovery phase of the substorm, an auroral streamer is detected by these instruments and the EISCAT radar, while simultaneously the Cluster satellites observe a bursty bulk flow in the conjugate portion of the plasma sheet in the magnetotail. The present combined data analysis reveals significant differences between the ionospheric equivalent current signature of this streamer (Figure 17) within a double-oval configuration, as compared

to previously studied streamer events without such a configuration. These differences are attributed to the presence of an additional poleward polarisation electric field between the poleward and the equatorward portions of the double oval, and simple model shows that such an assumption can conceptually explain the observations. Further, an estimation was made of the total current transferred in meridional direction by this recovery phase streamer to be ≈ 80 kA, significantly less than for previously analysed expansion phase streamer events. Both results indicate that the development of auroral streamers depends on the ambient background conditions in the magnetosphere-ionosphere system. The auroral streamer event studied was simultaneously observed in the conjugate Northern and Southern Hemisphere ionosphere.

O. Amm, et al., “A statistical investigation of the Cowling channel efficiency in the auroral zone”, *J. Geophys. Res.* 116, A02304, doi:10.1029/2010JA015988, 2011.

Dynamics and characteristics of black aurora as observed by high resolution ground-based imagers and radar

Archer et al. (2011) used ESR measurements, together with high-resolution multi-spectral data from the ASK imager, to study the fine struc-

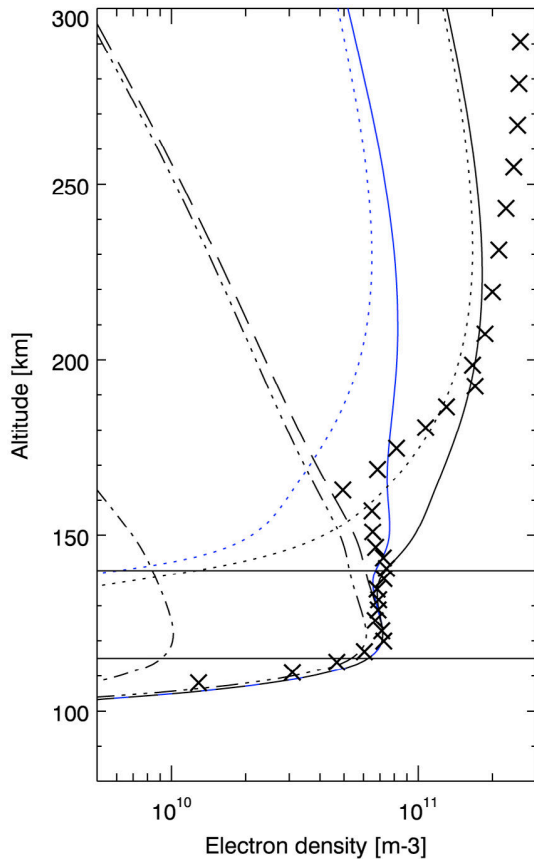


Figure 14: Measured (crosses) and modeled ESR electron densities at the time of the peak ionisation at 04:00 UT. Model electron precipitation (dotted lines) is shown for two different peak input energy fluxes of 0.5 mW m^{-2} (blue) and 3.0 mW m^{-2} (black). Other contributions are protonoelectrons (dash-dotted line), protoionisation (dash-triple dotted line) and total proton ionisation (long-dashed line). The solid lines correspond to total modelled electron densities.

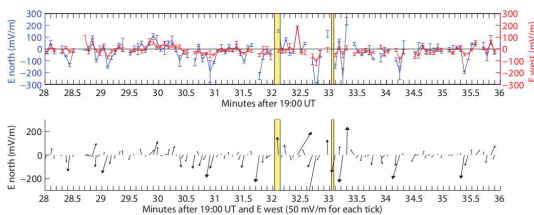


Figure 15: Top: north and west components of the derived electric field from EISCAT, as a function of time. Bottom: direction and amplitude of the electric field vector at each instant of time.

ture of “black aurora”, the dark lanes or patches between regions of bright emission. Sixteen events were analysed, corresponding to sheared and un-sheared black arcs, as well as black patches and

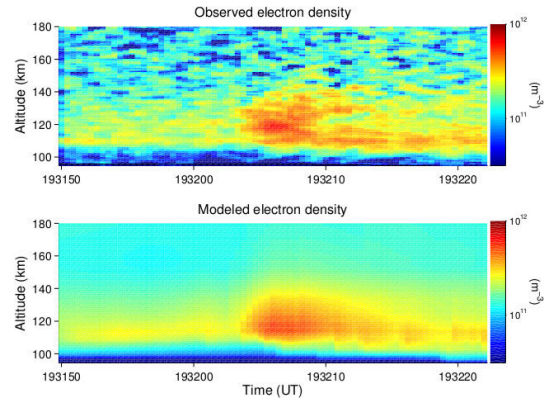


Figure 16: Top: electron density profiles from EISCAT measurements, for the 1932 arc. Bottom: corresponding modelled electron density. The bite-out in the data at 19:32:10 UT is not reproduced by the model, and is believed to be caused by horizontal convection of plasma near the arc.

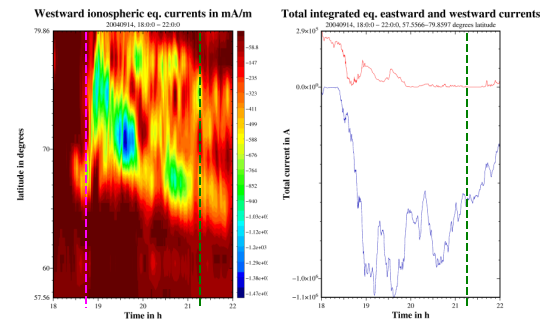


Figure 17: Keogram-style overview of ionospheric equivalent current development during the substorm within which the bursty bulk flow (BBF) event occurred (green dashed line). Left panel: westward component of ionospheric equivalent currents as a function of geographic latitude and time (substorm onset marked red dashed line); right panel: total meridionally integrated westward (blue) and eastward (red) currents as a function of time, in A.

rings. By relating the observed auroral structures to measurements of particle energy, Archer et al. were able to test different theories of how “black auroras” are created. They reported that the large reduction in high-energy precipitation observed in conjunction with the observation of black aurora favoured a model in which the dark patches correspond to regions where the highest energy particles are blocked by magnetospheric processes from entering the precipitation loss cone.

J. Archer, et al., “Dynamics and characteristics of black aurora as observed by high resolution ground-based im-

Polar mesospheric summer echoes

Evidence of isotropic scattering from PMSE

In an EISCAT campaign in the summer of 2011, the Kiruna EISCAT_3D Demonstrator Array was employed to make measurements of Polar Mesospheric Summer Echoes (PMSE). The demonstrator is a small array of yagi antennas connected to a digital receiver. It was built to make tests of EISCAT_3D software and hardware. It operates at the EISCAT VHF frequency (224 MHz) and its beam intersects the VHF beam at a point on the vertical above the VHF radar. The initial tests were made with the intersection point in the F-region. Shortly before the summer in 2011 the intersection was changed to the D-region. It was a surprise to discover that the demonstrator measured strong signals coming from PMSE above Tromsø when it was illuminated by the VHF radar, as shown in Figure 18, since the scattering angle is quite large, that is $\theta = 69^\circ$.

It is believed that the cause of PMSE is turbulence of the neutral atmosphere that couples to the ionised part of it via collisions. A decisive role is played by large (radius 10 nm to 50 nm) charged ice particles (a dusty plasma) that prolongs the inertial regime of turbulence such that electron irregularities may exist with scale sizes that meet the Bragg condition for scattering. Thus, the radar measurements function as a tracer of plasma and neutral turbulence. These Kiruna measurements of an absence of aspect sensitivity of the PMSE echoes show that this turbulence is nearly isotropic which agrees with Kolmogorov's hypothesis that regardless of the anisotropy of the turbulence at large scales, the cascading of energy to the inertial subrange is such that in this regime the turbulence becomes isotropic (and homogeneous). It is to be noted that there have been in the past numerous measurements of aspect sensitivity of PMSE, none of them having reported such large scattering angles. To our knowledge, these measurements have been made in monostatic mode, that is, by tilting the transmitting/receiving antenna off vertical and measuring the decrease of the scattered power. Typically, these measure-

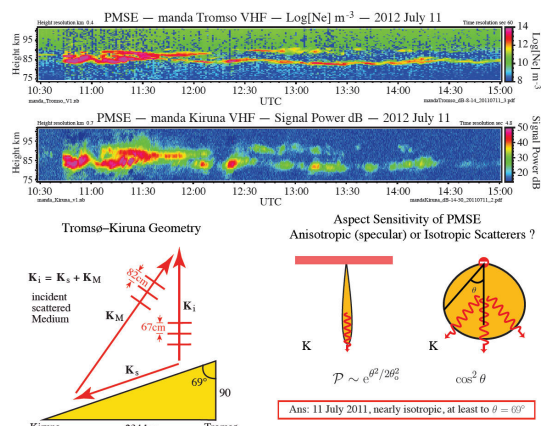


Figure 18: The top two panels show measurements of scattered power of PMSE from Tromsø and Kiruna respectively. The lower left panel shows a schematic of the T-K bistatic geometry. The cartoon on the lower right panel illustrates the geometry of anisotropic and isotropic scattering. The observed large scattering angle from Kiruna (69°) is an indication of isotropic scattering, meaning that the irregularities of electron density that cause the scattering have nearly isotropic distributions. It was surmised that Komogorov's hypothesis that turbulence becomes isotropic (and homogeneous) at the scale sizes of the inertial regime is valid for turbulence in the polar mesosphere.

ments result in 10° to 20° as the angle at which the signal vanishes.

C. La Hoz, H. Pinedo and O. Havnes, "Aspect sensitivity of PMSE observed at large scattering angles by the EISCAT radar", to be submitted.

PMSE research highlights from German EISCAT users

The EISCAT users in Germany (especially in Leibniz-Institute of Atmospheric Physics (IAP)) have been involved in several research activities in the frame of CAWSES priority program, eg. the investigation of frequency dependence of polar mesosphere summer echoes (PMSE) using simultaneous and common-volume measurements. The available experimental record impressively demonstrates that the radar volume reflectivity of PMSE (that is the scattering cross section per unit volume) reveals a tremendous frequency dependence such that simultaneous and common-volume observations at two different frequencies should be an ideal tool for studying the validity of theoretical expectations. Along this line, systematic studies of PMSE were carried out based on the

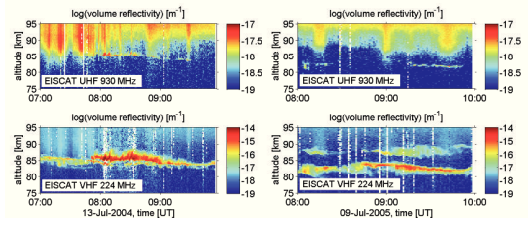


Figure 19: Volume reflectivity obtained with the EISCAT UHF radar at 930 MHz (upper panels) and the EISCAT VHF radar at 224 MHz (low panels) on 13 July 2004 (left column) and 9 July 2005 (right column), respectively. The heating parts were removed before being integrated into 1 min. Blanks in both panels indicate times where meteor echoes were removed.

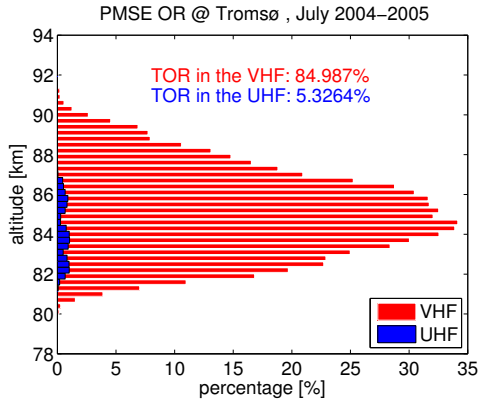


Figure 20: Comparison of PMSE occurrence rate at 930 MHz (in blue) and 224 MHz (in red) respectively derived from the EISCAT UHF and VHF observations in July 2004 and 2005. The total occurrence rates are indicated in the insert.

analysis of simultaneous and common-volume observations of PMSE with the ESR and SSR as well as with the EISCAT VHF and UHF radar, respectively, to study the statistical properties of PMSE at frequencies more than the “standard” frequency of 50 MHz, to derive microphysical parameters of the involved ice particles, and to discern the coherent scattering mechanism of PMSE at two different frequencies. The corresponding important results have been presented and published whilst there are also a number of EISCAT highlights reported in the previous Annual Report Germany.

In Figure 19 two typical examples are presented of simultaneous PMSE observed with the EISCAT VHF and UHF radars on July 13th 2004 and July 9th 2005, respectively. It is noted that pronounced echoes were simultaneously observed by both radars for a quite long duration. The VHF-echoes, however, generally extend over a larger

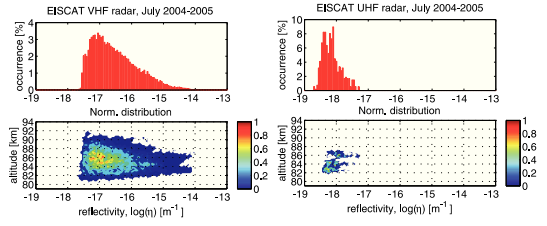


Figure 21: Relative occurrence of reflectivities (upper panels) and normalised distribution of the reflectivities along the altitudes (lower panels) obtained with EISCAT VHF radar (left panels) and EISCAT UHF radar (right panels) in July 2004–2005.

altitude range than the UHF-echoes and show more variations in the morphology (sometimes appearing with double-layer or even multi-layer structures), whereas the UHF-echoes appear intermittently as a very thin layer. In order to statistically demonstrate the difference between the VHF- and UHF-PMSE, next a comparison is made between PMSE at both frequencies in terms of occurrence rate and volume reflectivity, η . Making use of the observations in July 2004 and 2005 with the EISCAT VHF and UHF radars, the derived altitude profiles are presented of the occurrence rates of PMSE at both frequencies in Figure 20. UHF-PMSE show much smaller occurrence rates than VHF-PMSE and UHF-PMSE were observed in a considerably narrower altitude range, i.e., from 81 km to 87 km. Furthermore, the volume reflectivities of PMSE observations are compared at both frequencies. Histograms of η , as well as corresponding altitude-resolved distributions, are presented in Figure 21. η -values obtained from the EISCAT VHF and UHF observations fall within the range from $1.35 \times 10^{-18} \text{ m}^{-1}$ to $1.58 \times 10^{-14} \text{ m}^{-1}$ with the maximum around 10^{-17} m^{-1} and from $1.95 \times 10^{-19} \text{ m}^{-1}$ to $7.01 \times 10^{-18} \text{ m}^{-1}$ with the maximum smaller than 10^{-18} m^{-1} , respectively. Focusing on the lower panels, it is stressed that there are two patches in the distribution of the UHF PMSE which are consistent with corresponding maxima of the η -distribution for VHF-PMSE around 86 km and from 82 km to 84 km.

Besides the previous analysis of PMSE, another exercise was to study the influence of the involved ice particles in PMSE on ambient electron densities with the simultaneous observations with the EISCAT VHF and UHF radars. It is common belief that the occurrence of PMSE is closely connected to the presence of ice particles which become negatively charged due to electron attachment and

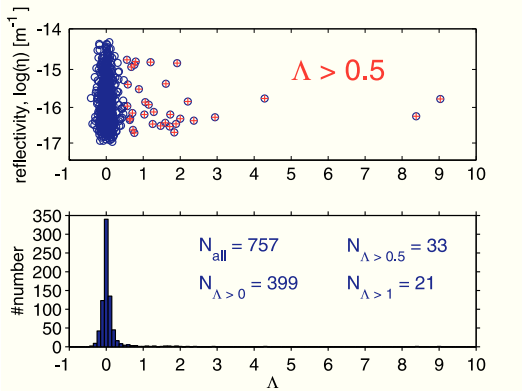


Figure 22: Upper panel: Scatter plot of the derived Λ values from the UHF observations against the corresponding volume reflectivities of the VHF PMSE (Λ with values larger than 0.5 are marked with red crosses); Lower panel: Histogram of Λ with the number of Λ in the different ranges indicated in the insert.

hence effectively scavenge electrons. This process occasionally leads to large electron density depletions which have also been called “biteouts”. The EISCAT radars are both incoherent scatter (IS) radars and archive measurements from a superposition of coherent scatter from PMSE and incoherent scatter from ambient plasma in the ionospheric D-region (i.e., at altitudes below ~ 95 km). Due to the frequency dependence of PMSE mentioned above, the VHF radar observes PMSE much more frequently than the UHF radar. Given a sufficiently large electron density, however, the UHF observations may be dominated by incoherent scatter from the D-region electrons such that they can be used to infer electron densities in the presence of PMSE simultaneously observed with the VHF radar. This analysis has been applied to all 25 h of simultaneous observations and derived 757 Λ -values from the UHF observations in the presence of VHF PMSE. Here Λ is the ratio between the charge number density of ice particle and free electron number densities. That $\Lambda = 1$, for example, means there are 50% of electrons attached on ice particles and 50% of free electrons left. The lower panel of Figure 22 presents the distribution of the derived Λ -values. For the large majority of cases (699 cases), the Λ values are within the range from -0.3 to 0.3 which can be considered close to 0 and hence no strong electron biteouts are observed. Please note that the occurrence of negative Λ -values simply reveals the imperfection of our algorithm to determine the undisturbed electron density and may hence be

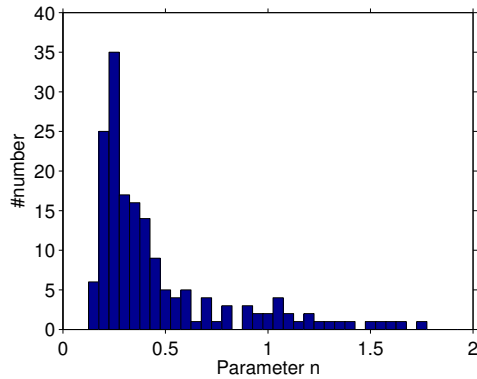


Figure 23: Distribution of parameter n derived from the UHF-observations in the presence of PMSE observed with the EISCAT VHF radar. For large majority of cases, $n < 1$ indicative of the presence of charged ice particles and no UHF-PMSE.

considered as a systematic error of our analysis. This means that the quoted Λ -values should be considered to have error bars of ± 0.3 because of this effect. Nevertheless, this method still allows to quantify depletions with Λ -values larger than say 0.5. From 757 cases, there are only 33 cases with $\Lambda > 0.5$ marked with red crosses in the upper panel (21 cases with $\Lambda > 1$), i.e., only 4.4% of all the observations.

In addition, the upper panel of Figure 22 reveals that the distribution of Λ -values versus the volume reflectivities of VHF PMSE shows no obvious correlation between them. This is, however, expected: According to the turbulence with large Schmidt number theory (TWLS-theory) of PMSE, the volume reflectivity of PMSE is most strongly controlled by the Schmidt number which can change the volume reflectivity at given wavenumber k by many orders of magnitude whereas the dependence on Λ is much less pronounced.

Before any final conclusions can be drawn on the statistical distribution of Λ , it should be noted that the UHF observations could be a superposition of incoherent scatter from the disturbed electron densities and coherent scatter from the UHF PMSE which, however, does not stand well out of the ambient incoherent scatter from the ionospheric plasma. Next the spectral shapes are checked of corresponding auto-correlation functions (ACF) in order to find out whether such cases of superposition do frequently occur and create a bias in the data. The expression of the ACF magnitude is approximated as:

$$\text{ACF}(\tau) = \text{ACF}_{\tau=0} \cdot \exp\{-\tau/\tau_e\} \quad (1)$$

Here n is an exponent to describe the shape of the spectrum. That is, $n = 1$ and $n = 2$ represent a Lorentzian (=pure incoherent scatter) and a Gaussian (=coherent scatter), respectively, whereas $n < 1$ marks the cases with the presence of charged ice particles. According to the above discussion, there should be two possibilities for the spectral shapes derived from the simultaneous observations with both radars when the VHF radar observed pronounced PMSE and the UHF observations show an apparently undisturbed electron density profile. I.e., the parameter n should be close to 2 for the VHF observations whereas it should either also be close to 2 for the cases in the presence of UHF PMSE or smaller than 1 in the presence of charged ice particles (and pure incoherent scatter). This analysis was applied to all the observations. The corresponding results of the derived parameters n (for UHF-observations at altitudes with VHF-PMSE) is shown in Figure 23. The parameter n shows that large majority of cases with values smaller than 1, which indicates that there are charged ice particles present in the vicinity of VHF PMSE but no PMSE were observed with the EISCAT UHF radar. This finding confirms that the distribution of Λ -values is not biased by a superposition of coherent and incoherent scatter. In addition, this result underlines the importance of the presence of charged ice particles for the generation of PMSE and demonstrates that small relative concentrations of charged ice particles are sufficient to create these very strong coherent echoes.

N. Engler and M. Rapp, "Analysis of spectral parameters of polar mesosphere winter echoes using the EISCAT VHF radar", 15th International EISCAT Workshop, Qingdao, China, 5–9 September, 2011 (talk).

Q. Li and M. Rapp, "EISCAT radars: Potentials to study the properties of PMSE and the ambient environment", 15th International EISCAT Workshop, Qingdao, China, 5–9 September, 2011 (talk).

Q. Li and M. Rapp, "PMSE-observations with the EISCAT VHF and UHF-Radars: Statistical properties", *J. Atmos. Sol. Terr. Phys.* 73(9), 944–956, doi:10.1016/j.jastp.2010.05.015, 2011.

Q. Li, "Multi-frequency radar observations of polar mesosphere summer echoes: Statistical properties and microphysical results", Ph.D. thesis, University of Rostock, Germany, 2011.

J. Kieser, "The influence of precipitating solar and magnetospheric energetic charged particles on the entire atmosphere: Simulations with HOMMONIA", Ph.D. thesis, University of Hamburg, Germany, 2011.

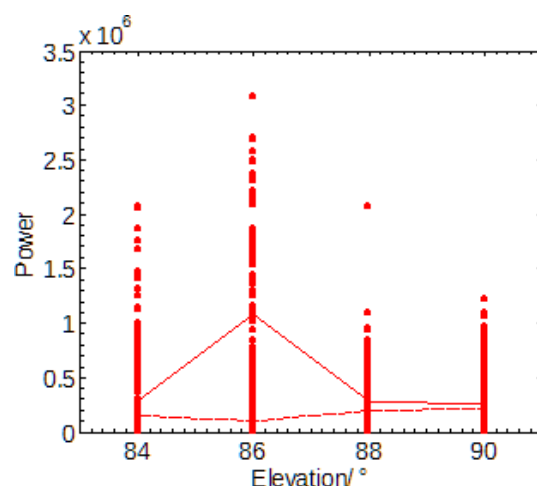


Figure 24: The measured PMSE return power at different elevations of the EISCAT VHF radar.

M. Rapp et al., "Localized mesosphere-stratosphere-troposphere radar echoes from the E region at 69°N: Properties and physical mechanisms", *J. Geophys. Res.*, 116, A02320, doi: 10.1029/2010JA016167, 2011.

EISCAT VHF measurements of aspect sensitivity in the vicinity of polar mesospheric summer echoes

The aspect sensitivity describes the radar signal dependence when the beam is tilted from the vertical direction. The Chinese campaign in July 2010 shows that the echo power is varying at different elevations as indicated in Figure 24. The strongest echoes do not lie in the vertical direction, which show that the turbulence theory used to explain PMSE may be not an optimum tool.

In addition, PMSE observation on 13 July, 2010 shows a double layer as indicated by Figure 25 (top). Figure 25 (bottom) indicates that the top layer shows the decreasing echo power with the offset from vertical, and the bottom layer does not show an obvious aspect sensitivity, which is very different from results obtained before.

Li Hailong et al., "VHF radar measurements of aspect sensitivity in the vicinity of polar mesosphere summer echoes during Chinese campaign", 15th International EISCAT Workshop, Qingdao China, September 2011.

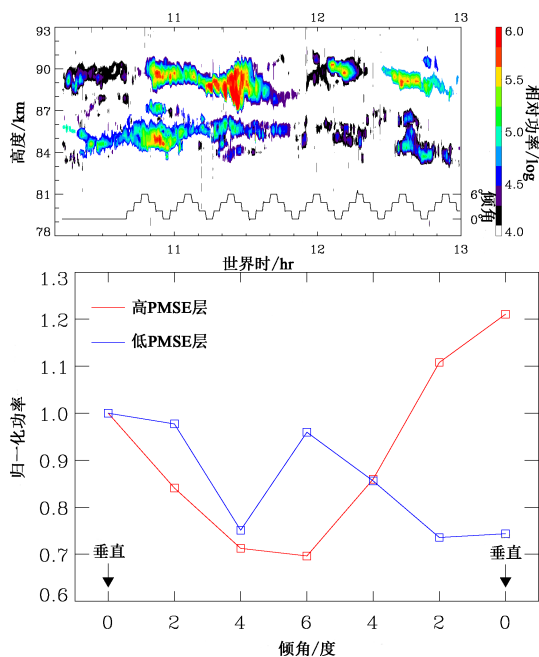


Figure 25: PMSE measured by EISCAT VHF radar. Top panel: The two layers of the PMSE. Bottom panel: Echo power from the PMSE as function of offset from the vertical. The top layer is shown in red and the bottom layer in blue. The arrows indicate vertical.

Majority of PMSE spectral widths at UHF and VHF are compatible with a single scattering mechanism

Motivated by a recent controversy in the literature about the agreement or disagreement of spectral widths (after conversion to Doppler-velocities) of PMSE observed simultaneously with the EISCAT VHF and UHF radars in Tromsø, Norway, this issue was reconsidered taking into account a much larger data set than in any of the previous studies. While these previous studies only considered case studies of a few minutes in length, this study considered a total of 380 min of simultaneous and common volume observations with these two radars at a time resolution of 30 s, i.e., a total of 760 samples. This study is important to discern whether PMSE at these two frequencies originate from the same coherent scattering mechanism or if different physical mechanisms are at work.

It was found that the VHF spectra are on average well described by a Gauss shape (with spectral parameter $n = 2$ — which is derived from a generalised formulation of the autocorrelation func-

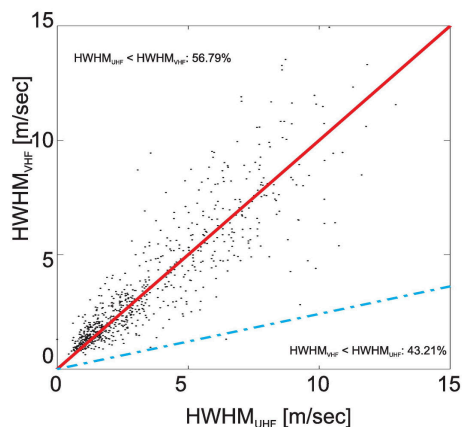


Figure 26: Half width at half maximum measured simultaneously by UHF and VHF radar. Red solid line shows 1 : 1 slope. Blue dash-dotted line shows the relationship of two spectral widths in the case of incoherent scattering mechanism.

tion), whereas the UHF-spectra show a small deviation from this shape with an average n of 1.6.

In Figure 26 a scatter plot is shown of spectral widths derived from the simultaneous VHF- and UHF-observations described above. The 1 : 1 slope marked by the red solid line shows values where the spectral widths derived from the VHF observations (ordinate) equal those ones derived from the UHF measurements (abscissa). Figure 26 demonstrates that most data have spectral widths which are very close at both frequencies with only weak scattering around equality (red line). Spectral widths do largely agree but show a small systematic difference, i.e., the UHF spectra are on average 0.1 m s^{-1} narrower than the VHF spectra at an average spectral width of 3.5 m s^{-1} . This small systematic effect is largely explained considering the overall effect of beam-, shear-, and wavebroadening. This means that the slightly different beam widths of the VHF and UHF-radars and the hence slightly different observing volumes account for the small systematic difference in mean spectral width.

Finally, it was demonstrated that the small deviation of UHF-spectra from a perfect Gauss shape can be either due to relatively small signal-to-noise ratios of the UHF-data and/or a superposition of incoherent and coherent scatter in cases where both contributions add equally to the total observed power. Since VHF PMSE are much more stronger than the incoherent scatter background this effect can not be recognized in VHF observations. This superposition effect may occasion-

ally also lead to larger deviations between VHF and UHF spectra in that it can potentially narrow the UHF-spectra significantly. However, excluding these rather rare and exotic cases, it was concluded that the majority of the observations are compatible with a single coherent scattering at both VHF and UHF.

I. Strelnikova and M. Rapp, "Majority of PMSE spectral widths at UHF and VHF are compatible with a single scattering mechanism", *J. Atmos. Sol. Terr. Phys.* 73, 2142–2152, doi:10.1016/j.jastp.2010.11.025, 2011.

Dusty space plasma diagnosis using temporal behavior of polar mesospheric summer echoes during active modification

Mahmoudian et al. (2011) studied the different behaviour of Polar Mesospheric Summer Echoes during EISCAT heating experiments, in an attempt to diagnose the variations in parameters such as electron temperature enhancement during heating, dust density, dust charge polarity, ion-neutral collision frequency, electron density and dust radius, from the different ways that the layers behaved as the Heater was turned off and on (Figure 27). They produced a model which predicted the results of PMSE modulation experiments at a range of different frequencies (7.9 MHz, 56 MHz, 139 MHz, 224 MHz and 930 MHz) corresponding to the existing radar facilities, and compared this with observations in order to obtain the dust parameters.

A. Mahmoudian, et al., "Dusty space plasma diagnosis using temporal behavior of polar mesospheric summer echoes during active modification", *Ann. Geophys.* 29, 2169-2179, 2011.

Statistical survey of electron temperature enhancements in heater modulated polar mesospheric summer echoes

Routledge et al. (2011) presented a statistical analysis of 26 PMSE modulation experiments (Figure 28), conducted between 2002 and 2007, using a model to estimate the enhancement of D region electron temperature caused by the heating, showing that the modulation of the PMSE layer for a fixed electron temperature enhancement is essentially independent of height. They also studied a number of cases (Figure 29) in which the heating experiment failed to achieve any modulation

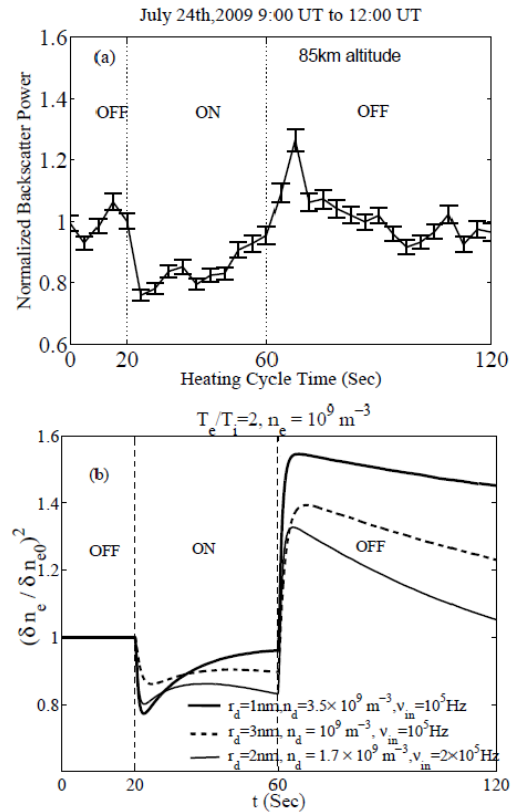


Figure 27: A comparison of VHF radar superposed epoch data during radiowave heating and results from the computational model. Panel (a) shows the superposed epoch of PMSE VHF backscatter power, and panel (b) the computational model result.

of the PMSE layer, and showed that, in those cases, the atmospheric attenuation of the HF heater wave was too great for it to have any effect on the PMSE layer.

G. Routledge, et al., "A statistical survey of electron temperature enhancements in heater modulated polar mesospheric summer echoes at EISCAT", *J. Atmos. Sol. Terr. Phys.* 73, 4, 472-482, doi:10.1016/j.jastp.2010.11.004, 2011.

Active experiments

Temporal development of the magnetic zenith effect

Honary et al. (2011) made an experimental study of the "magnetic zenith effect", a time-dependent phenomenon observed when the ionosphere is heated by high-power electromagnetic waves. It

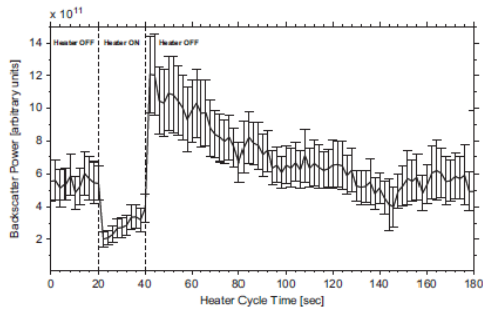


Figure 28: Superposed epoch analysis of PMSE backscatter intensity variations due to HF pumping on 15/07/2004. The dashed vertical lines represent the boundaries between the HF pump ON/OFF cycle. The vertical error bars represent the standard error of the backscatter power and account for the variation in backscatter power from cycle to cycle.

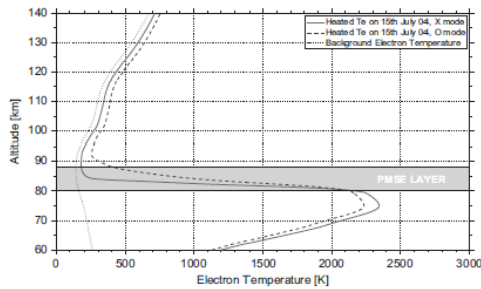


Figure 29: Modelled profile of enhanced electron temperature for the successful PMSE modulation experiment of 15/07/2004. The grey band from 80 km to 88 km denotes the altitude span of the PMSE layer. For this particular experiment, X-mode modulation was used and its predicted temperature enhancement is shown as the solid curve. The dashed curve represents the predicted temperature effect had O-mode heating been used on this occasion. The dotted curve represents the background electron temperature for this day.

is known that, during the first few seconds after heating, the strongest electron density irregularities and the greatest enhancements in electron temperature appear to migrate towards the magnetic zenith direction. Honary et al. showed that the time taken for the electron temperature to reach a stable state is between 5 s and 10 s, which is consistent with the growth time of electron density irregularities in the heated region, with transverse sizes on the order of several metres. The authors demonstrated that, when heating occurred in the direction of the magnetic field, as opposed to vertically, the resulting electron temperature enhance-

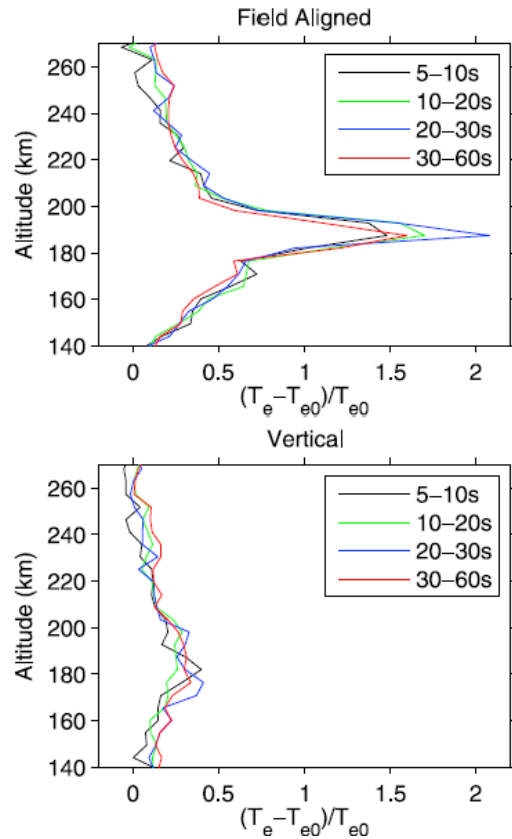


Figure 30: The relative increase in electron temperature during heating. (top panel) Both radar and heater in the field-aligned direction. (bottom panel) Radar and heater both vertical.

ments were greater by at least a factor of two (Figure 30). They also found a new position, between the magnetic zenith and the Spitz angle, where the heating effect appears to maximize, leading them to propose a new explanation of the magnetic zenith effect, in which Upper Hybrid Resonance modes can be trapped in plasma striations, localised above the level where the plasma frequency coincides with the frequency of the heater pump wave, within a region which is 2° to 3° in width (Figure 30). The increase of the electron temperature in striations is known to take place very rapidly, hence explaining the rapid dynamics of the magnetic zenith effect. This new theory also appears to explain recent heating and airglow observations reported at HAARP.

F. Honary, et al., "Temporal development of the magnetic zenith effect", *J. Geophys. Res.* 116, A06309, doi:10.1029/2010JA016029, 2011.

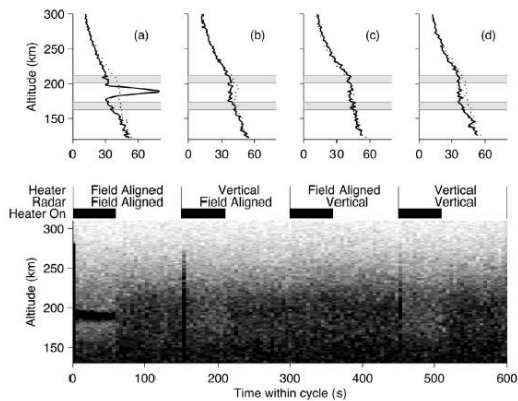


Figure 31: (top panel) Altitude profiles of power (12 μ s lag profile in arbitrary units), averaged over multiple heater cycles, and over each of the different heater and radar beam configurations: (a) both heater and radar beams are field aligned, (b) heater beam is vertical and radar beam is directed toward the local magnetic field, (c) heater beam is field aligned and the radar beam is in vertical position, and finally, (d) heater and radar beams are both vertical. Solid lines are heater-on measurements, and dotted lines are heater-off. The shaded regions show range gates that are not contaminated (162.8 km to 173.6 km and 200.7 km to 211.5 km) which are used for the measurement of electron temperatures. (bottom panel) The complete set of 12 μ s lag profiles, averaged over the cycles.

EISCAT incoherent scatter radar measurements of artificial ionospheric modification at sub-ms time scales

Efficient generation of ELF/VLF waves through the modulation of ionospheric currents requires reliable measurements of the modulated current for different heater parameters. Incoherent scatter radar (ISR) measurements of modified plasma densities/temperatures would be ideal in quantifying the heating and cooling cycles in response to modulated heating by high-power HF waves. Considering the ms time scales of ELF/VLF generation processes, it is necessary to resolve the heating and cooling cycles at sub-ms time scales. Such measurements using ISRs have largely been avoided due to the common knowledge that the instrument requires minutes of integration.

Results are presented of an epoch averaging experiment using EISCAT that provides 0.2 ms resolution ISR power measurements as a function of phase into the HF heater ON and OFF cycle. In ELF/VLF generation, it is the electron temperature (T_e) modulation that results in the modulation

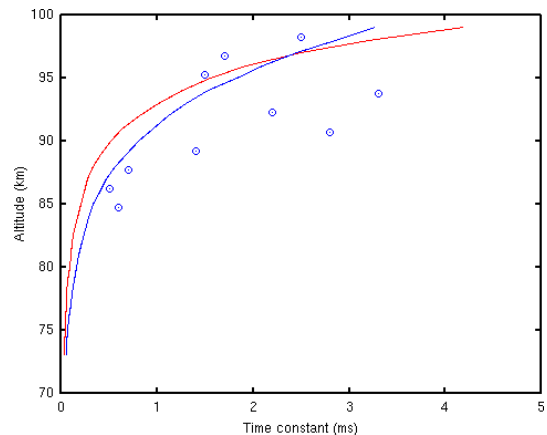


Figure 32: EISCAT measurements of electron cooling time constants (circles) compared to theoretical values computed from Banks (red line) and Wait and Spies (blue line).

of electron collision frequency/mobility and therefore the electrojet modulation. Assuming a reliable electron collision frequency for transport as a function of T_e , it is necessary to measure T_e and electron density (N_e) simultaneously to predict the ionospheric current modulation. This is possible if two incoherent scatter radars operating at sufficiently different frequencies are used and if the Debye length and Bragg wavelengths are comparable.

For the experiment results presented here, the ionospheric volume modified by the EISCAT heater were probed by both EISCAT UHF and VHF incoherent scatter radars operating at 0.16 m and 0.67 m Bragg wavelengths. Considering $N_e = 10^9 \text{ m}^{-3}$ in the D region ionosphere, for electron temperature $T_e = 300 \text{ K}$, the Debye length is 0.38 m, where as for $T_e = 1000 \text{ K}$ the Debye length is 0.69 m; these parameters are reasonably appropriate to extract T_e/N_e from simultaneous UHF/VHF data.

ISR power modulation was successfully detected both in the E and F region heated ionosphere. The findings are as follows:

1. D region ISR spectral broadenings are identified as evidence of plasma heating from 100 km down to 75 km altitude.
2. During the 1.4 ms ON and 1.4 ms OFF heating cycle at 4 MHz X mode, D region modulations of ISR power were successfully detected (Figure 32), with the modulations never recovering to the non-heated state. This implies a time-scale for heating/cooling greater than several ms or longer.

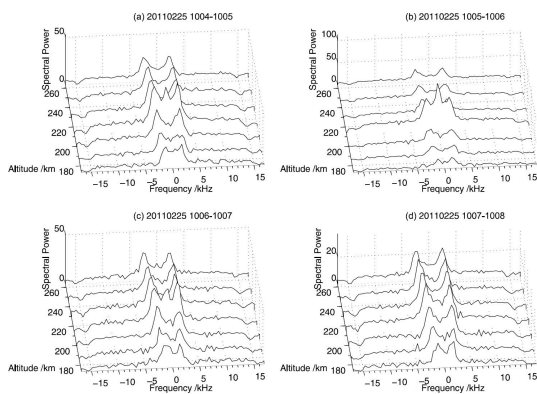


Figure 33: Ion line spectra at altitudes from 170 km to 270 km from data that have been post-integrated to one minute during the SPEAR heater-ON period between 10:04 and 10:08 UT on 25 February 2011.

3. In the F region, the time scale of the development of plasma turbulence is measured to be near 0.3 ms, and the decay is around 0.2 ms.

In addition, are working on inferring T_e and N_e profiles by combining UHF and VHF radar measurements.

H. Bahcivan and M. Nicolls, “EISCAT incoherent scatter radar measurements of artificial ionospheric modification at sub-ms time scales”, AGU fall meeting, San Francisco, USA, 2011.

Alternative estimation of the RF-enhanced plasma temperature during SPEAR experiments

Vickers and Baddeley (2011) investigated the apparent lack of electron temperature enhancements as seen in ESR data during HF heating by SPEAR (Figure 33). They showed that contamination of the incoherent scatter spectrum by the Purely Growing Mode (PGM) of plasma instability can make the realistic estimation of temperatures very difficult, especially because PGM signatures can be very persistent. Using a recently developed method to remove the PGM signatures from the measured incoherent scatter spectra, Vickers and Baddeley were able to demonstrate that the corrected measurements produced temperatures in good agreement with theory, ranging from a few tens to a few hundreds of Kelvin above background level, once effects such as absorption had been accounted for (Figure 34).

H. M. S. Vickers, and L. J. Baddeley, “An alternative estimation of the RF-enhanced plasma

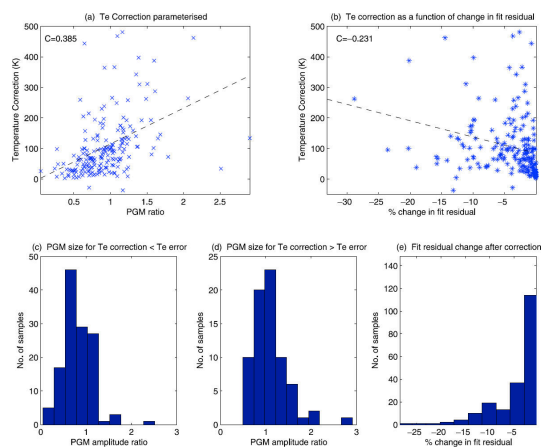


Figure 34: (a) The temperature correction (corrected temperature—uncorrected temperature) shown as a function of PGM amplitude ratio, defined as the PGM amplitude divided by the mean of the up-shifted and down-shifted ion line amplitudes. The scatterplot uses results from one minute integrated data, taken from ~ 70 SPEAR-on periods in 2004, during campaigns in April, September/October and December. The strength of the correlation between the two parameters assumes a linear fit of 0.385. The best linear fit is shown by the dashed black line. (b) The relationship between the temperature correction and the percentage change in the GUISDAP fit residual, calculated using the residual values from fits made to the uncorrected and corrected spectra, using the same data set as in panel (a). Again, the best linear fit is indicated by the dashed black line, and the correlation between the two parameters is only -0.231. Histograms of the PGM amplitude ratio for samples where the temperature correction was (c) less, or (d) greater, than the uncorrected electron temperature error. (e) The percentage change in fit residual is represented as a histogram, which shows that the majority of samples (85%) experienced a reduction in the fit residual which was less than 10%.

temperature during SPEAR artificial heating experiments: Early results”, *J. Geophys. Res.* 116, A11323, doi:10.1029/2011JA016795, 2011.

Scientific highlights from Russian EISCAT users

Two HF heating campaigns were held by the Arctic and Antarctic Research Institute (Russia) in March and October 2011. The main attention was paid to plasma modifications induced by X-mode powerful HF radio waves injected towards the magnetic zenith into the high latitude F region of the ionosphere. The EISCAT HF heating fa-

cility, located near Tromsø in Northern Norway (geographical coordinates 69.6° N, 19.2° E; magnetic dip angle $I = 78^\circ$) was used to modify the ionosphere in the high-latitude F region. The heating facility operated at 5.423 MHz, 6.2 MHz, 6.77 MHz, 7.1 MHz and 7.9 MHz, with X-mode polarization, and with 10 min continuous HF pulses. The phased array 1, with the width of the HF antenna beam of about 7° , was used in October 2011, resulting in an effective radiated power (ERP) of 520 MW to 1100 MW. The HF heater antenna beam was tilted 12° to the south of zenith, thus allowing HF pumping in the field-aligned direction (magnetic zenith, MZ).

The HF heating facility at Tromsø is located adjacent to the EISCAT UHF incoherent radar which operates at a frequency of 930 MHz. During the experiments the UHF radar measured the ionospheric plasma parameters, such as the electron density and temperature (N_e and T_e), the ion temperature (T_i), and the ion velocity (V_i), in the altitude range from 90 km to 600 km mostly in the direction of the magnetic zenith. Ionograms were taken every four minutes using the EISCAT dynasonde, which is co-located with both the EISCAT UHF and heater array at Tromsø.

The results obtained in the course of experiments for the first time clearly demonstrate that the X-mode HF pump wave with high effective radiated power of 520 MW to 1100 MW can generate very strong electron density enhancements in the field-aligned direction (artificial ducts) in the high-latitude F-region ionosphere when the heater frequency is above f_{oF2} .

Table 1 describes the heater and ionosphere parameters for the experiments on 7, 8, 10, 11, and 12 October 2011 during which the ionosphere was modified by X-mode HF pump waves. In all events listed in Table 1, extremely strong electron density enhancements ($\sim 60\%$ to 70%) in a wide altitude range up to the upper limit of the EISCAT UHF radar measurements (600 km) occurred. By way of illustration Figure 35 presents the altitude-temporal variations of N_e and T_e from the EISCAT UHF radar observations during HF heating experiment on 10 October 2011. The appearance of electron density enhancements in a wide altitude range was accompanied by increases in the electron temperature. In contrast to the N_e changes, the T_e increases took place in a limited altitude range (mainly from 200 km to 300 km).

During the first two heater-on periods from 14:20–14:30 and 14:35–14:45 UT the UHF radar was scanned between 90° and 78° (see Figure 35).

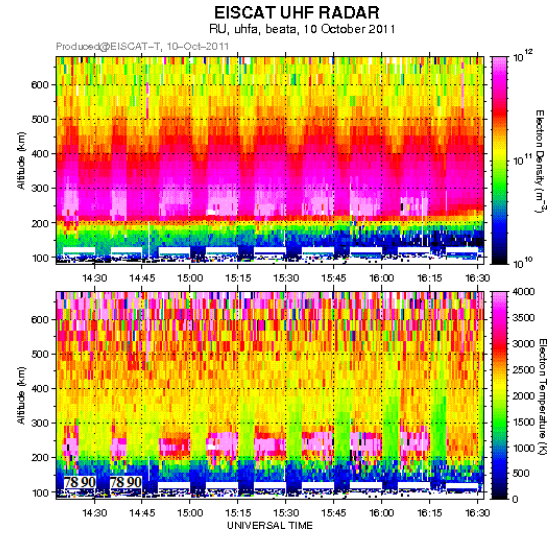


Figure 35: Altitude-temporal variations of N_e and T_e from the EISCAT UHF radar observations during HF heating experiment on 10 October 2011 from 14:20–16:30 UT. X-mode heater-on periods are marked in the time axis. UHF radar measured in the magnetic zenith (78°) in all heater-on cycles except for 14:20–14:30 and 14:35–14:45 UT cycles in which it was scanned between 78° and 90° . The duration of each position was of 5 min.

It was found, that the N_e and T_e enhancements were observed only in the magnetic field-aligned direction (78°). There were no changes in the vertical direction (90°). It was found that the frequency range, in which extremely strong N_e and T_e enhancements occurred under X-mode heating, lies in the interval of $f_H - f_{ce}/2 \leq f_{xF2} \leq f_H + f_{ce}/2$. Thus, the frequency range is bound above by the value of the extraordinary-mode critical frequency $f_{xF2max} = f_H + f_{ce}/2$ and below by $f_{xF2min} = f_H - f_{ce}/2$.

It has to be mentioned that the EISCAT UHF radar spectra during X-mode HF pumping demonstrate strongly heater-enhanced ion-acoustic and plasma lines, which are unusual for X-mode heating. These heater-enhanced ion and/or plasma line backscatter enhancements are typical signatures of parametric decay instability. Figure 36 shows plasma lines obtained from the EISCAT UHF radar data in the course of HF heating experiments, when the X-mode HF pump wave was radiated towards the MZ.

It is seen from Figure 36 that plasma lines were excited at the heater frequency of X-mode powerful HF radio wave injected towards the magnetic zenith. Remember that on 10 October 2011 (Figure 36, left panel) in the first two heater-on peri-

Table 1: List of the EISCAT Heating experiments when the strong N_e enhancements accompanied by the increased T_e occurred under X-mode heating of the F-region of the high latitude ionosphere with the use of the phased array 1.

| N | Date | Time of observations, UT | Total number of "ON" cycles | f_H , MHz | ERP, MHz | f_{oF2} , MHz |
|-----|----------|--------------------------|-----------------------------|-------------|----------|-----------------|
| 1 | 7.10.11 | 16:05–17:00 | 4 | 6.77 | 760 | 6.2–5.8 |
| 2 | 8.10.11 | 14:05–15:15 | 5 | 7.9 | 1100 | 7.0–6.5 |
| 3 | 10.10.11 | 14:20–16:30 | 9 | 7.1 | 940 | 7.1–5.7 |
| 4 | | 17:20–18:30 | 5 | 5.423 | 520 | 4.8–4.1 |
| 5 | 11.10.11 | 13:50–15:45 | 8 | 7.9 | 1100 | 7.7–6.7 |
| 6 | 12.10.11 | 14:50–15:15 | 2 | 7.9 | 1100 | 7.3–7.1 |
| 7 | | 15:20–16:30 | 5 | 7.1 | 940 | 7.1–5.7 |

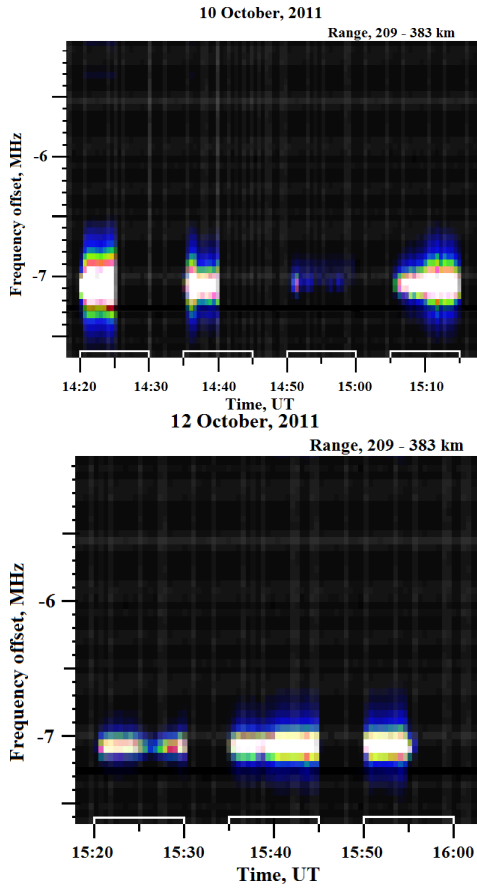


Figure 36: Plasma lines obtained from the EISCAT UHF radar data in the course of HF heating experiments, when the X-mode HF pump wave was radiated towards the MZ. Left panel: 10 October, 2011, $f_H=7.1$ MHz; Right panel: 12 October, 2011, $f_H=7.1$ MHz.

ods the UHF radar was scanned between 78° and 90° . Similar to the strong N_e enhancements (see Figure 35) plasma lines were excited only in the magnetic zenith.

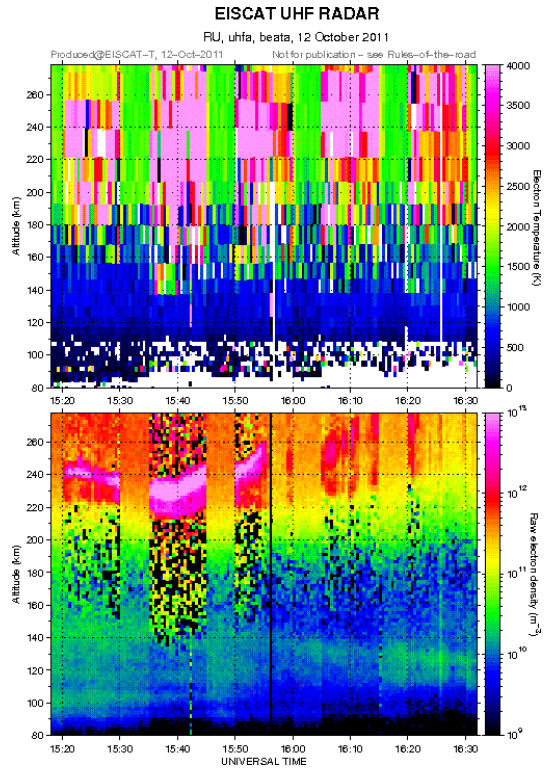


Figure 37: The altitude-temporal distribution of electron temperature and raw electron density for X-mode heating at $f_H=7.1$ MHz on 12 October, 2011. HF pump wave was radiated towards the magnetic zenith from 15:20 UT by 10 min on, 5 min off cycles.

Figure 37 depicts the altitude-temporal distribution of electron temperature and raw electron density for X-mode heating on 12 October, 2011.

The results, obtained from numerous X-mode HF pumping experiments in the high-latitude F region of the ionosphere, have shown an evidence of formation of artificial ducts with strongly en-

hanced electron density (up to 70%) in a wide altitude range up to the upper limit of the UHF radar measurements. The formation of artificial ducts is accompanied by the electron temperature increases, generation of small-scale artificial field-aligned irregularities, and heater-enhanced ion and/or plasma line backscatter enhancements. It was found that observed N_e enhancements under X-mode HF heating cannot be explained by temperature-dependent reaction rates. Enhanced production of ionization by accelerated electrons is an alternative mechanism for N_e increases induced by an X-mode heating. Fluxes of accelerated electrons can be produced by Langmuir turbulence. Taking into account that an X-mode wave can not produce the Langmuir waves, it is assumed that the X-mode may first be converted to the Z-mode, which can induce intense plasma turbulence above the X-mode reflection altitude. In addition to processes involving direct electrostatic conversion of the Z-mode wave, the Z-mode waves can be scattered by AFAs that, in turn, can also lead to the producing Langmuir turbulence.

N. F. Blagoveshchenskaya, et al., "Artificial small-scale field-aligned irregularities in the high latitude F region of the ionosphere induced by an X-mode HF heater wave", *Geophys. Res. Lett.* 38, doi: 10.1029/2011GL046724, 2011.

N. F. Blagoveshchenskaya, et al., "The effects of modification of a high-latitude ionosphere induced by high-power HF radio waves. 1. Results of multi-instrument ground-based observations", *Radiophysics & Quant. Electr.* 53, 512–531, 2011 (Engl. Transl.).

N. F. Blagoveshchenskaya, et al., "Modification of the high-latitude ionosphere by high-power HF radio waves. 2. Results of coordinated satellite and ground-based observations", *Radiophysics & Quant. Electr.* 54, 89–101, 2011 (Engl. Transl.).

T. D. Borisova, et al., "Characteristics of Pc4–5 pulsations obtained using the method of bistatic backscatter of HF radio waves, the EISCAT HF Heating facility, and ground-based magnetometers", *Geomagnetism and Aeronomy* 51, 620–632, 2011 (Engl. Transl.).

N. F. Blagoveshchenskaya, et al., "Results of Russian experiments dealing with the impact of powerful HF radio waves on the high latitude ionosphere using EISCAT facilities", *Geomagnetism and Aeronomy*, 51, 1109–1120, 2011 (Engl. Transl.).

Unusually broadened HF radar spectra from heater-induced artificial plasma irregularities

Vickers and Robinson (2011) used the SPEAR heater and the ESR, in conjunction with the SuperDARN CUTLASS radars, to examine the spectral width of the density irregularities produced by SPEAR heating (Figure 38). In contrast to normal heating results, which characteristically show irregularities with very narrow spectra during heating, a broad range of spectral widths was encountered, especially in the data from the CUTLASS Iceland radar, while the spectral widths observed by the CUTLASS Finland Radar remained low (Figure 39). The observations were made under disturbed conditions, with fast flows poleward of the heated volume and a flow gradient across the heated region. The authors attributed the broad spectral widths in the CUTLASS Iceland data to a combination of the look direction of the radar beams from that site, together with inhomogeneities in the ionospheric velocity within the heated region.

H. Vickers, and T. Robinson, "Observations of unusually broadened HF radar spectra from heater-induced artificial plasma irregularities", *J. Geophys. Res.* 116, A05301, doi:10.1029/2010JA015516, 2011.

Investigation of the HF heater induced effects in the ionosphere

Investigations carried out by the Institute of Radio Astronomy (IRA) in Kharkiv, Ukraine, in 2011 were basically directed on studying ionospheric effects induced by HF heating. Among the main subjects, one was the "self-scattering" effect consisting in the scattering of the pump radio waves on ionospheric irregularities produced by the same HF emission. Apparently, this effect was first observed in 2002 during simultaneous observations of EISCAT heater signal at three greatly dispersed sites located in Ukraine, Saint Petersburg and at the Ukrainian Antarctic Station (Zalizovski, et al., 2009). It was found that time variations in the Doppler frequency shifts of the heater signal measured at the three spaced positions were highly correlated in most cases. After the 2002 experiment, several special measuring campaigns with the EISCAT and HAARP heaters have been conducted. As a result some additional information about the morphology of the effect has been obtained (Galushko, et al., 2008).

SUPERDARN PARAMETER PLOT

30 Oct 2000⁽⁰⁰⁴⁾

WIDTH_L: PYK Beam 13,14,15 and HAN Beam 5

unknown scan mode (-6318)

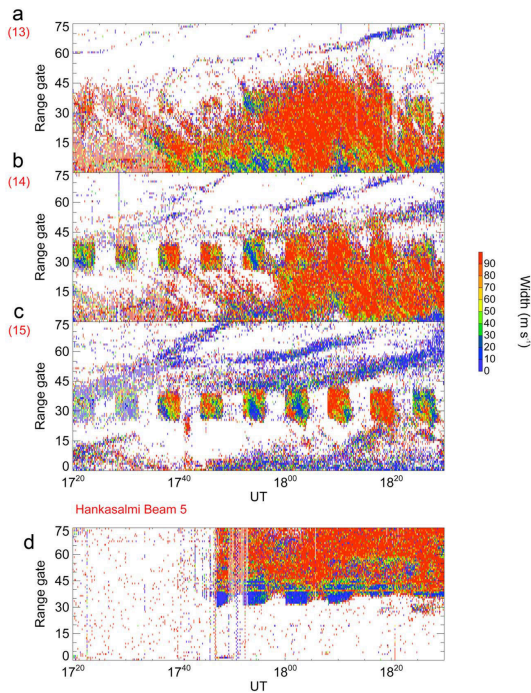


Figure 38: Range-time plots of the SuperDARN FITACF analysis spectral width recorded by the CUTLASS Iceland radar in (a–c) beams 13, 14, and 15 and by the CUTLASS Finland radar (d) beam 5 between 1720 and 1830 UT on 30 October 2000.

However, these observations were carried out during the minimum phase of the solar cycle and the characteristic features of the “self-scattering” were not so clearly seen as in the first experiment. Since 2011 the solar activity started to increase which stimulated a new measurement campaign with the EISCAT heater to be conducted on November 1 to 4, 2011. The heater radiated simultaneously at two frequencies separated by 10 Hz to 10 kHz. It was expected that due to the strong nonlinear interaction of the pumped waves with the ionospheric plasma an ion-acoustic turbulence (IAT) will be generated near the reflection point the incident wave, with the estimated scale-sizes of the IAT ranging from tens of meters to tens of centimeters and velocities about several hundreds of meters per second. To detect such processes the EISCAT UHF radar and digital Doppler HF receivers of IRA NASU were used. The HF receivers were located at the Radio Astronomy Observatory (RAO, Ukraine), Ukrainian Antarctic Station (UAS, Antarctica), Low-Frequency Observatory (LFO, Ukraine), KHO Observatory (Sval-

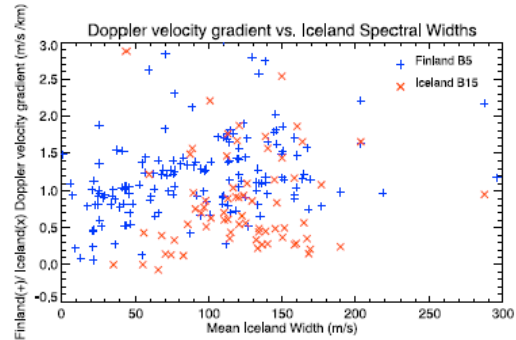


Figure 39: A scatterplot illustrating the relationship between the Doppler velocity gradient within the heated volume and the spectral widths measured by Iceland beam 15. The Doppler velocity gradient measured by the Finland radar (shown by the blue plus signs) was calculated using the observed range extent of artificial scatter and the difference between Doppler velocities at the near and far edges of the artificial backscatter for each heater-ON period. For the Iceland measurements (shown as red Xs), the Doppler velocity gradient was calculated by dividing the difference between the range-averaged line-of-sight velocities measured in beams 13 and 15 by 200 km. This is the approximate spatial separation between the centers of beam 13 and beam 15 at a distance of 2000 km from the Iceland bore site, with beam separation of the order of 6.5° .

bard) and near the EISCAT heater in Tromsø (Norway). The last three sites operate in unattended Internet-controlled mode since 2009, 2008 and of 2011, respectively. At Radio Astronomy Observatory an additional three-channel coherent HF receiver designed by IRA was used to provide measurements of angles of arrival of EISCAT heater signal. It should be noted, the “Joint Geospace Research Program by the National Academy of Sciences of Ukraine and EISCAT for 2012–2015” envisages a similar equipment to be installed near the EISCAT heater in Norway. Totally 15 h of heating and 7.5 h of UHF ISR observations were used. The operation schedule was as follows: 1 November 14:00–16:30 UT (Heating facility and UHF ISR); 2 November 03:00–05:30 UT (Heating facility), and 14:00–15:30 UT (Heating facility and UHF ISR); 3 November 03:00–05:30 UT (Heating facility), and 12:30–16:00 UT (Heating facility and UHF ISR); 4 November 03:00–05:30 UT (Heating facility).

Preliminary processing of the observational data of the November 2011 measurement campaign allowed detecting the “self-scattering” ef-

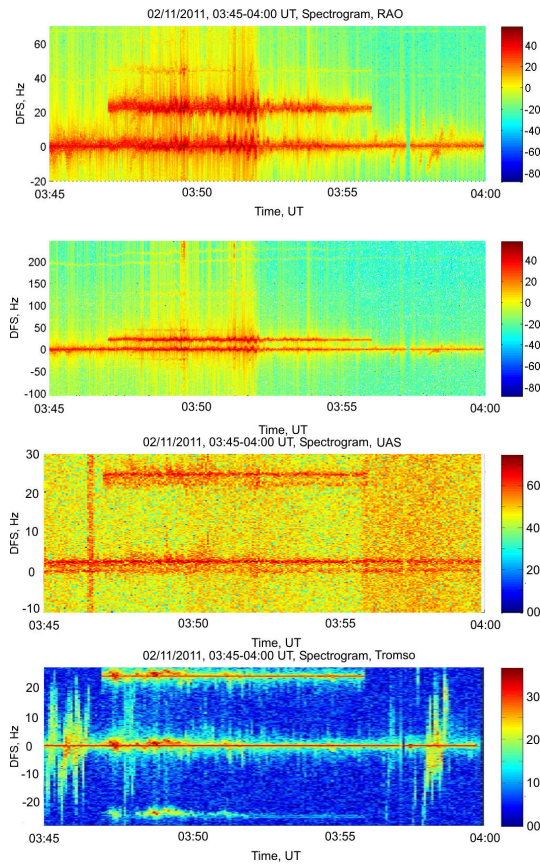


Figure 40: Spectrogram of the EISCAT heater signal as observed on November 2, 2011 at RAO (top two panels), UAS (third panel) and in Tromsø (bottom panel) between 03:45 and 04:00 UT.

fect, similar to that observed in 2002. As an example, Figure 40 presents typical spectrograms of the EISCAT heater signals recorded at the RAO (Ukraine), UAS (Antarctica) and Tromsø (Norway). One can clearly see quasiperiodic variations in the Doppler frequency shift of the received signals with characteristic period about 10 s occurred about 03:52 UT. Generally, the spectrograms of the signal received at UAS differ from those observed at RAO. However, the time intervals where the “self-scattering” was detected at RAO coincide with the time moments of increased magnitudes of the scattered signal observed in Antarctic. One can also see the appearance of the scattered components in the signal observed in Tromsø, at the distance about 15 km from the heating facility.

Figure 41 presents color-coded Doppler frequency-time distributions of the azimuth (top panel) and elevation (bottom panel) angles of the EISCAT heater signal received at RAO. As can be seen, the spectral components corres-

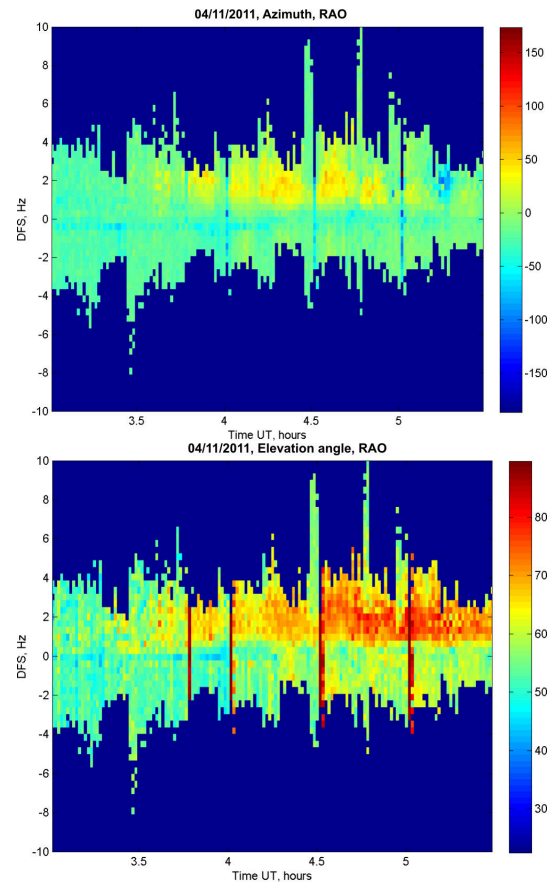


Figure 41: Doppler frequency-time distributions of the azimuth (top panel) and elevation angle (bottom panel) of the EISCAT heater signal measured at RAO between 03:00 and 05:30 UT on November 4, 2011. The angle of arrival magnitudes are color-coded (see scale on the right).

ponding to a positive Doppler frequency shift demonstrate a 15 min periodicity which effect is more pronounced in the azimuth angle variations. Specifically, magnitudes of angles of arrival over the time intervals when the heater radiated the full power noticeably differ from those measured when the probe signal of a lower power was transmitted alone.

Ukrainian scientists continued a theoretical analysis of possible mechanisms of the “self-scattering effect” of powerful HF signals in the ionosphere. A paper by V.G. Galushko, V.G. Bezrodny, A.V. Koloskov, and A.V. Zalizovski on the preliminary results of the study has been submitted to the “Radio Physics and Radio Astronomy” journal. The paper presents results of numerical simulations which have been performed with the use of data from the EISCAT incoherent scatter radar. The calculations show that phase path

deviations at the upgoing segment of the pump wave trajectory might play the determinative role in producing synchronous variations in the Doppler frequency shifts of the self-scattered signals observed in the November 2002 experiments. In addition the characteristics of HF fields scattered in aspect-sensitive directions are determined with allowance for the regular refraction effects in the ionosphere, and a condition for excitation of the ionospheric interlayer duct channel by HF signals aspect-sensitive scattered in a given direction is analyzed. The geometrical optics calculations are made within the Born approximation for an anisotropic power-law model spectrum of random irregularities of the upper ionosphere. It is shown that the suggested mechanism could provide practically identical HF signal scattering characteristics toward all the spaced receiving sites involved in the experiment.

In November 2011 the “Joint Geospace Research Program by the National Academy of Sciences of Ukraine and EISCAT for 2012-2015” was approved by the NASU. The Program was announced and endorsed at the 10th EISCAT Science Oversight Committee meeting, Tromsø, Norway, 29–30 March 2012. The principal scientific concept of the Program is the development and deployment of new facilities and techniques for 3D diagnostics of natural and artificially stimulated ionospheric inhomogeneities in the Arctic region. Some of the facilities have been already put into operation and are used for making measurements. Small-sized unattended HF receivers were deployed at Svalbard (2008) and in Tromsø (2011) to monitor emissions from broadcast radios and heating facilities. In 2009 an additional receiver was set active in Ukraine at the Low Frequency Observatory. Data from these instruments have successfully used for studying ionospheric processes during the measuring campaigns in 2009, 2010 and 2011. The further steps envisaged by the Program are as follows:

1. Development and implementation of new radar-based, GNSS-TEC and radio astronomy techniques for remote sensing of the near Earth plasma environment at observatories of EISCAT and Ukraine.
2. Development and validation of physical models of ionospheric and magnetospheric disturbances of natural and artificial origin at high- and mid-latitudes of the European continent.

The activities proposed by the program include:

1. Study of a variety of natural and stimulated plasma fluctuations in auroral region and mid-latitudes, particularly, artificial plasma turbulence, polar mesospheric summer and winter echoes, field-aligned inhomogeneities and traveling ionospheric disturbances.
2. Investigation of mechanisms of top-down (from interplanetary space and Sun) and bottom-up (from Earth’s surface and troposphere) transfer of powerful geospace disturbances.
3. Improvement of the physical models of ionospheric disturbance motion from auroral to mid-latitude ionosphere.
4. Refinement of models of wave interaction between neutral and charged atmospheric gas components.
5. Study of the spatial distribution and intensity of global thunderstorm activity in view of the global climate changes.

A. V. Zalizovski, et al., “Self-scattering of a powerful HF radio wave on stimulated ionospheric turbulence”, *Radio Science* 44, RS3010, doi:10.1029/2008RS004111, 2009.

V.G. Galushko, et al., “Self-Scattering of the Heater Emissions Observed at Geographically Dispersed Receiving sites”, *IEEE Antennas and Propagation Magazine* 50, 155–161, 2008.

Angular dependence of pump-induced bottom- and top-side ionospheric plasma turbulence

Kosch et al. (2011) used the Tromsø radars and the HF heater, scanning the radar in small steps to study the location and angular extent of the “Z-mode radio window”, through which radio waves above a certain frequency can propagate beyond the ionospheric peak. The Heater cycle was deliberately kept low, in order to minimise the growth of field-aligned irregularities. They found that the equatorward radio window had an angular width of 2° to 3°, most often appearing 7° to 8° south of the heater (Figure 42). These properties were broadly as expected from theory, with the locations of the bottomside radio window and topside enhanced radar echoes being consistent with the expected position determined by ray tracing performed on the basis of the observed plasma densities, especially when a tilt was imposed on the

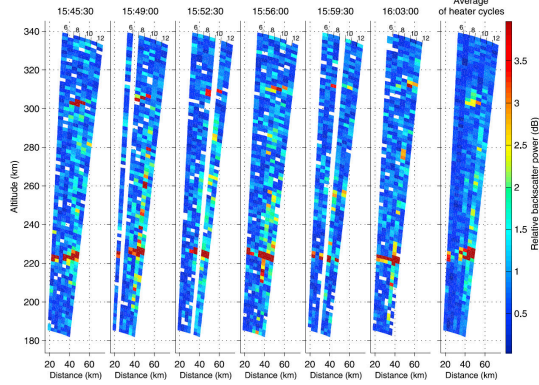


Figure 42: Relative backscatter power, not corrected for range, as a function of range and angle from 6° to 12° zenith angle south of EISCAT. The range and angular resolution are 1.8 km and 1° , respectively. The first through sixth panels show individual radar scans assembled from 7 HF pump cycles. The seventh panel shows the average of all the available data. Data gaps indicate technical problems with the radar.

ionosphere, consistent with observations obtained from an HF sounder.

M. J. Kosch, et al., "Angular dependence of pump-induced bottom- and top-side ionospheric plasma turbulence at EISCAT", *J. Geophys. Res.* 116, A03322, doi:10.1029/2010JA016014, 2011.

Heating induced temperature enhancement in the polar summer ionosphere

The ionospheric heating observation by ISR in August 2009 in Tromsø, Norway, was analyzed as Figure 43. There are two types of increases in electron temperature: the increases in a narrow height range near 150 km and the increases in a wide height range at 150 km to 400 km. As shown in Figure 44 obtained by regression analysis, the increase of temperature in percentage linearly increases with heating power. And the regression lines are

$$\Delta T = 0.53P + 4.07 \quad (2)$$

and

$$\Delta T = 0.15P + 5.60 \quad (3)$$

for type 1 and type 2 respectively.

A clear two-dimensional distribution was presented for the measurement performed on August 15. The heating effects obviously depend on the angle offset from the geomagnetic field. Figure 45 indicates the heating effect function as the angle offset, where the red line means the

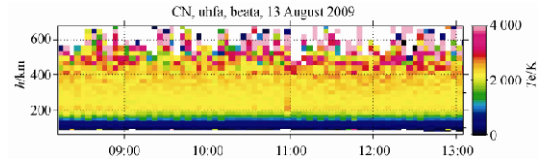


Figure 43: Increase in electron temperature on August 13, 2009.

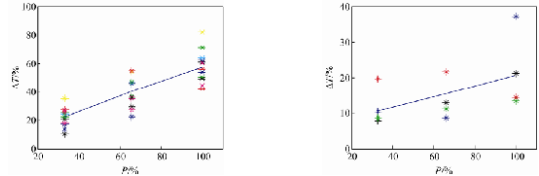


Figure 44: Regression analysis of the temperature increase for type 1 and type 2 respectively.

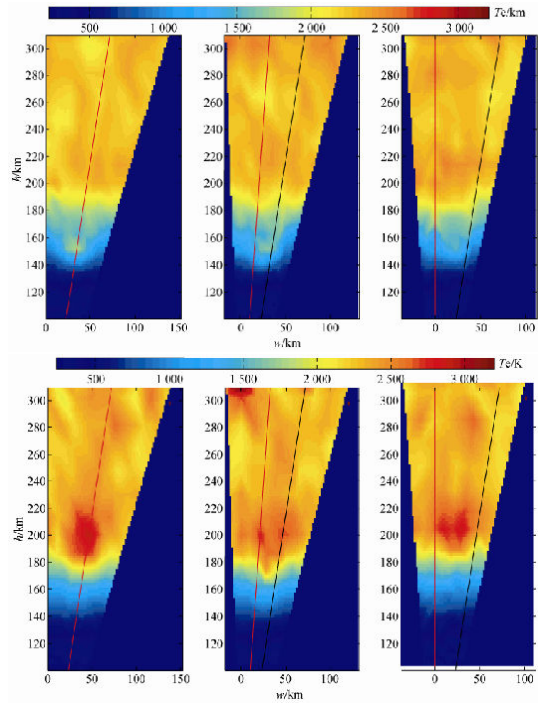


Figure 45: 2D distribution of electron temperature induced by heating on August 15, 2009 (top: type 1, bottom: type 2)

heating beam and the black one the geomagnetic field.

The disturbance of ion line spectra induced by ionospheric heating (HF frequency 5.423 MHz, reflecting height 214 km, 8 min on and 4 min off) on 13 September 2010, was analyzed. An enhancement of ion line spectra is present near reflected altitude under the condition of dense heating, as shown in Figure 46, where at 10:58 and 11:08 HF

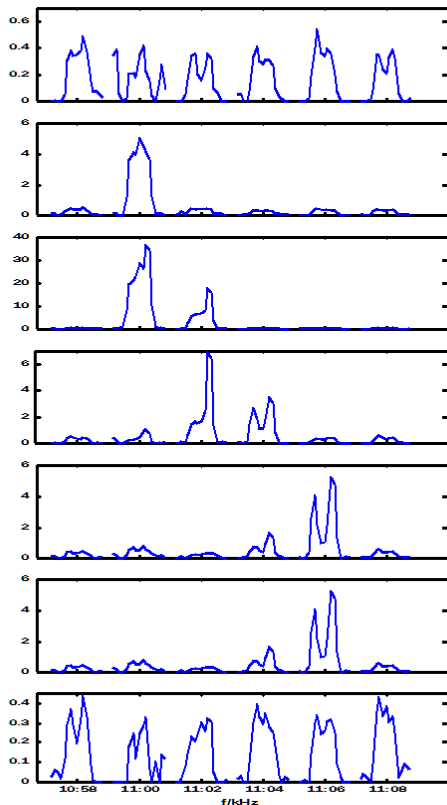


Figure 46: The disturbed ion line at height 219.75 km, 216.75 km, 213.75 km, 210.75 km, 207.75 km, 204.75 km and 201.75 km respectively.

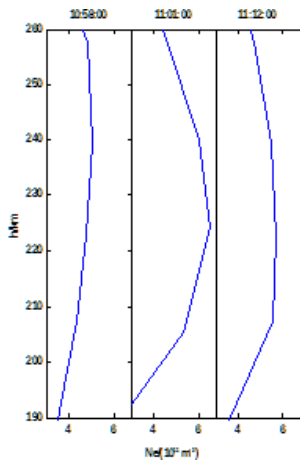


Figure 47: The electron density profile.

was off, at 11:00, 11:02, 11:04 and 11:06 HF was on. It should be possible that the disturbance of ion line spectra is due to a coherent echo, which can be the scattering from irregularity of electron density induced by ionospheric heating indicated by Figure 47.

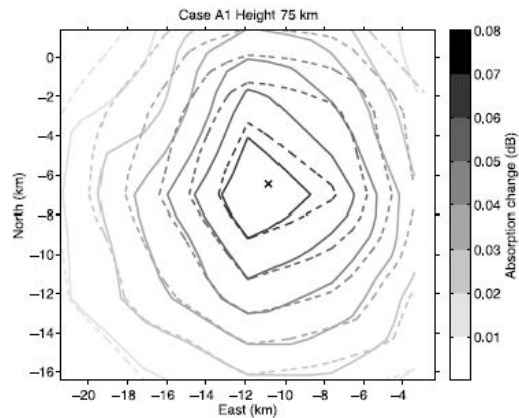


Figure 48: Contour plots of the change in CNA during heating observed by ARIES (solid lines) and modelled (dashed lines). The peak modeled CNA has been scaled to the peak observed CNA in this plot, in order to compare the morphology rather than the absolute values. The vertical over the heater is marked by the cross.

Xu Bin, et al., "Heat-induced temperature enhancement in the polar summer ionosphere", *Advance in Polar Science* 22(2), 101–110, 2011.

Cheng Musong, et al., "Observation of VHF incoherent scatter spectra disturbed by HF heating", 15th International EISCAT Workshop, Qingdao China, 5–9 September 2011.

Cosmic noise absorption changes due to radio heating of the D region ionosphere

Senior et al. (2011) studied the way in which artificially heating the D region of the ionosphere increases the electron-neutral collision frequency, and hence the amount of radio wave absorption. They used a high-resolution imaging riometer to estimate the level of absorption for various degrees of heating, and compared the results with a theoretical model which used the measured electron densities as an input (Figure 48). While the model successfully reproduced the spatial morphology of the absorption, it initially underestimated the absorption level by factor 2. This discrepancy was reduced to around 30 % by using a more realistic ground conductivity in the modelling of the heater ERP (Figure 49).

A. Senior, et al., "Measurements of cosmic noise absorption changes due to radio heating of the D-region ionosphere", *J. Geophys. Res.*, 116, A04310, doi:10.1029/2010JA016189, 2011

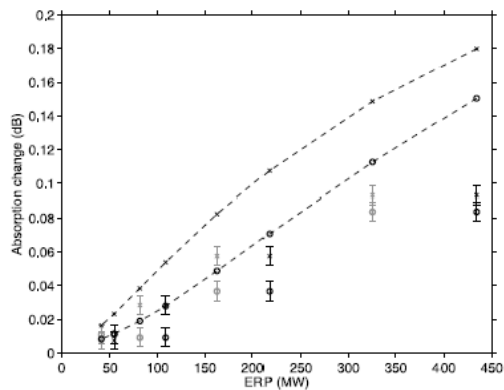


Figure 49: The observed (black points with error bars) and modeled (dashed lines) CAN change due to heating for the experiment of July 1st 2008. O-mode polarization is denoted by circles and X-mode polarization is denoted by crosses. The grey points with error bars show the observations plotted at 75 % of the original ERP.

New radar techniques

Fractional baud-length coding

A novel approach is presented for modulating radar transmissions in order to improve target range and Doppler estimation accuracy. This is achieved by using non-uniform baud lengths. With this method it is possible to increase sub-baud range-resolution of phase coded radar measurements while maintaining a narrow transmission bandwidth. First target backscatter amplitude estimation error covariance matrix for arbitrary targets are derived when estimating backscatter in amplitude domain. Target optimality is defined and different search strategies are discussed that can be used to find well performing transmission envelopes. Several simulated examples of the method are given showing that fractional baud-length coding results in smaller estimation errors than conventional uniform baud length transmission codes when estimating the target backscatter amplitude at sub-baud range resolution. The method is also demonstrated in practice by analysing the range resolved power of a low-altitude meteor trail echo that was measured using a fractional baud-length experiment with the EISCAT UHF system (Figure 50).

J.-P. Vierinen, "Fractional baud-length coding", *Ann. Geophys.* 29, 1189–1196, 2011.

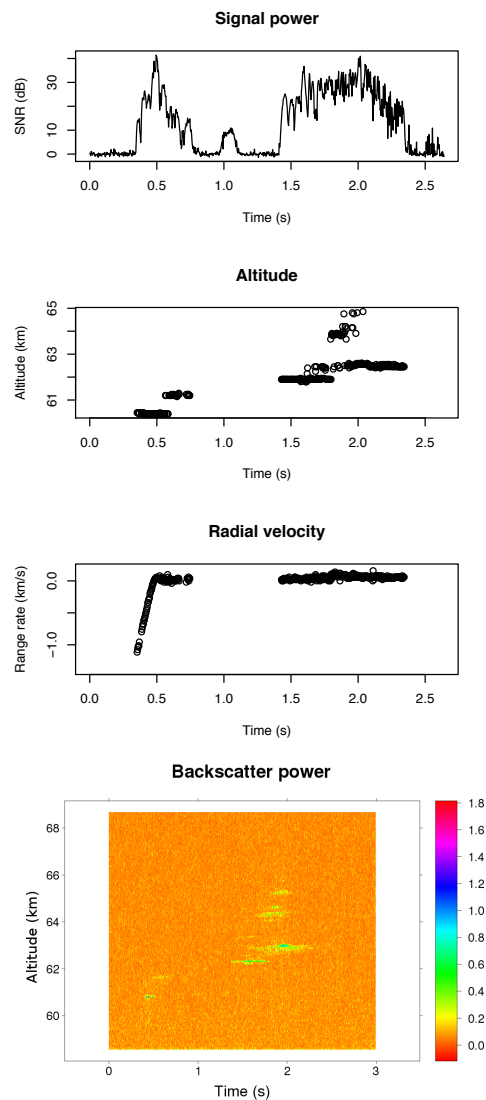


Figure 50: A low-altitude meteor echo at 60 km seen with the EISCAT UHF radar on 19 November 2009 at 05:16 UT during a low-elevation meteor experiment. The meteor echo can be seen decelerating from 1 km/s down to 0 km/s, and then echoes from a trail-like structure are seen for a while. The three top panels show the results from moving point-target model that determines the most likely range, Doppler shift and power of a point target. The fourth panel shows the range resolved backscatter power from a spread target model. After the initial head echo, many layers appear at altitudes above the initial detection. Most of the layers show 100 m to 400 m range spread.

Meteor head echo polarization at 930 MHz studied with the EISCAT UHF HPLA radar

The polarisation characteristics of 930 MHz meteor head echoes have been studied for the first

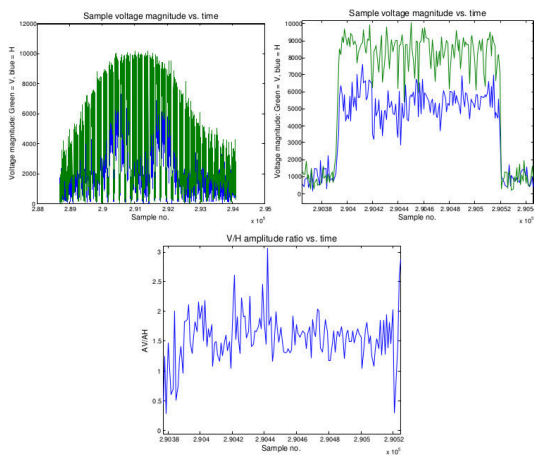


Figure 51: Showing the passage of a typical head echo target through the common scattering volume at Q in $0.6 \mu\text{s}$ time resolution. Top left panel shows the full event in raw amplitude format. The time interval between successive radar pulses is $1656 \mu\text{s}$ and the event lasts for 30 pulses or about 50 ms (the first four pulses are not shown). Top right panel shows the development of the scattered signal during a single $76.8 \mu\text{s}$ radar pulse (pulse number 10, counting from the left). Bottom panel shows the V-H amplitude ratio during the same pulse.

time, using data obtained in a series of radar measurements carried out with the tristatic EISCAT UHF high power, large aperture (HPLA) radar system in October 2009. An analysis of 44 tristatic head echo events shows that the polarisation of the echo signal recorded by the Kiruna receiver often fluctuates strongly on time scales of tens of microseconds, illustrating that the scattering process is essentially stochastic (Figure 51). On longer timescales (larger than milliseconds), more than 90% of the recorded events show an average polarisation signature that is independent of meteor direction of arrival and echo strength and equal to that of an incoherent-scatter return from underdense plasma filling the tristatic observation volume. This shows that the head echo plasma targets scatter isotropically, which in turn implies that they are much smaller than the 33 cm wavelength and close to spherically symmetric, in very good agreement with results from a previous EISCAT UHF study of the head echo RCS/meteor angle-of-incidence relationship.

Significant polarisation is present in only three events with unique target trajectories. These all show a larger effective target cross section transverse to the trajectory than parallel to it. It is proposed that the observed polarisation may be a signature of a transverse charge separation plasma

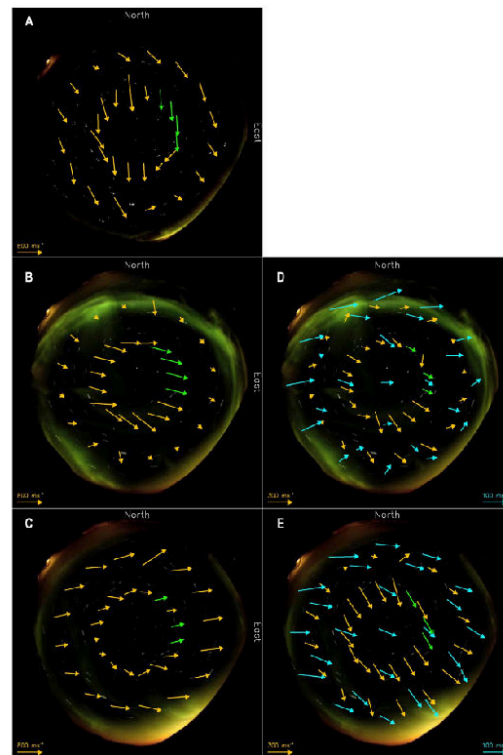


Figure 52: Averaged all-sky images of the aurora with F region ion (yellow) flow vectors overlaid for (a) 2312–2330 UT, (b) 2336–2354 UT, (c) 2436–2454 UT and with E region ion (yellow) and neutral (blue) flow vectors overlaid for (d) 2336–2354 UT and (e) 2436–2454 UT on 2 February 2010. The green vectors are modelled without line-of-sight data.

resonance in the region immediately behind the meteor head, similar to the resonance effects previously discussed in connection with meteor trail echoes by Herlofson, Billam and Browne, Jones and Jones and others.

G. Wannberg, A. Westman, and A. Pellinen-Wannberg, “Meteor head echo polarization at 930 MHz studied with the EISCAT UHF HPLA radar”, *Ann. Geophys.* 29, 1197–1208, doi:10.5194/angeo-29-1197-2011, 2011.

Joule heating near an auroral arc and ion-neutral collision frequency in the polar cap E region

Kosch et al. (2011) reported on the first combined mesoscale ionospheric and thermospheric observations, obtained partly in the vicinity of an auroral arc. The EISCAT Svalbard Radar was scanned in a novel observing mode, to obtain E and F region velocities in an annulus centred on

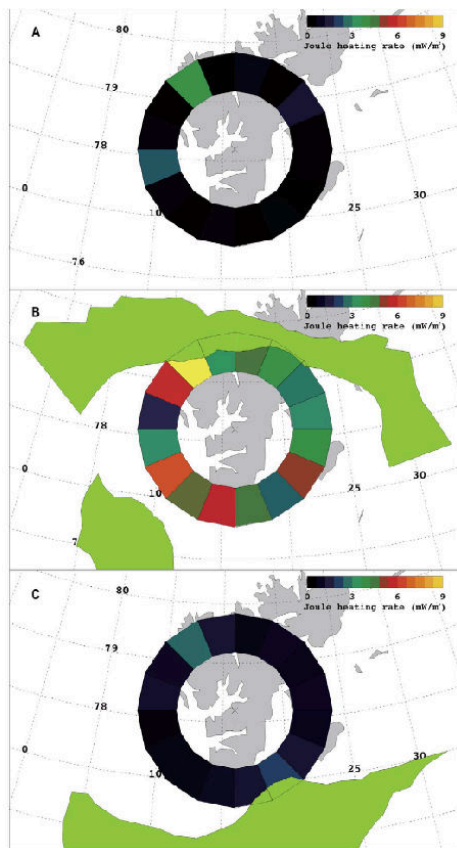


Figure 53: The spatial distribution of Joule heating in 22.5° sectors about Longyearbyen projected to 110 km for (a) 2312–2330 UT, (b) 2336–2354 UT, and (c) 2436–2454 UT on 2 February 2010. In the two lower panels, the aurora is overlaid for 110 km altitude.

the radar. At the same time, the Scanning Doppler Imager observed E-region winds and temperatures using 557.7 nm optical emissions (Figure 52). Combining the ion and neutral density observations permitted the E region Joule heating to be estimated with an azimuthal spatial resolution of ~ 64 km at a radius of ~ 163 km from the radar. The results showed that the Joule heating of the polar thermosphere contained significant mesoscale structure (Figure 53), while the average ion-neutral collision frequency at the altitude of the emission (~ 113 km) was in good agreement with current MSIS model.

M. J. Kosch, et al., "Mesoscale observations of Joule heating near an auroral arc and ion-neutral collision frequency in the polar cap E region", *J. Geophys. Res.* 116, A05321, doi:10.1029/2010JA016015, 2011.

List of publications 2011

- Amm, O., R. Nakamura, T. Takada, K. Kauristie, H.U. Frey, C.J. Owen, A. Aikio, and R. Kuula, Observations of an auroral streamer in a double oval configuration, *Ann. Geophys.*, 29, 701-716, doi:10.5194/angeo-29-701-2011, 2011.
- Amm, O., R. Fujii, K. Kauristie, A. Aikio, A. Yoshikawa, A. Ieda, and H. Vanhamäki, A statistical investigation of the Cowling channel efficiency in the auroral zone, *J. Geophys. Res.*, 116, A02304, doi:10.1029/2010JA015988, 2011.
- Archer, J., H. Dahlgren, N. Ivchenko, B.S. Lanchester, G.T. Marklund, Dynamics and characteristics of black aurora as observed by high resolution ground-based imagers and radar, *Int. J. Remote Sens.*, 32, 2973-2985, doi:10.1080/01431161.2010.541517, 2011.
- Barthélémy, M., J. Liliensten, F. Pitout, C. Simon Wedlund, R. Thissen, D. Lorentzen, F. Sigernes, J. Moen, G. Gronoff, I. McCrea, H. Rothkael, H. Ménager, and A. Aruliah, Polarisation in the auroral red line during coordinated EISCAT Svalbard Radar/optical experiments, *Ann. Geophys.*, 29, 1101-1112, 2011.
- Biebricher, A., Numerical Analysis of Polar Mesosphere Summer and Winter Echoes: The Overshoot Effect, Ph. D. thesis, University of Tromsø, Norway, 2011.
- Blagoveshchenskaya, N. F., T. D. Borisova, M. T. Rietveld, T. K. Yeoman, D. M. Wright, M. Rother, H. Lühr, E. V. Mishin, and C. Roth, Results of Russian Experiments Dealing with the Impact of Powerful HF Radiowaves on the High-Latitude Ionosphere Using the EISCAT Facilities, *Geomagnetism and Aeronomy*, ISSN 0016-7932, 51, 8, 1109-1120, 2011.
- Blagoveshchenskaya, N.F., T.D. Borisova, T.K. Yeoman, M.T. Rietveld, I.M. Ivanova, and L.J. Baddeley, Artificial small-scale field-aligned irregularities in the high latitude F region of the ionosphere induced by an X-mode HF heater wave, *Geophys. Res. Lett.*, 38, L08802, doi:10.1029/2011GL046724, 2011.
- Blagoveshchenskaya, N. F., T. D. Borisova, V. A. Kornienko, M. T. Rietveld, T. K. Yeoman, D. M. Wright, M. Rother, H. Lühr, E. V. Mishin and C. Roth, V.L. Frolov, M. Parot, J.L. Rauch, Modification of the high-latitude ionosphere by high-power hf radio waves. 2. Results of coordinated satellite and ground-based observations, *Radiophys. & Quant. Electr.*, 54, 2, 89-101, DOI: 10.1007/s11141-011-9273-9 2011. (Translated from *Izvestiya Vysshikh Uchebnykh Zavedenii, Radiofizika*, 54, 2, pp. 97-112, February 2011).
- Borisova, T. D., N. F. Blagoveshchenskaya, V. A. Kornienko, and M. T. Rietveld, Characteristics of Pc4-5 Pulsations Obtained Using the Method of Bistatic Backscatter of HF Radio Waves, the EISCAT HF Heating Facility, and Ground-Based Magnetometers, *Geomagnetism and Aeronomy*, ISSN 0016-7932, 51, 5, 620-632, 2011.
- Cai, H. T., F. Yin, S. Y. Ma, and I. W. McCrea, Observations of AGW/TID propagation across the polar cap: a case study, *Ann. Geophys.*, 29, 1355-1363, 2011.
- Dahlgren, H., B. Gustavsson, B. S. Lanchester, N. Ivchenko, U. Brandstrom, D. K. Whiter, T. Sergienko, I. Sandahl, and G. Marklund, Energy and flux variations across thin auroral arcs, *Ann. Geophys.*, 29, 1699-1712, doi:10.5194/angeo-29-1699-2011, 2011.
- Ekeberg, J., Solitary Waves and Enhanced Incoherent Scatter Ion Lines, Doctoral Thesis, University of Umeå, Kiruna, Sweden, 2011.
- Enell, C.-F., J. Hedin, J. Stegman, G. Witt, M. Friedrich, W. Singer, G. Baumgarten, B. Kaifler, U.-P. Hoppe, B. Gustavsson, U. Brändström, M. Khaplanov, A. Kero, T. Ulich, E. Turunen, The Hotel Payload 2 campaign: Overview of NO, O and electron density measurements in the upper mesosphere and lower thermosphere, *J. Atmos. Sol. Terr. Phys.*, 73, 14-15, 2228-2236, 2011.
- Fontdecaba i Baig, J., F. Martinerie, M. Sutter, V. Martinot, E. Fletcher, Radar Tracking Campaigns for ESA CO-VI, proceedings of European Space Surveillance Conference, Madrid, 7-9 June 2011.
- Friedrich, M. and G. Landauer, An extension for the model IMAZ for large absorption, *Earth Planets Space, Earth Planets Space*, 63, 4, 383-390, doi:10.5047/eps.2010.12.008, 2011.
- Havnes, O., C. La Hoz, M. T. Rietveld, M. B. Kassa, G. Baroni, and A. Biebricher, Dust charging and density conditions deduced from observations of PMWE modulated by artificial electron heating, *J. Geophys. Res.*, 116, D24203, doi:10.1029/2011JD016411, 2011.

- Honary, F., N. Borisov, M. Beharrell, and A. Senior, Temporal development of the magnetic zenith effect, *J. Geophys. Res.*, 116, A06309, doi:10.1029/2010JA016029, 2011.
- Hultqvist, B., History of EISCAT - Part 1: On the early history of EISCAT with special reference to the Swedish part of it, *Hist. Geo Space. Sci.*, 2, doi:10.5194/hgss-2-115-2011, 115-121, 2011.
- Kieser, J., The influence of precipitating solar and magnetospheric energetic charged particles on the entire atmosphere: Simulations with HAMMONIA, Ph.D. thesis, University of Hamburg, Germany, 2011.
- Kitamura, N., Y. Ogawa, Y. Nishimura, N. Terada, T. Ono, A. Shinbori, A. Kumamoto, V. Truhlik, and J. Smilauer, Solar zenith angle dependence of plasma density and temperature in the polar cap ionosphere and low-altitude magnetosphere during geomagnetically quiet periods at solar maximum, *J. Geophys. Res.*, 116, A08227, doi:10.1029/2011JA016631, 2011.
- Kosch, M.J., E. Mjølhus, M. Ashrafi, M.T. Rietveld, T. Yeoman and S. Nozawa, Angular dependence of pump-induced bottom- and top-side ionospheric plasma turbulence at EISCAT, *J. Geophys. Res.*, 116, A03322, 9 PP, doi:10.1029/2010JA016014, 2011.
- Kosch, M. J., I. Yiu, C. Anderson, T. Tsuda, Y. Ogawa, S. Nozawa, A. Aruliah, V. Howells, L. J. Baddeley, I. W. McCreary, and J. A. Wild, Mesoscale observations of Joule heating near an auroral arc and ion-neutral collision frequency in the polar cap E region, *J. Geophys. Res.*, 116, A05321, doi:10.1029/2010JA016015, 2011.
- Lanchester, B., O.-P. Jokioho, M. Galand, N. Ivchenko, D. Lummerzheim, J. Baumgardner, and S. Chakrabarti, Separating and quantifying ionospheric responses to proton and electron precipitation over Svalbard, *J. Geophys. Res.*, 116, A09322, doi:10.1029/2011JA016474, 2011.
- Li, Q., Multi-frequency radar observations of polar mesosphere summer echoes: Statistical properties and microphysical results, Ph.D. thesis, University of Rostock, Germany, 2011.
- Li, Q., M. Rapp, PMSE-observations with the EISCAT VHF and UHF-radars: Statistical properties, *J. Atmos. Sol. Terr. Phys.*, 73, 9, 944-956, 2011.
- Lukianova, R., and A. Kozlovsky, IMF By effects in the plasma flow at the polar cap boundary, *Ann. Geophys.*, 29, 1305-1315, 2011.
- Mahmoudian, A. W. A. Scales, M. J. Kosch, A. Senior, and M. Rietveld, Dusty space plasma diagnosis using temporal behavior of polar mesospheric summer echoes during active modification, *Ann. Geophys.*, 29, 2169-2179, 2011.
- Mikhailov, A.V. and T.Yu. Leschinskaya, Ionospheric altitude profiles in the main ionospheric trough as observed by field-aligned EISCAT incoherent scatter radar observations, *J. Atmos. Solar-Terr. Phys.*, 73, 4, 488-498, doi:10.1016/j.jastp.2010.11.007, 2011.
- Nygrén, T., A.T. Aikio, R. Kuula, and M. Voiculescu, Electric fields and neutral winds from monostatic incoherent scatter measurements by means of stochastic inversion, *J. Geophys. Res.*, 116, A05305, doi:10.1029/2010JA016347, 2011.
- Ogawa, Y., S.C. Buchert, I. Häggström, M.T. Rietveld, R. Fujii, S. Nozawa, and H. Miyaoka, On the statistical relation between ion upflow and naturally enhanced ion-acoustic lines observed with the EISCAT Svalbard radar, *J. Geophys. Res.*, 16, A03313, 12 PP, doi:10.1029/2010JA015827, 2011.
- Oksman, J., History of EISCAT - Part 2: The early history of EISCAT in Finland, *Hist. Geo Space. Sci.*, 2, doi:10.5194/hgss-2-123-2011, 123-128, 2011.
- Oyama, S., A. Brekke, T. T. Tsuda, J. Kurihara, and B. J. Watkins, Variance of the vertical ion speed measured with the European Incoherent Scatter (EISCAT) UHF radar in the polar lower ionosphere at Tromsø, Norway, *J. Geophys. Res.*, 116, A00K06, doi:10.1029/2010JA016129, 2011.
- Partamies, N., L. Juusola, E. Tanskanen, K. Kauristie, J. M. Weygand, and Y. Ogawa, Substorms during different storm phases, *Ann. Geophys.*, 29, 2031-2043, 2011.
- Pellinen-Wannberg, A., The Radio Physics of Meteors: High Resolution Radar Methods Offering New Insights, *Radio Science Bulletin*, 339, 32-45, 2011, 2011.
- Pitkänen, T., A.T. Aikio, O. Amm, K. Kauristie, H. Nilsson, and K.U. Kaila, EISCAT-Cluster observations of quiet-time near-Earth magnetotail fast flows and their signatures in the ionosphere, *Ann. Geophys.*, 29, 299-319, 299-319, 2011.
- Rapp, M., L. Leitert, R. Latteck, M. Zecha, P. Hoffmann, J. Höffner, U.-P. Hoppe, C. La Hoz, and E.V. Thrane, Localized mesosphere-stratosphere-troposphere radar echoes from the E region at 69°N: Properties and physical mechanisms, *J. Geophys. Res.*, 116, A02320, doi:10.1029/2010JA016167, 2011.
- Rinne, Y., J. Moen, J.B.H. Baker, and H.C. Carlson, Convection surrounding mesoscale ionospheric flow channels, *J. Geophys. Res.*, 116, A05213, doi:10.1029/2010JA015997, 2011.

- Routledge, Graham, Polar mesospheric summer echoes - studied by active radio wave experiments, PhD thesis, University of Lancaster, UK, 16 March 2011.
- Routledge, G., M.J. Kosch, A. Senior, A.J. Kavanagh, I.W. McCrea and M.T. Rietveld, A statistical survey of electron temperature enhancements in heater modulated polar mesospheric summer echoes at EISCAT, *J. Atmos. Solar-Terr. Phys.*, 73, 4, 472-482, doi:10.1016/j.jastp.2010.11.004, 2011.
- Senior, A., M.T. Rietveld, F. Honary, W. Singer, and M. J. Kosch, Measurements and Modelling of Cosmic Noise Absorption Changes due to Radio Heating of the D-Region Ionosphere, *J. Geophys. Res.*, 116, A04310, doi:10.1029/2010JA016189, 2011.
- Skjæveland, Å., J. Moen, and H. C. Carlson, On the relationship between flux transfer events, temperature enhancements, and ion upflow events in the cusp ionosphere, *J. Geophys. Res.*, 116, A10305, doi:10.1029/2011JA016480, 2011.
- Sojka, J.J., M. Nicolls, A. van Eyken, C. Heinselman and D. Bilitza, 24/7 Solar minimum polar cap and auroral ion temperature observations, *Adv. Space Res.*, 48, 1, 1-11, dx.doi.org/10.1016/j.asr.2011.03.005, 2011.
- Strelnikova, I., M. Rapp, Majority of PMSE spectral widths at UHF and VHF are compatible with a single scattering mechanism, *Journal of Atmospheric and Solar-Terrestrial Physics*, 73, 14-15, 2142-2152, 2011.
- Tanaka, Y.-M., T. Aso, B. Gustavsson, K. Tanabe, Y. Ogawa, A. Kadokura, H. Miyaoka, T. Sergienko, U. Brändström, and I. Sandahl, Feasibility study on Generalized-Aurora Computed Tomography, *Ann. Geophys.*, 29, 551-562, 2011.
- Vickers, Hannah, Radar Observations of Artificial Ionospheric Modification Effects, PhD thesis, University of Leicester, 2011.
- Vickers, H. M. S., and L. J. Baddeley, An alternative estimation of the RF-enhanced plasma temperature during SPEAR artificial heating experiments: Early results, *J. Geophys. Res.*, 116, A11323, doi:10.1029/2011JA016795, 2011.
- Vickers, H., and T. Robinson, Observations of unusually broadened HF radar spectra from heater-induced artificial plasma irregularities, *J. Geophys. Res.*, 116, A05301, doi:10.1029/2010JA015516, 2011.
- Vierinen, J., Fractional baud-length coding, *Ann. Geophys.*, 29, 1189-1196, doi:10.5194/angeo-29-1189-2011, 2011.
- Vlasov, A., K. Kauristie, M. van de Kamp, J.-P. Luntama, and A. Pogoreltsev, A study of Traveling Ionospheric Disturbances and Atmospheric Gravity Waves using EISCAT Svalbard Radar IPY-data, *Ann. Geophys.*, 29, 2101-2116, 2011.
- Wannberg, G., A. Westman, and A. Pellinen-Wannberg, Meteor head echo polarization at 930 MHz studied with the EISCAT UHF HPLA radar, *Ann. Geophys.*, 29, 1197-1208, doi:10.5194/angeo-29-1197-2011, 2011.
- Wissing, Jan Maik, Analysis of particle precipitation and development of the Atmospheric Ionization Module OSnabrück AIMOS, Ph. D. Thesis, University of Osnabrück, Germany, 2011.
- Wissing, J.M., M.-B. Kallenrode, J. Kieser and H. Schmidt, M.T. Rietveld, A. Strømme, P. J. Erickson, Atmospheric Ionization Module OSnabrück (AIMOS) 3: Comparison of electron density simulations by AIMOS/HAMMONIA and incoherent scatter radar measurements, *J. Geophys. Res.*, 116, A08305, doi:10.1029/2010JA016300, 2011.
- Zhang, Q.-H., B.-C. Zhang, R.-Y. Liu, M. W. Dunlop, M. Lockwood, J. Moen, H.-G. Yang, H.-Q. Hu, Z.-J. Hu, S.-L. Liu, I. W. McCrea, and M. Lester, On the importance of interplanetary magnetic field |By| on polar cap patch formation, *J. Geophys. Res.*, 116, A05308, doi:10.1029/2010JA016287, 2011.
- Zhang, Q.-H., M. W. Dunlop, R.-Y. Liu, H.-G. Yang, H.-Q. Hu, B.-C. Zhang, M. Lester, Y. V. Bogdanova, I. W. McCrea, Z.-J. Hu, S. R. Crothers, C. La Hoz, and C. P. Nielsen, Coordinated Cluster/Double Star and ground-based observations of dayside reconnection signatures on 11 February 2004, *Ann. Geophys.*, 29, 1827-1847, 2011.

EISCAT Operations 2011

The EISCAT radars operate in two basic modes, using approximately half the available observing time for each. In the Special Programme mode, users conduct individual experiments dedicated to specific experiments and objectives. The resulting data are reserved for the exclusive use of the experimenters for one year from the date of collection. Special programmes often make use of the well developed pulse schemes and observing modes of the Common Programme. EISCAT Common Programmes are conducted for the benefit of the entire user community and the resulting data are immediately available to all. The Common Programme modes are developed and maintained by EISCAT staff, and the overall programme is monitored by the Scientific Oversight Committee (SOC). Common Programme operations are often conducted as part of the coordinated World Day programme organised by the International Union of Radio Scientists (URSI) Incoherent Scatter Working Group (ISWG).

Common Programme One, CP-1, uses a fixed transmitting antenna, pointing along the geomagnetic field direction. The three-dimensional velocity and anisotropy in other parameters are measured by means of the receiving stations at Kiruna and Sodankylä (see map, inside front cover). CP-1 is capable of providing results with very good time resolution and is suitable for the study of substorm phenomena, particularly auroral processes where conditions might change rapidly. The basic time resolution is 5 s. Continuous electric field measurements are derived from the tri-static F-region data. On longer time scales, CP-1 measurements support studies of diurnal changes, such as atmospheric tides, as well as seasonal and solar-cycle variations. The observation scheme uses alternating codes for spectral measurements.

Common Programme Two, CP-2, is designed to make measurements from a small, rapid transmitter antenna scan. One aim is to identify wave-like phenomena with length and time scales comparable with, or larger than, the scan (a few tens of kilometers and about ten minutes). The present version consists of a four-position scan which is

completed in six minutes. The first three positions form a triangle with vertical, south, and south-east positions, while the fourth is aligned with the geomagnetic field. The remote site antennas provide three-dimensional velocity measurements in the F-region. The pulse scheme is identical with that of CP-1.

Common Programme Three, CP-3, covers a 10° latitudinal range in the F-region with a 17-position scan up to 74°N in a 30 min cycle. The observations are made in a plane defined by the magnetic meridian through Tromsø, with the remote site antennas making continuous measurements at 275 km altitude. The coding scheme uses alternating codes. The principle aim of CP-3 is the mapping of ionospheric and electrodynamic parameters over a broad latitude range.

Common Programmes One, Two, and Three are run on the UHF radar. Three further programmes are designed for use with the VHF system. The UHF and VHF radars are often operated simultaneously during the CP experiments. Such observations offer comprehensive data sets for atmospheric, ionospheric, and magnetospheric studies.

Common Programme Four, CP-4, covers geographic latitudes up to almost 80°N (77°N invariant latitude) using a low elevation, split-beam configuration. CP-4 is particularly suitable for studies of high latitude plasma convection and polar cap phenomena. However, with the present one-beam configuration of the VHF radar, CP-4 is run with either both UHF and VHF radars or with UHF only in a two position scan.

Common Programme Six, CP-6, is designed for low altitude studies, providing spectral measurements at mesospheric heights. Velocity and electron density are derived from the measurements and the spectra contain information on the aeronomy of the mesosphere. Vertical antenna pointing is used.

Common Programme Seven, CP-7, probes high altitudes and is particularly aimed at polar wind studies. The present version, with only one of the VHF klystrons running, is designed to cover



Ingemar Häggström, EISCAT head of operations, demonstrating the pointing direction of the test array from the EISCAT_3D Design Study.

altitudes up to 1500 km vertically above Ramfjordmoen.

Equivalent Common Programme modes are available for the EISCAT Svalbard Radar. CP-1 is directed along the geomagnetic field (81.6° inclination). CP-2 uses a four position scan. CP-3 is a 15 position elevation scan with southerly beam swinging positions. CP-4 combines observations in the F-region viewing area with field-aligned and vertical measurements. Alternating code pulse schemes have been used extensively

for each mode to cover ranges of approximately 80 km to 1200 km with integral clutter removal below 150 km. CP-6 is similar to the mainland radar CP-6.

The tables on the next pages summarise the accounted hours on the various facilities for each month and for each Common Programme mode (CP) or Associate (SP).

*Dr. Ingemar Häggström
Senior Scientist, EISCAT Scientific Association*

KST COMMON PROGRAMMES

| 2011 | Jan | Feb | Mar | Apr | May | Jun | Jul | Aug | Sept | Oct | Nov | Dec | Total | % | Target% |
|--------------|-----|-------|-----|-----|-----|-----|-----|-----|------|-----|------|------|--------------|------------|---------|
| CP1 | 0.5 | 1 | | 0.5 | | | 4.5 | | | 3.5 | | 0.5 | 10.5 | 1 | 16 |
| CP2 | | 218.5 | | | | | 2 | 299 | | | | 16 | 535.5 | 63 | 16 |
| CP3 | | | | | | | 8.5 | | | 0.5 | 80.5 | 12 | 101.5 | 12 | 12 |
| CP4 | | | | | | | | | | | | | 0 | 0 | 10 |
| CP6 | | | 62 | | 1 | 75 | | | 61.5 | 3 | | | 202.5 | 24 | 20 |
| CP7 | | | | | | | | | | 0.5 | | | 0.5 | 0 | 18 |
| UP1 | | | | | | | | | | | | | 0 | 0 | |
| UP2 | | | | | | | | | | | | | 0 | 0 | |
| UP3 | | | | | | | | | | | | | 0 | 0 | |
| Total | 0.5 | 219.5 | 62 | 0.5 | 1 | 75 | 15 | 299 | 61.5 | 7.5 | 80.5 | 28.5 | 850.5 | 100 | |
| % | 0 | 26 | 7 | 0 | 0 | 9 | 2 | 35 | 7 | 1 | 9 | 3 | 100 | | |

KST SPECIAL PROGRAMMES

| 2011 | Jan | Feb | Mar | Apr | May | Jun | Jul | Aug | Sept | Oct | Nov | Dec | Total | Incl AA | Target |
|--------------|-----|-----|-----|-----|------|-----|------|-----|------|-----|------|-------|--------------|------------|------------|
| CN | | | | | 57 | | | | | | 32.5 | | 89.5 | 90 | 60 |
| FI | | | 12 | | | | | | | | | 88.5 | 100.5 | 101 | 102 |
| GE | | | | | | | 7.5 | | | | | 53.5 | 61 | 61 | 59 |
| NI | 24 | | | | | | 5 | | | | 83 | 29.5 | 141.5 | 142 | 120 |
| NO | | | | | | | 152 | | | | 28 | 11 | 191 | 191 | 232 |
| SW | | | | | | | 23 | | | 13 | 6 | | 42 | 42 | 167 |
| UK | | | | | 18.5 | | 31.5 | | 4.5 | | 42.5 | | 97 | 97 | 156 |
| AA | | | | | | | | | | | | | 0 | | |
| Total | 24 | 0 | 12 | 0 | 75.5 | 0 | 219 | 0 | 4.5 | 13 | 192 | 182.5 | 722.5 | 723 | 896 |
| % | 3 | 0 | 2 | 0 | 10 | 0 | 30 | 0 | 1 | 2 | 27 | 25 | 100 | | |

| | EI | CN | FI | GE | NI | NO | SW | UK |
|--------|----|-----|------|------|-------|-------|------|-------|
| Target | | 6.7 | 11.4 | 6.56 | 13.41 | 25.91 | 18.6 | 17.43 |

KST OTHER PROGRAMMES

| 2011 | Jan | Feb | Mar | Apr | May | Jun | Jul | Aug | Sept | Oct | Nov | Dec | Total | Target |
|--------------|-----|-----|------|-----|-----|-----|-----|-----|------|-----|-----|------|------------|------------|
| PP | | 6 | 1 | | 23 | 30 | | | | | | 17.5 | 77.5 | 92 |
| EI | | | | | | | | | | | 17 | 4 | 21 | 30 |
| RU | | | 74.5 | | | | | | | 89 | | | 163.5 | 170 |
| TB | | 36 | | | | | | | | | 29 | | 65 | 65 |
| Total | 0 | 42 | 75.5 | 0 | 23 | 30 | 0 | 0 | 0 | 89 | 46 | 21.5 | 327 | 357 |

KST CUMULATIVE TOTALS

| 2011 | Jan | Feb | Mar | Apr | May | Jun | Jul | Aug | Sept | Oct | Nov | Dec | Total | Target |
|--------------|------|-------|-------|-----|------|-----|-----|-----|------|-------|-------|-------|-------------|-------------|
| CP | 0.5 | 219.5 | 62 | 0.5 | 1 | 75 | 15 | 299 | 61.5 | 7.5 | 80.5 | 28.5 | 850.5 | 825 |
| SP | 24 | 0 | 12 | 0 | 75.5 | 0 | 219 | 0 | 4.5 | 13 | 192 | 182.5 | 722.5 | 896 |
| OP | 0 | 42 | 75.5 | 0 | 23 | 30 | 0 | 0 | 0 | 89 | 46 | 21.5 | 327 | 357 |
| Total | 24.5 | 261.5 | 149.5 | 0.5 | 99.5 | 105 | 234 | 299 | 66 | 109.5 | 318.5 | 232.5 | 1900 | 2078 |

USAGE BREAKDOWN

| 2011 | Jan | Feb | Mar | Apr | May | Jun | Jul | Aug | Sept | Oct | Nov | Dec | Total | Target |
|-------------|------|-------|-------|------|------|------|-----|-----|------|-----|-------|------|-------|--------|
| UHF | 20 | 166.5 | 40.5 | 0.5 | 29.5 | 20 | 79 | 198 | | 55 | 176.5 | 111 | 896.5 | 867 |
| VHF | | 20 | 74.5 | | 20 | 75 | 86 | | 61.5 | 10 | 67 | 83.5 | 497.5 | 801 |
| Heating | | | 2 | 34.5 | | 31.5 | | 65 | | 44 | 60 | 32 | 269 | 260 |
| Passive UHF | 15.5 | 291.5 | | | 74 | 40 | 21 | 404 | 17 | 3 | 63.5 | 23 | 952.5 | 600 |
| Bolt array | | | | | | 49 | 66 | | 63 | 7 | | 3.5 | 188.5 | |
| ESR | 126 | 279 | 105.5 | 21 | 10.5 | 64 | 6.5 | 0 | 0 | 6 | 161.5 | 152 | 932 | 1535 |
| Passive ESR | | | | | 56 | 2 | | | | | | | 58 | |

ESR COMMON PROGRAMMES

| 2011 | Jan | Feb | Mar | Apr | May | Jun | Jul | Aug | Sept | Oct | Nov | Dec | Total | % | Target% |
|--------------|-----|-----|------|-----|-----|------|-----|-----|------|-----|------|------|--------------|------------|---------|
| CP1 | 1.5 | | | 8 | 2 | | | | | 1 | 55 | 20.5 | 88 | 24 | 54 |
| CP2 | | 144 | | | | | | | | | | | 144 | 39 | 16 |
| CP3 | | | | | | | | | | | 4.5 | | 4.5 | 1 | 12 |
| CP4 | | | | | | | | | | | | | 0 | 0 | 10 |
| CP6 | | | 62.5 | 1 | 1 | 58 | | | | | | | 122.5 | 34 | |
| CP7 | | | | | | | | | | | | | 0 | 0 | |
| UP1 | | | | | | | | | | | | | 0 | 0 | |
| UP2 | | | | | | | | | | | | | 0 | 0 | |
| UP3 | | | | | | 6.5 | | | | | | | 6.5 | 2 | |
| Total | 1.5 | 144 | 62.5 | 9 | 3 | 64.5 | 0 | 0 | 0 | 1 | 59.5 | 20.5 | 365.5 | 100 | |
| % | 0 | 39 | 17 | 2 | 1 | 18 | 0 | 0 | 0 | 0 | 16 | 6 | 100 | | |

ESR SPECIAL PROGRAMMES

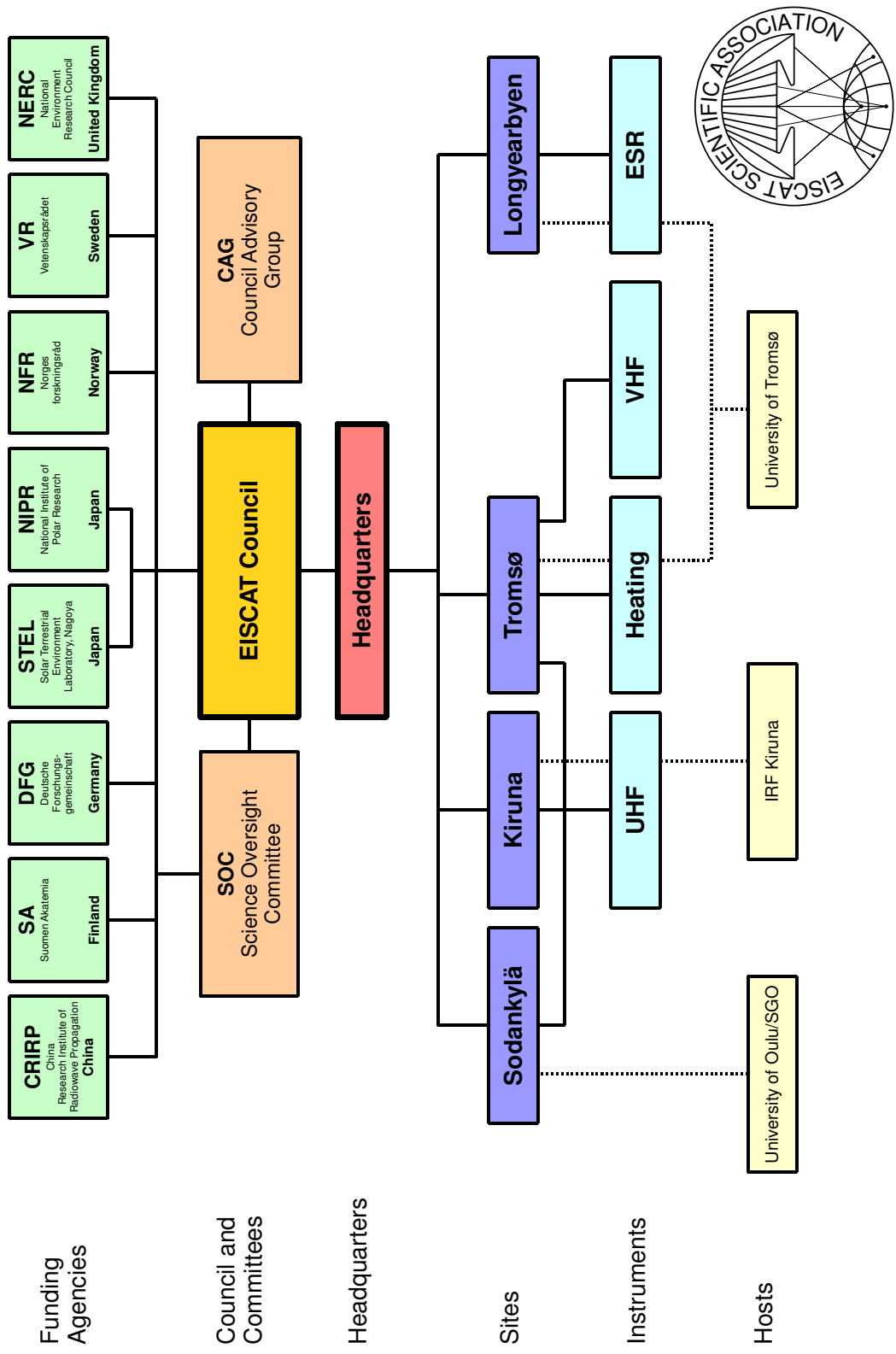
| 2011 | Jan | Feb | Mar | Apr | May | Jun | Jul | Aug | Sept | Oct | Nov | Dec | Total | Incl AA | Target |
|--------------|------|------|-----|-----|-----|-----|-----|-----|------|-----|-----|------|------------|------------|------------|
| CN | | | | | | | | | | | | | 0 | 0 | 40 |
| FI | | | | | | | | | | | 11 | 61.5 | 72.5 | 73 | 68 |
| GE | | | | | | | 2 | | | | | | 2 | 2 | 39 |
| NI | 21 | 12 | | | | | | | | | 3 | 53.5 | 89.5 | 90 | 80 |
| NO | 15 | 27.5 | 43 | | | | 1.5 | | | 5 | 33 | 1 | 126 | 126 | 154 |
| SW | 15 | | | | | | | | | | 12 | | 27 | 27 | 111 |
| UK | 7.5 | 24.5 | | | 14 | | 3 | | | | 12 | | 61 | 61 | 104 |
| AA | | | | | | | | | | | | | 0 | | |
| Total | 58.5 | 64 | 43 | 0 | 14 | 0 | 6.5 | 0 | 0 | 5 | 71 | 116 | 378 | 378 | 596 |
| % | 15 | 17 | 11 | 0 | 4 | 0 | 2 | 0 | 0 | 1 | 19 | 31 | 100 | | |

ESR OTHER PROGRAMMES

| 2011 | Jan | Feb | Mar | Apr | May | Jun | Jul | Aug | Sept | Oct | Nov | Dec | Total | Target | |
|--------------|-----|------|-----|-----|-----|-----|-----|-----|------|-----|-----|-----|-------|------------|------------|
| PP | | 25.5 | | | | | | | | | | | 14.5 | 40 | 93 |
| EI | | | | | | | | | | | | | | 0 | 20 |
| RU | | | | | 12 | | | | | | | 20 | | 32 | 20 |
| TB | 66 | 45.5 | | | | 7.5 | | | | | | 11 | 1 | 131 | 131 |
| Total | 66 | 71 | 0 | 12 | 7.5 | 0 | 0 | 0 | 0 | 0 | 0 | 31 | 15.5 | 203 | 264 |

ESR CUMULATIVE TOTALS

| 2011 | Jan | Feb | Mar | Apr | May | Jun | Jul | Aug | Sept | Oct | Nov | Dec | Total | Target |
|--------------|------|-----|-------|-----|------|------|-----|-----|------|-----|-------|------|--------------|-------------|
| CP | 1.5 | 144 | 62.5 | 9 | 3 | 64.5 | 0 | 0 | 0 | 1 | 59.5 | 20.5 | 365.5 | 675 |
| SP | 58.5 | 64 | 43 | 0 | 14 | 0 | 6.5 | 0 | 0 | 5 | 71 | 116 | 378 | 596 |
| OP | 66 | 71 | 0 | 12 | 7.5 | 0 | 0 | 0 | 0 | 0 | 31 | 15.5 | 203 | 264 |
| Total | 126 | 279 | 105.5 | 21 | 24.5 | 64.5 | 6.5 | 0 | 0 | 6 | 161.5 | 152 | 946.5 | 1535 |



EISCAT organisational diagram, December 2011.

EISCAT Scientific Association

December 2011

Council

The Council consists of a Delegation with a maximum of three persons from each Associate. Germany leaves EISCAT Scientific Association at the end of 2011.

P. R. of China

Prof. Q. Dong
Prof. J. Wu *Vice-Chairperson, Delegate*

Finland

Dr. A. Aikio
Dr. K. Kauristie
Dr. K. Sulonen *Delegate*

Germany

Prof. J. Röttger
Dr. K. Zach *Delegate*

Japan

Dr. H. Miyaoka *Delegate*
Dr. S. Nozawa

Norway

Prof. A. Brekke
Dr. B. Jacobsen *Delegate*
Dr. L. Lønnum

Sweden

Dr. T. Andersson *Chairperson, Delegate*
Prof. D. Murtagh

United Kingdom

Dr. I. McCrea
Dr. M. Schultz *Delegate*

Scientific Oversight Committee

The EISCAT scientific community organises the Scientific Oversight Committee (SOC), under the guidance of the Council.

| | |
|---------------------------|----------------------------|
| Dr. N. Blagoveshchenskaya | External member |
| Dr. S. Buchert | Sweden |
| Dr. J. Chau | External member |
| Dr. M. Kosch | United Kingdom |
| Prof. C. La Hoz | <i>Chairperson, Norway</i> |
| Prof. R. Liu | P. R. of China |
| Dr. Y. Ogawa | Japan |
| Prof. J. Röttger | Germany |
| Dr. T. Ulich | Finland |

Director

Dr. E. Turunen

Council Advisory Group

The Council Advisory Group (CAG) prepares matters to be brought to the Council.

| | |
|------------------|------------------------|
| Dr. A. Aikio | Council Member |
| Mr. H. Andersson | Head of Administration |
| Dr. T. Andersson | Council Chairperson |
| Prof. A. Brekke | Council Member |
| Dr. I. McCrea | Council Member |
| Dr. H. Miyaoka | Council Member |
| Dr. E. Turunen | Director |

Executives

Senior Management

| | |
|------------------|---------------------------|
| Mr. H. Andersson | Head of Adm., Deputy Dir. |
| Dr. E. Turunen | Director |

Site Leaders

Station Managers

| | |
|---------------------|-----------------------|
| Mr. H. Boholm | EISCAT Svalbard Radar |
| Mr. R. Jacobsen | Tromsø Radar |
| Mr. J. Markkanen | Sodankylä Site |
| Dr. M. Rietveld | Tromsø Heating |
| Mr. L.-G. Vanhainen | Kiruna Site |



EISCAT staff and invited guests at the Annual Review Meeting and 30 year celebrations, 23–26 August 2011, at Svalbard. Picture taken at the Hansbreen glacier, Hornsund.

Appendix:

**EISCAT Scientific Association
Annual Report, 2011**

EISCAT Scientific Association Annual Report 2011

EISCAT Scientific Association
Registered as a Swedish non-profit organisation
Organisation number: 897300-2549

Annual report for the financial year 2011-01-01 – 2011-12-31

The EISCAT Council and the Director for the Association submits herewith the annual report for 2011.

| Content | Page |
|--------------------------|-------------|
| Administration report | 1 |
| Profit and loss accounts | 5 |
| Balance sheet | 6 |
| Statement of cash flows | 7 |
| Notes | 8 |

ADMINISTRATION REPORT

Ownership, organisation and objective

The EISCAT Scientific Association was established in 1975 through an agreement between six European organisations. Japan joined in 1996 and the Peoples Republic of China in 2007.

The EISCAT Associates at 2011-12-31 are: China Research Institute of Radiowave Propagation (Peoples Republic of China), Deutsche Forschungsgemeinschaft (Germany), National Institute of Polar Research (Japan), Natural Environment Research Council (United Kingdom of Great Britain and Northern Ireland), Norges forskningsråd (Norway), Solar-Terrestrial Environment Laboratory, Nagoya University (Japan), Suomen Akatemia (Finland), and Vetenskapsrådet (Sweden).

A new EISCAT Agreement came into force 2007-01-01, with all Associates making long term funding commitments to the Association. The Association has its formal seat in Kiruna, Sweden, and is registered as a non-profit organisation.

The aim of the Association is to make significant progress in the understanding of physical processes in the high latitude atmosphere by means of experimental programmes generally conducted using the incoherent scatter radar technique, which may be carried out as part of wider international projects. For this purpose, the Association has developed, constructed, and now operates, a number of radar facilities at high latitudes. At present, these comprise a system of stations at Tromsø (Norway), Kiruna (Sweden), Sodankylä (Finland), and Longyearbyen (Svalbard).

The Association is fully funded by the Associates but additional operations may also be funded by short term additional contributions from both Associate and non-Associate bodies. Depending on the available funding, scientific priorities and operational targets are adjusted on an annual basis.

The EISCAT Council is charged with the overall administration and supervision of the Association's activities. The Council appoints a Director, who is responsible for the daily management and operation of the facilities of the Association.

Operation and scientific development

The EISCAT Radars delivered a full programme of operations for the user community and operated reliably throughout the year with only some interruptions due to equipment or operational problems.

The various EISCAT radars operated for a total of 2 846 accounted hours (3 496 hours in 2010).

The UHF tristatic mode of operation had to be phased out in November after a Finnish mobile operator started to use a newly deployed GSM base station 6.1 km away from the Sodankylä site and thus effectively blocking the UHF frequency band from then on. Council

decided in the autumn meeting to convert the Kiruna and Sodankylä antennas to VHF use such that tristatic operations would be possible again. The new needed hardware will be installed summer 2012.

Common Programmes amounted to 43% (42%) of the operations. Special Programmes amounted to 39% (37%) and other operations amounted to 18% (21%) of the total hours.

Scientists from France, Ukraine and Russia paid for the use of the facilities. Totally 391.5 hours (254.5 hours) were accounted on behalf of these countries. Both Ukraine and Russia have Affiliate agreements. The introduced Peer-Review Programme attracted several applications and user groups from USA, Germany and UK were granted time, at no costs, on the systems. Peer-Review time amounted to 117.5 accounted hours (new scheme for the year).

The EISCAT_3D_2 preparatory phase continued as planned during the year. Two additional EU Framework Programme 7 projects started 1 November 2011 with EISCAT being a Partner. Both projects are related to data provision or procedures. Both will be running for about three years and one project, ESPAS, "Near-Earth Space Data Infrastructure for e-Science" will be a major undertaking with a total committed effort amounting to 612 kEUR over 41 work-months. The second project, ENVRI, will not draw so much resource. EISCAT joined in also on two further EU FP7 bids; COOPEUS and IMPRES. The outcome of these applications will be known during spring 2012.

The "third antenna system on Svalbard with dual mode capabilities" development continued during the year. The needed Norwegian concept plan was submitted to the local authorities on Svalbard for consideration in the beginning of 2012. The plan will undergo a public hearing and a formal response should be expected probably some time mid 2012.

Future operation and scientific development

During 2012, EISCAT will continue to support the wide range of existing and new programmes proposed by the various Associates' scientific communities, including the hosting of user-supplied equipment.

The now lacking mainland tristatic capabilities will be reintroduced in summer 2012 but then using the 224 MHz VHF frequency. Since this frequency is much different from UHF, new science opportunities should arise. The monostatic UHF radar and the Svalbard Radar will continue to be available for users. Also the small VHF receive-only array in Kiruna is available for use and the Heating system continues to be developed allowing new utilisation modes.

The work of the Council and its committees

The Council had two ordinary meetings under the leadership of the Chairperson, Dr. Tomas Andersson. Council had its spring meeting at the Academy of Finland, in Helsinki. The autumn meeting was held at the Deutsche Forschungsgemeinschaft (DFG) in Bonn, Germany. The Council Advisory Group had two meetings under the leadership of the Chairperson, Dr. Tomas Andersson. The spring meeting was held at the Research Council Norway, Oslo, and the autumn meeting was held at the Swedish Research Council, Stockholm. The Scientific Oversight Committee had two meetings during the year. The first

meeting was held at the Jicamarca Radio Observatory, Peru with Prof. Ruiyuan Liu as Chairperson. The chairpersonship then changed and the new Chairperson, Prof. Cesar La Hoz lead the second meeting that was held in Qingdao, P. R. of China.

The German Associate, DFG, had a fixed five year agreement running from 2007 to end 2011. The departure meant that the annual operating budget for 2012 onwards had to be adjusted to the new, without Germany, funding level. Council decided in 2010 that a proactive approach should be implemented involving preferably improved income but also, if needed, adjustments to the cost level. As a way of improving the income, the Associates agreed to inflationary compensate their annual contribution for 2012 and thus shifting the annual funding level to a somewhat higher level. To reduce re-occurring costs, the overall regular staff level was reduced by two positions. With these measures, the cost budget for 2012 and 2013 will be tolerable and 2014 can probably be balanced too if taking in use own reserves.

Around 2014 - 2015 it is expected that the Associate work related to EISCAT_3D has arrived at an updated Agreement structure and additional funding.

Budget development during the year

The 2011 operations ended below the operating target set for the year. Some of the systems were underused by users. In addition the Svalbard Radar had a long down period caused by an unusual fault in the RF-feed.

EISCAT celebrated its 30-years anniversary in August and staff and a limited set of guests celebrated the occasion on Svalbard by enjoying a boat cruise followed by a public seminar and an anniversary dinner in the evening. Staff costs became lower than budgeted due to a year-long vacancy on Svalbard which was deliberately kept vacant. Project staff was hired for the ongoing projects. Project staff and costs are mostly refunded by the project financier, EU.

External users, particularly French scientists, continued to make use of the facilities. The recovery in 2011 of SEK meant that Associate contributions, paid in national currencies, became lower than budget, but since about half of the operations are in Norway and Finland (NOK and EUR), the overall currency effect was low in total.

The long-term budget plan

The long-term budget plan will be challenging but measures taken during the year created an improved spend profile that will be explored during the coming few years.

The result for 2011 and the surplus handling

The year was balanced by transferring 1 898 kSEK to the Surplus fund.

PROFIT AND LOSS ACCOUNTS

in thousands of Swedish Crowns

| | Note 1 | 2011 | 2010 |
|--|--------|----------------|----------------|
| Associate contributions | Note 2 | 23 164 | 24 248 |
| Other operating income | | 5 061 | 3 219 |
| | | <u>28 225</u> | <u>27 467</u> |
| Operation costs | | -6 914 | -6 243 |
| Administration costs | | -4 448 | -4 413 |
| Personnel costs | Note 3 | -16 967 | -17 854 |
| Depreciation of fixed assets | | -1 203 | -1 214 |
| | | <u>-29 533</u> | <u>-29 724</u> |
| <i>Operating profit/loss</i> | | -1 308 | -2 257 |
| Interest income | | 230 | 52 |
| Other financial income and cost | | 740 | -41 |
| Own reserves and funds | Note 4 | 1 033 | 949 |
| | | <u>2 002</u> | <u>960</u> |
| <i>Profit/loss after financial items</i> | | 694 | -1 297 |
| Appropriations | Note 5 | -1 898 | 83 |
| Transfer from funds invested | Note 6 | 1 203 | 1 214 |
| | | <u>-694</u> | <u>1 297</u> |
| <i>Net profit/loss for the year</i> | | 0 | 0 |

BALANCE SHEET

in thousands of Swedish Crowns

| | | 2011 | 2010 |
|--------------------------------------|---------|---------------|---------------|
| ASSETS | | | |
| <u>Fixed assets</u> | | | |
| <i>Tangible fixed assets</i> | Note 7 | | |
| Buildings | | 3 194 | 3 557 |
| Radar systems | | 832 | 748 |
| Equipment and tools | | 1 622 | 1 664 |
| | | <u>5 648</u> | <u>5 968</u> |
| <u>Current assets</u> | | | |
| Receivables | | 2 435 | 3 050 |
| Prepayments and accrued income | Note 8 | 2 202 | 1 129 |
| Cash at bank and in hand | Note 9 | 24 166 | 24 711 |
| | | <u>28 803</u> | <u>28 889</u> |
| <i>Total assets</i> | | <i>34 450</i> | <i>34 858</i> |
| CAPITAL AND LIABILITIES | | | |
| <u>Capital</u> | | | |
| Funds invested | Note 10 | 5 648 | 5 968 |
| Funds held on reserve | Note 11 | 17 289 | 17 312 |
| | | <u>22 937</u> | <u>23 280</u> |
| <u>Current liabilities</u> | | | |
| Liabilities, trade | Note 12 | 11 320 | 11 425 |
| Provisions | | 0 | 0 |
| Other liabilities | | 193 | 152 |
| | | <u>11 513</u> | <u>11 578</u> |
| <i>Total capital and liabilities</i> | | <i>34 450</i> | <i>34 858</i> |
| <i>Pledged assets</i> | | <i>none</i> | <i>none</i> |
| <i>Contingent liabilities</i> | | <i>none</i> | <i>none</i> |

STATEMENT OF CASH FLOWS

in thousands of Swedish Crowns

| | 2011 | 2010 |
|---|---------------|---------------|
| <u>Operating activities</u> | | |
| Operating result before financial items | -1 308 | -2 257 |
| Transfer from funds invested | 1 203 | 1 214 |
| Interest received | 230 | 52 |
| Currency exchange rate changes | 695 | -57 |
| Extra ordinary income and cost | 45 | 15 |
| Increase/decrease of receivables | 615 | 821 |
| Increase/decrease of prepayments and accrued income | -1 073 | -489 |
| Increase/decrease of creditors and liabilities | -64 | 6 608 |
| <i>Cash flow from operations</i> | <i>343</i> | <i>5 907</i> |
| <u>Investment activities</u> | | |
| Investments in tangible assets | -888 | -419 |
| <i>Cash flow from investment activities</i> | <i>-888</i> | <i>-419</i> |
| <i>Cash flow for the year</i> | <i>-545</i> | <i>5 488</i> |
| <i>Liquid assets at the beginning of the year</i> | <i>24 711</i> | <i>19 222</i> |
| <i>Liquid assets at the end of the year</i> | <i>24 166</i> | <i>24 711</i> |

EISCAT Scientific Association Annual Report 2011

NOTES

Note 1 Accounting principles

The accounting and valuation principles applied are consistent with the provisions of the Swedish Annual Accounts Act and generally accepted accounting principles (bokföringsnämnden allmänna råd och vägledning).

All amounts are in thousands of Swedish kronor (SEK) unless otherwise stated.

Receivables

Receivables are stated at the amounts estimated to be received, based on individual assessment.

Receivables and payables in foreign currencies

Receivables and payables in foreign currencies are valued at the closing day rate. Where hedging measures have been used, such as forwarding contracts, the agreed exchange rate is applied. Gains and losses relating to operations are accounted for under other financial income and cost.

Bank accounts in foreign currencies

Bank balances in foreign currencies are valued at the closing day rate.

Fixed assets

Tangible fixed assets are stated at their original acquisition values after deduction of depreciation according to plan. Assets are depreciated systematically over their estimated useful lives. The following periods of depreciation are applied: Buildings 5 - 50 years, Radar systems 3 - 20 years and Equipment and tools 1 - 5 years.

Note 2 Associate contributions

The Associates contributed to the operation during the year in accordance with the agreement. The commitments are in local currencies. The received contributions have been accounted in SEK.

| | <u>2011</u> |
|------------------------|---------------|
| CRIRP (P. R. of China) | 2 757 |
| DFG (Germany) | 1 614 |
| NIPR (Japan) | 1 639 |
| RCN (Norway) | 5 365 |
| SA (Finland) | 3 126 |
| NERC (United Kingdom) | 3 264 |
| VR (Sweden) | 5 400 |
| | <u>23 164</u> |

Accumulated contributions status as of 2011-12-31

| | <u>1976 - 2011</u> |
|------------------------|--------------------|
| Previous Associates | 190 074 |
| CRIRP (P. R. of China) | 16 214 |
| DFG (Germany) | 192 094 |
| NIPR (Japan) | 70 311 |
| RCN (Norway) | 145 486 |
| SA (Finland) | 65 314 |
| NERC (United Kingdom) | 221 039 |
| VR (Sweden) | 118 829 |
| | <u>1 019 360</u> |

Note 3 Personnel costs and average number of employees

The Association employs directly the Headquarters staff, currently about seven positions, including the Director. The Headquarters is located in Kiruna, Sweden. The personnel working at the Kiruna (Sweden), Sodankylä (Finland), Svalbard and Tromsö (Norway) sites are not employed by the Association. Instead, the personnel are provided via site contracts by the Swedish Institute of Space Physics (Kiruna site staff), Oulu University (Sodankylä staff) and Tromsö University (Tromsö and Svalbard staff). The Association refunds all expenses related to the provided staff, as well as an additional overhead.

Personnel costs in total

| | <u>2011</u> | <u>2010</u> |
|--|-------------|-------------|
| Salaries and emoluments paid to the Director | 1 335 | 1 286 |
| Other personnel, employed and provided via site contracts | 10 835 | 10 971 |
| Social security contributions amounted to of which for pension costs | 3 888 | 4 106 |
| | 1 923 | 2 086 |

The Director, Dr. Esa Turunen, started his employment 2009-01-01. His employment contract with Council was extended one further year and is now for four years.

Of the pension costs, 344 kSEK (333 kSEK) relates to the Director. He and all other directly employed staff are included in ITP like occupational pension plans. For the personnel provided via site contracts, the pension plans are handled by their respective employer.

The members of the board (EISCAT Council) and members of committees, who represents Associates, do not receive remunerations from the Association. Travel expenses in connection with Council and committee meetings are normally covered by the Associates. For the Council Advisory Group, the Association cover meeting and travel costs.

Salaries and emoluments and average number of staff per country

| | | |
|---|--------|--------|
| Finland | | |
| Salaries and emoluments | 1 001 | 1 029 |
| Average number of staff - men and women | 2 + 0 | 2 + 0 |
| Norway (including Svalbard) | | |
| Salaries and emoluments | 5 996 | 5 818 |
| Average number of staff - men and women | 10 + 0 | 10 + 0 |
| Sweden | | |
| Salaries and emoluments | 5 173 | 5 410 |
| Average number of staff - men and women | 6 + 2 | 7 + 1 |

Members of the board and Directors at year-end - men and women

The board consist of delegations from every Associate country each having a Delegate (formal member) and up to two Representatives.

| | | |
|--------------------------------|--------|--------|
| Board members (EISCAT Council) | 12 + 4 | 12 + 4 |
| Directors | 1 + 0 | 1 + 0 |

Note 4 Own reserves and funds

Transactions involving own reserves and funds.

| | | |
|----------------------------------|--------|------|
| Capital Operating reserve | | |
| Budgeted transfer to the reserve | -1 105 | -884 |
| Transfer from the reserve | 888 | 419 |
| Investments made | -888 | -419 |

| | | |
|----------------------------------|-----|-----|
| Spare parts reserve | | |
| Budgeted transfer to the reserve | -18 | -28 |
| Transfer from the reserve | 159 | 109 |

| | | |
|---------------------------------|-------|--------|
| Surplus fund | | |
| Budgeted transfer from the fund | 2 362 | 4 196 |
| Budgeted transfer to the fund | -365 | -2 445 |

| | | |
|-----------------------------------|--------------|------------|
| Sum own reserves and funds | 1 033 | 949 |
|-----------------------------------|--------------|------------|

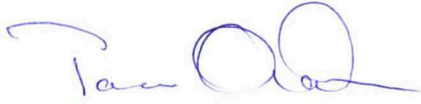
EISCAT Scientific Association Annual Report 2011

| | 2011 | 2010 | | 2011 | 2010 |
|---|--------------|--------------|---|---------------|---------------|
| Note 5 Appropriations | | | Prepaid rents | 100 | 92 |
| The outcome for this year became a surplus relative to the budget amounting to 1 898 kSEK. The amount has been transferred to the surplus fund. The 2010 outcome resulted in a deficit (-83 kSEK), which was covered by a transfer from the surplus fund. | | | Prepaid insurances | 507 | 462 |
| | | | Accrued income, EISCAT_3D_2 project | 1 221 | 139 |
| | | | Accrued income, ENVRI project | 14 | 0 |
| | | | Accrued income, ESPAS project | 19 | 0 |
| | | | Other items | 342 | 437 |
| | | | | <u>2 202</u> | <u>1 129</u> |
| Note 6 Transfer from funds invested | | | Note 9 Bank balances status | | |
| The depreciation cost is covered by funds from Capital - funds invested | | | Nordea | 24 164 | 24 709 |
| | | | Cash in hand | 1 | 2 |
| | | | | <u>24 166</u> | <u>24 711</u> |
| Note 7 Tangible fixed assets | | | Note 10 Funds invested status | | |
| Changes in tangible fixed assets during 2011. | | | Buildings | 3 603 | 3 557 |
| Buildings | | | Radar Systems | 832 | 748 |
| Opening acquisition value | 42 382 | 42 374 | Equipment and Tools | 1 213 | 1 664 |
| Acquisitions during the year | 46 | 8 | | <u>5 648</u> | <u>5 968</u> |
| Disposals during the year | 0 | 0 | | | |
| Closing acquisition value | 42 428 | 42 382 | Note 11 Funds held on reserve | | |
| Opening accumulated depreciation | -38 825 | -38 531 | Less investments were made but more spare parts than budgeted were bought. Both actions were budget neutral since the differences were covered by reserve transfers. The surplus for this year (1 898 kSEK) was added to the surplus fund. The other transfers were as budgeted. | | |
| Depreciations during the year | -409 | -295 | Capital operating reserve | 2 051 | 1 834 |
| Disposals during the year | 0 | 0 | Equipment repair fund | 754 | 754 |
| Closing accumulated depreciation | -39 234 | -38 825 | Investment fund | 7 971 | 7 971 |
| Closing residual value | 3 194 | 3 557 | Restructuring reserve | 4 101 | 4 101 |
| Radar systems | | | Spare parts reserve | 149 | 290 |
| Opening acquisition value | 244 542 | 244 484 | Surplus fund | 2 262 | 2 362 |
| Acquisitions during the year | 151 | 59 | | <u>17 289</u> | <u>17 312</u> |
| Disposals during the year | 0 | 0 | Note 12 Liabilities, trade | | |
| Closing acquisition value | 244 693 | 244 542 | Three projects financed by EU's European Commission through the Framework Programme 7 scheme are ongoing. All projects work with prefinancing. The prefinancing is kept as liability until taken in use. The prefinancing is released when a periodic report is made. Costs arising in a project are covered by build up of accrued income, which becomes a part of the periodic reporting. A periodic report is coupled with a financial claim. The ESPAS prefinancing was received only in 2012. The guarantee fund is kept as contingency by the Commission for the EISCAT_3D_2 project, which EISCAT is the Co-ordinator of. The guarantee fund will be released at the end of the project, 2014-09-30. | | |
| Opening accumulated depreciation | -243 795 | -243 662 | EISCAT_3D_2 guarantee fund, whole project | 2 003 | 2 023 |
| Depreciations during the year | -67 | -132 | EISCAT_3D_2 prefinancing | 5 069 | 5 120 |
| Disposals during the year | 0 | 0 | ENVRI prefinancing | 539 | 0 |
| Closing accumulated depreciation | -243 861 | -243 795 | ESPAS prefinancing | 0 | 0 |
| Closing residual value | 832 | 748 | Liabilities, trade | 3 709 | 4 282 |
| Equipment and tools | | | | <u>11 320</u> | <u>11 425</u> |
| Opening acquisition value | 33 011 | 33 057 | | | |
| Acquisitions during the year | 691 | 352 | | | |
| Disposals during the year | 237 | -398 | | | |
| Closing acquisition value | 33 459 | 33 011 | | | |
| Opening accumulated depreciation | -31 347 | -30 958 | | | |
| Depreciations during the year | -728 | -787 | | | |
| Disposals during the year | 237 | 398 | | | |
| Closing accumulated depreciation | -31 838 | -31 347 | | | |
| Closing residual value | 1 622 | 1 664 | | | |
| Sum tangible fixed assets | 5 648 | 5 968 | | | |

Note 8 Prepayments and accrued income

The main buildings and systems insurance for 2012 was paid in December. Costs relating to the Antenna III feasibility work were invoiced in January 2012. Costs spent during 2011 in the now three ongoing EC projects will be claimed from EC when the periodic report is due. The largest, the EISCAT_3D_2 project will have its first periodic report in April 2012.

Stockholm 2012-05-29



Dr. Tomas Andersson



Prof. Qing-sheng Dong



Dr. Bjørn Jacobsen



Dr. Hiroshi Miyaoka



Dr. Michael Schultz



Dr. Kati Sulonen



Dr. Esa Turunen
Director

Our audit report was issued on 2012-06-20.



Mrs. Annika Wedin
Authorised Public Accountant



Audit report

To the council of EISCAT Scientific Association, Corporate Identity Number 897300-2549

Report on the annual accounts

I have audited the annual accounts of EISCAT Scientific Association for the year 2011.

Responsibilities of the council and the director for the annual accounts

The council and the director are responsible for the preparation and fair presentation of the annual accounts in accordance with the Annual Accounts Act, and for such internal control as the council and the director determine is necessary to enable the preparation of annual accounts that are free from material misstatement, whether due to fraud or error.

Auditor's responsibility

My responsibility is to express an opinion on the annual accounts based on my audit. I conducted my audit in accordance with International Standards on Auditing and generally accepted auditing standards in Sweden. Those standards require that I comply with ethical requirements and plan and perform the audit to obtain reasonable assurance about whether the annual accounts are free from material misstatement.

An audit involves performing procedures to obtain audit evidence about the amounts and disclosures in the annual accounts. The procedures selected depend on the auditor's judgment, including the assessment of the risks of material misstatement of the annual accounts, whether due to fraud or error. In making those risk assessments, the auditor considers internal control relevant to the association's preparation and fair presentation of the annual accounts, in order to design audit procedures that are appropriate in the circumstances, but not for the purpose of expressing an opinion on the effectiveness of the association's internal control. An audit also includes evaluating the appropriateness of accounting policies used and the reasonableness of accounting estimates made by the council and the director, as well as evaluating the overall presentation of the annual accounts.

I believe that the audit evidence I have obtained is sufficient and appropriate to provide a basis for my audit opinion.

Opinion

In my opinion, the annual accounts have been prepared in accordance with the Annual Accounts Act and presented fairly, in all material respects. The financial position of the association as of 31 December 2011 and of its financial performance and cash flows for the year then ended is also in accordance with the Annual Accounts Act. The statutory administration report is consistent with the other parts of the annual accounts.

Report on other legal and regulatory requirements

In addition to my audit of the annual accounts, I have also examined the administration of the council and the director of EISCAT Scientific Association for the 2011.

Responsibilities of the council and the director

The council and the director are responsible for the administration.

Auditor's responsibility

My responsibility is to express an opinion with reasonable assurance on the administration based on my audit. I conducted the audit in accordance with generally accepted auditing standards in Sweden.

As a basis for my opinion on the council and the director's administration, in addition to my audit of the annual accounts, I examined significant decisions, actions taken and circumstances of the association in order to determine whether any member of the council or the director have undertaken any action or is guilty of negligence which may entail a liability for damages. I also examined whether any council member or the director has, in any other way, acted in contravention of the Annual Accounts Act or the statutes.

I believe that the audit evidence I have obtained is sufficient and appropriate to provide a basis for my opinion.

Opinion

The council and the director have not acted in contravention of the statutes.

Gävle, 20 June 2012

Annika Wedin
Authorized Public Accountant

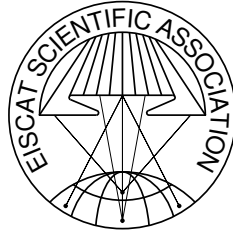
Report 2011 of the EISCAT Scientific Association

©EISCAT Scientific Association

EISCAT Headquarters

Box 812, SE-981 28 Kiruna, Sweden

Scientific contributions: EISCAT Associates and staff



The EISCAT Associates

December 2011

CRIRP

China Research Institute of Radiowave Propagation
China
www.crip.ac.cn

DFG

Deutsche Forschungsgemeinschaft
Germany
www.dfg.de

NERC

Natural Environment Research Council
United Kingdom
www.nerc.ac.uk

NFR

Norges forskningsråd
Norway
www.forskningsradet.no

NIPR

National Institute of Polar Research
Japan
www.nipr.ac.jp

SA

Suomen Akatemia
Finland
www.aka.fi

STEL

Solar Terrestrial Environment Laboratory, Nagoya
Japan
www.stelab.nagoya-u.ac.jp

VR

Vetenskapsrådet
Sweden
www.vr.se

EISCAT Scientific Association

Headquarters

EISCAT Scientific Association
Box 812
SE-981 28 Kiruna, Sweden
Phone: +46 980 79150
Fax: +46 980 79159
www.eiscat.se

Sites

Kiruna

EISCAT Kiruna Site
Box 812
SE-981 28 Kiruna, Sweden
Phone: +46 980 79136
Fax: +46 980 29276

Longyearbyen

EISCAT Svalbard Radar
Postboks 432
N-9171 Longyearbyen, Svalbard
Phone: +47 790 21236
Fax: +47 790 21751

Sodankylä

EISCAT Sodankylä Site
Tähteläntie 54B
FIN-99600 Sodankylä, Finland
Phone: +358 16 619880
Fax: +358 16 610375

Tromsø

EISCAT Tromsø Site
Ramfjordmoen
N-9027 Ramfjordbotn, Norway
Phone: +47 776 20730
Fax: +47 776 20740